

Online Non-linear Prediction of Financial Time Series Patterns



Joel da Costa

Supervisor: A/Prof. T. Gebbie

A dissertation submitted in partial fulfilment of the requirement

for the Master of Science degree in Advanced Analytics,

School of Statistical Sciences,

University of Cape Town

2019

Abstract

We consider a mechanistic non-linear machine learning approach to learning signals in financial time series data, and establish a modularised and decoupled algorithm framework that is proved on daily sampled closing time-series data for JSE equity markets. The input patterns are based on input data vectors of data windows pre-processed into a sequence of daily, weekly and monthly or quarterly sampled feature measurement changes (log feature fluctuations). The data processing is split into a batch processed step where features are learnt using a Stacked AutoEncoder (SAE) via unsupervised learning, and then both batch and online supervised learning are carried out using these features learnt, with the output being a point prediction of

measured time-series feature fluctuations (log differenced data) in the future (ex-post). Weight initializations for these networks are implemented with restricted Boltzmann machine (RBM) pre-training, and variance based initializations. The historical simulation is then run using an online feedforward neutral network (FNN) initialised with the weights from the batch training and validation step. The validity of results are shown under a rigorous assessment of backtest overfitting using both Combinatorially Symmetrical Cross Validation and Probabilistic and Deflated Sharpe Ratios. Results are further used to develop a view on the phenomenology of financial markets and the value of complex historical data under unstable dynamics.

Keywords: online learning, feedforward neural network, restricted boltzmann machine, variance weight initialization, stacked autoencoder, pattern prediction, JSE, non-linear, financial time series, combinatorially symmetrical cross validation, back-test overfitting, deflated Sharpe ratio, probabilistic Sharpe ratio s

Contents

| | |
|---|-----------|
| List of Figures | 7 |
| List of Tables | 8 |
| 1 Introduction | 11 |
| 2 Literature Review | 14 |
| 2.1 Technical Analysis | 14 |
| 2.2 Neural Networks | 15 |
| 2.2.1 Training and Backpropagation | 16 |
| 2.2.2 Activation Functions | 17 |
| 2.2.3 Deep Learning | 18 |
| 2.2.4 Weight Initialization Improvements | 19 |
| 2.3 Stacked AutoEncoders | 19 |
| 2.3.1 High Dimensional Data Reduction | 19 |
| 2.3.2 Deep Belief Networks | 20 |
| 2.3.3 Stacked Denoising AutoEncoders | 21 |
| 2.3.4 Pre-training | 22 |
| 2.3.5 Time Series Applications | 22 |
| 2.3.6 Financial Applications | 23 |
| 2.4 Online Learning Algorithms and Gradient Descent | 24 |
| 2.5 Gradient Learning Improvements | 25 |
| 2.5.1 Gradient Adjustments and Regularization | 25 |
| 2.5.2 Dropout | 25 |
| 2.5.3 Learning Rate Schedules | 26 |
| 2.6 Backtesting and Model Validation | 27 |
| 2.6.1 Sharpe Ratio Assessment Methodologies | 28 |
| 2.6.2 Generalised Assessment Methodologies | 29 |
| 2.6.3 Test Data Length | 30 |
| 3 Data Processing and Generation | 32 |
| 3.1 Data Processing | 32 |
| 3.1.1 Log Difference Transformation and Aggregation | 32 |
| 3.1.2 Data Scaling | 32 |
| 3.1.2.1 Standardization | 33 |
| 3.1.2.2 Normalization | 33 |
| 3.1.2.3 Limited Standardization | 33 |
| 3.1.2.4 Limited Normalization | 33 |
| 3.1.3 Reverse Data Scaling | 33 |
| 3.1.3.1 Reverse Standardization | 33 |
| 3.1.3.2 Reverse Normalization | 33 |
| 3.1.3.3 Reverse Limited Standardization | 34 |
| 3.1.3.4 Reverse Limited Normalization | 34 |
| 3.1.4 Price Reconstruction | 34 |
| 3.1.5 Decorrelation | 34 |
| 3.2 Synthetic Data Generation | 34 |
| 3.2.1 GBM Data Distributions | 35 |
| 3.3 Price Considerations | 35 |

| | |
|---|-----------|
| 4 Models and Algorithms | 36 |
| 4.1 Process Overview | 36 |
| 4.2 Feedforward Neural Networks | 36 |
| 4.2.1 Notation and Network Representation | 37 |
| 4.2.2 Activation Functions | 37 |
| 4.2.2.1 Sigmoid | 38 |
| 4.2.2.2 ReLU | 38 |
| 4.2.2.3 Leaky ReLU | 38 |
| 4.2.2.4 Linear Activation | 39 |
| 4.2.3 Backpropagation | 39 |
| 4.2.4 Gradient Descent Algorithms | 41 |
| 4.2.5 Regularization | 42 |
| 4.2.6 Learning Rate Schedule | 43 |
| 4.2.7 Dropout | 44 |
| 4.3 Restricted Boltzmann Machines | 44 |
| 4.3.1 RBM Stochastic Descent | 45 |
| 4.3.2 Contrastive Divergence | 46 |
| 4.3.3 CD-1 and SGD | 47 |
| 4.4 Stacked AutoEncoders | 48 |
| 4.4.1 Sigmoid Based Greedy Layerwise SAE Training | 48 |
| 4.4.2 ReLU based SAE Training | 49 |
| 4.4.3 Denoising AutoEncoders | 50 |
| 4.4.3.1 Additive Gaussian Noise | 50 |
| 4.4.3.2 Masking Noise | 50 |
| 4.5 Variance Based Weight Initializations | 51 |
| 4.5.1 Initialization Rationale | 51 |
| 4.5.2 Initializations | 51 |
| 4.5.2.1 “Xavier” Initialization | 51 |
| 4.5.2.2 “He” Initialization | 52 |
| 4.5.2.3 “He-Adjusted” Initialization | 52 |
| 4.6 Money Management Strategy and Returns | 52 |
| 4.6.1 Input Variables | 53 |
| 4.6.2 Calculated Asset Variables | 53 |
| 4.6.3 Calculated Strategy Variables | 55 |
| 4.7 Combinatorially Symmetric Cross-Validation and Probability of Back-test Overfitting | 56 |
| 4.8 Deflated Sharpe Ratio | 59 |
| 4.8.1 Optimal Number of Clusters Algorithm | 59 |
| 4.8.2 Sharpe Ratio Normality and Probabilistic Sharpe Ratio | 61 |
| 4.8.3 False Strategy Theorem | 62 |
| 4.8.4 Deflated Sharpe Ratio | 62 |
| 4.8.4.1 Estimating $\mathbb{E}[\mathbf{K}]$ and $\text{Var}[\widehat{\mathbf{SR}_k}]$ | 63 |
| 5 Framework Implementation | 65 |
| 5.1 Full Framework Process | 65 |
| 5.2 Process Diagram | 66 |
| 5.3 Parameter Space Exploration | 68 |
| 5.4 Reproducibility | 68 |
| 5.5 Synthetic Data | 68 |
| 5.6 Data Preparation | 69 |
| 5.6.1 Data Window Aggregations | 69 |
| 5.6.2 Point Predictions | 69 |

| | | |
|----------|--|-----------|
| 5.6.3 | Scaling | 70 |
| 5.7 | Data Segregation | 70 |
| 5.8 | Unsupervised Learning: SAE Training | 71 |
| 5.9 | Supervised Learning: Prediction Network Training | 71 |
| 5.10 | Price Reconstruction | 72 |
| 5.11 | Money Management Strategy | 72 |
| 5.12 | Probability of Backtest Overfitting | 73 |
| 5.13 | Deflated Sharpe Ratio | 73 |
| 6 | Software Libraries and Development | 74 |
| 6.1 | Programming Languages | 74 |
| 6.2 | Data Generation & Processing | 74 |
| 6.3 | Network Training | 75 |
| 6.4 | Process Implementation | 76 |
| 6.5 | Process Reproducibility | 76 |
| 6.6 | Database Implementation | 77 |
| 6.7 | Diagnostic Libraries | 77 |
| 6.7.1 | DSR Libraries | 78 |
| 7 | Datasets Used | 79 |
| 7.1 | Actual Datasets | 79 |
| 7.1.1 | “Actual10” | 79 |
| 7.1.2 | “Scaling10” | 79 |
| 7.1.3 | “AGL” and “AGL&ACL” | 79 |
| 7.2 | Synthetic Datasets | 81 |
| 7.2.1 | “Synthetic6” | 81 |
| 7.2.2 | “Synthetic10” | 81 |
| 8 | Results | 84 |
| 8.1 | Introduction | 84 |
| 8.1.1 | Technical Notes | 85 |
| 8.2 | Primary Determinants of OOS P&L | 87 |
| 8.2.1 | Effects of Data Horizon Aggregations | 87 |
| 8.2.2 | OGD Learning Rate | 89 |
| 8.2.3 | Feature Selection | 90 |
| 8.3 | Value of Historical Signal | 94 |
| 8.4 | Weight Initializaton Techniques | 96 |
| 8.4.1 | RBM Pretraining for Sigmoid Networks | 96 |
| 8.4.2 | Variance Based Weight Initialization Techniques | 97 |
| 8.5 | Synthetic Data | 100 |
| 8.5.1 | GBM Generated Data | 100 |
| 8.5.2 | Synthetic Data Horizon Effects | 100 |
| 8.5.3 | Synthetic Data Feature Selection | 101 |
| 8.6 | Complexity of Financial Time Series | 102 |
| 8.6.1 | Data Scaling | 102 |
| 8.6.2 | SAE Reproduction | 103 |
| 8.6.3 | FFN Prediction | 106 |
| 8.7 | Network Structure | 109 |
| 8.7.1 | Effects of Network Size | 109 |
| 8.7.1.1 | SAE Network Structures | 109 |
| 8.7.2 | Effects of Activation Functions | 110 |
| 8.7.3 | Predictive FFN Activations and Scaling | 111 |

| | | |
|-----------|--|------------|
| 8.7.4 | Sigmoid Activation Functions | 112 |
| 8.7.5 | Leaky ReLU vs ReLU | 112 |
| 8.8 | Money Management Strategy | 113 |
| 8.9 | Probability of Backtest Overfitting | 115 |
| 8.9.1 | Concerns Regarding the PBO Calculation | 115 |
| 8.9.2 | PBO Results | 117 |
| 8.9.3 | Framework Success | 119 |
| 8.10 | Deflated Sharpe Ratio | 120 |
| 8.10.1 | Computational Complexity | 120 |
| 8.10.2 | ONC Results | 120 |
| 8.10.3 | DSR and PSR Results | 122 |
| 8.10.4 | Framework Success | 123 |
| 8.11 | Summary of Actual and Synthetic Data Effects | 124 |
| 9 | Conclusion | 125 |
| 10 | Future Work | 129 |
| 11 | Appendix | 130 |
| 11.1 | Additional Results | 130 |
| 11.1.1 | Additional Results for Section 8.2 - Feature Selection | 130 |
| 11.1.2 | Additional Results for Section 8.4 - Weight Initialization Techniques | 130 |
| 11.1.3 | Additional Results for Section 8.6 - Complexity of Financial Time Series | 131 |
| 11.1.3.1 | Effects of Learning Rate Epoch Cycles | 131 |
| 11.1.3.2 | Effects of Learning Rate Epoch Cycles | 132 |
| 11.1.4 | Additional Results for Section 8.7 - Network Structure and Training | 133 |
| 11.2 | Additional Calculations for Section 8.10 - DSR and ONC | 136 |
| 11.2.1 | DSR and PSR calculations | 136 |
| 11.3 | Configuration Sets Used | 139 |
| 11.3.1 | Configuration 1 | 139 |
| 11.3.2 | Configuration 2 | 139 |
| 11.3.3 | Configuration 3 | 140 |
| 11.3.4 | Configuration 4 | 141 |
| 11.3.5 | Configuration 5 | 142 |
| 11.3.6 | Configuration 6 | 142 |
| 11.3.7 | Configuration 7 | 143 |
| 11.3.8 | Configuration 8 | 144 |
| 11.3.9 | Configuration 9 | 145 |
| 11.3.10 | Configuration 10 | 145 |
| 11.3.11 | Configuration 11 | 146 |
| 11.3.12 | Configuration 12 | 147 |
| 11.3.13 | Configuration 13 | 148 |
| 11.3.14 | Configuration 14 | 149 |
| 11.3.15 | Configuration 15 | 150 |
| 11.3.16 | Configuration 16 | 150 |
| 11.3.17 | Configuration 17 | 151 |
| 11.4 | Diagnostic Charts | 153 |
| 12 | References | 156 |

List of Figures

| | | |
|----|--|-----|
| 1 | The AutoEncoder Training Steps | 21 |
| 2 | Feedforward Neural Network Diagram | 37 |
| 3 | Cyclical Learning Rate Diagram | 44 |
| 4 | Restricted Boltzmann Machines Diagram | 45 |
| 5 | Overall Process Flow Diagram | 67 |
| 6 | “Actual10” Price Relatives | 80 |
| 7 | ‘Scaling10’ Price Relatives | 80 |
| 8 | ‘AGL&ACL’ Price Relatives | 81 |
| 9 | Synthetic6 Price Relatives | 83 |
| 10 | Synthetic10 Price Relatives | 83 |
| 11 | OGD MSE vs OOS P&L | 86 |
| 12 | SAE MSE Scores by Data Aggregations | 88 |
| 13 | OOS P&L by Data Aggregations | 88 |
| 14 | OOS P&L by OGD Learning Rates | 89 |
| 15 | OOS P&L by OGD Learning Rates and Data Aggregations | 90 |
| 16 | IS SAE Performance for MSE and P&L by Encoding Size | 91 |
| 17 | OOS P&L By Feature Selection Size and OGD Learning Rate | 92 |
| 18 | OOS P&L By Feature Selection Size, OGD Learning Rate and Data Horizons | 93 |
| 19 | OOS P&L by IS Training Epochs | 94 |
| 20 | OOS P&L by IS Training Dataset Size | 95 |
| 21 | Pre-training Effects on SAE MSE Scores | 97 |
| 22 | SAE MSE by Weight Initialization | 98 |
| 23 | OOS P&L by Weight Initialization | 99 |
| 24 | SAE MSE Scores for Synthetic Data | 100 |
| 25 | OOS P&L by Data Aggregation (Synthetic Data) | 101 |
| 26 | OOS P&L by Feature Selection Size and OGD Learning Rate (Synthetic Data) | 101 |
| 27 | SAE MSE by Scaling Function | 102 |
| 28 | OOS P&L by Scaling (Synthetic Data) | 103 |
| 29 | SAE MSE by L1 Regularization | 104 |
| 30 | SAE MSE by Denoising Variance | 104 |
| 31 | SAE MSE by Learning Rate Schedule Ranges | 105 |
| 32 | Effects of Epoch Cycle Lengths on P&L | 107 |
| 33 | Effects of L1 Regularization on P&L | 108 |
| 34 | Effects of Dropout on P&L | 108 |
| 35 | Network Performance by Size | 109 |
| 36 | MSE by Output Activations | 110 |
| 37 | MSE by Activations and Encoding Layer Size | 111 |
| 38 | P&L by Scaling and Activations (Synthetic Data) | 112 |
| 39 | MMS OOS P&L Distributions | 114 |
| 40 | MMS Sharpe Ratios and Correct Trades | 114 |
| 41 | PBO Scores by Split Values | 117 |
| 42 | Number of CSCV Combinations by Split Value | 117 |
| 43 | Logit Distribution for All Configurations | 118 |
| 44 | Logit Distribution for Subset of Configurations | 119 |
| 45 | Sharpe Ratios for ONC Clusters and Best Strategy | 121 |
| 46 | OGD MSE Scores for ONC Clusters | 122 |
| 47 | MSE By Feature Selection Size (Synthetic Data) | 130 |

| | | |
|----|--|-----|
| 48 | Prediction Accuracy by Training Epochs (MNIST Data) | 130 |
| 49 | SAE MSE by Initialization (Actual Data) | 131 |
| 50 | SAE MSE by Learning Rate Epoch Cycles (Actual Data) | 131 |
| 51 | SAE MSE by Learning Rate Epoch Cycles (Synthetic Data) | 132 |
| 52 | P&L by Learning Rates | 132 |
| 53 | MSE By Network Sizes (Actual Data) | 133 |
| 54 | MSE By Network Sizes (Synthetic Data) | 133 |
| 55 | P&L By Network Sizes (Actual Data) | 134 |
| 56 | P&L By Network Sizes (Synthetic Data) | 134 |
| 57 | Predictive P&L by OGD Learning Rate (Synthetic Data) | 135 |
| 58 | Predictive P&L by L1 Regularization (Synthetic Data) | 135 |
| 59 | SAE: Leaky ReLU vs ReLU (Synthetic Data) | 136 |
| 60 | P&L by ReLU Activations (Synthetic Data) | 136 |

List of Tables

| | | |
|---|--|-----|
| 1 | Database Schema Descriptions | 77 |
| 2 | Assets in the “Actual10” dataset, from 2003-2018. | 79 |
| 3 | Assets in the “Synthetic6” dataset, as detailed in Section 7.2.1. | 82 |
| 4 | Assets in the “Synthetic10” dataset, as detailed in Section 7.2.2. | 82 |
| 5 | P&L Diagnostic EDA Functions | 154 |
| 6 | P&L Diagnostic EDA Functions | 155 |

List of Acronyms

I

| | |
|---------------|--|
| BP | Backpropagation |
| CD1 | Contrastive Divergence 1 |
| CLR | Cyclical Learning Rate |
| CSCV | Combinatorially Symmetric Cross-Validation |
| DBN | Deep Belief Network |
| DSR | Deflated Sharpe Ratio |
| FDR | False Discovery Rate |
| FNN | Feedforward Neural Network |
| FST | False Strategy Theorem |
| FWER | Family Wise Error Rate |
| GBM | Geometric Brownian Motion |
| IID | Independently and Identically Distributed |
| IS | In Sample |
| LSTM | Long Short Term Memory |
| MCS | Model Confidence Set |
| MMS | Money Management Strategy |
| MSE | Mean Squared Error |
| NN | Neural Network |
| OHLC | Open High Low Close |
| OGD | Online Gradient Descent |
| ONC | Optimal Number Clusters |
| OOS | Out of Sample |
| PL | Profit and Loss |
| PBO | Probability of Backtest Overfitting |
| PCA | Principal Components Analysis |
| PSR | Probabilistic Sharpe Ratio |
| RBM | Restricted Boltzmann Machine |
| RNN | Recurrent Neural Network |
| SAE | Stacked AutoEncoder |
| (S)DAE | (Stacked) Denoising AutoEncoder |
| SGD | Stochastic Gradient Descent |
| SL | Supervised Learning |

| | |
|------------|---------------------------|
| SR | Sharpe Ratio |
| SVM | Support Vector Machine |
| SVR | Support Vector Regression |
| UL | Unsupervised Learning |

1 Introduction

This paper presents a novel framework with a non-linear and mechanistic approach to asset price fluctuation prediction in financial markets. The framework combines several concepts to this end: the training of deep neural networks, feature selection through the use of Stacked AutoEncoders and unsupervised learning, supervised learning through both batch and online methods for asset price fluctuation prediction and current assessment techniques such as Combinatorially Symmetric Cross-Validation (CSCV) and the Deflated Sharpe Ratio (DSR). In doing so, a modular process is presented, where individual components are decoupled and can be configured as necessary. This delivers a simplest high complexity framework which allows further adaptation for the exploration of a high dimensional solution space.

As Bailey et al. have noted, and which is discussed more fully in Section 2.6, backtesting overfitting for trading strategies have become problematically widespread in financial literature [7]. Neural networks, in their capacity as universal function approximators with few model limitations, offer an effective and appropriate methodology to generate predictions in an environment as complex as financial markets. However, the increased complexity and nature of backtest overfitting leave traditional validation methods such as hold-out or cross validation falling short. The framework presented investigates how more rigorous validation techniques can be applied to deep learning models in order to avoid such overfitting. Further validation takes place in assessing the potential profitability of the model in a live market.

The literature review in Section 2 has a fuller discussion of work that precedes the various techniques which have been implemented. A brief introduction to technical analysis in the financial sector, with it's perspective and history, is discussed and forms the basis for proposing and using the technical analysis methods throughout this paper (Section 2.1). The literature review then moves onto covering the usage and history of Neural Networks, which has progressed enormously in recent years. This section covers both the basic foundations, and also discusses the recent work which has resulted in the widespread use of deep learning models (Section 2.2). This is extended to the coverage of Stacked AutoEncoders, and their efficacy in data reduction for complex systems, which has lead them to be pivotal tools in deep learning models (Section 2.3). Online learning methods are discussed in Section 2.4 with a coverage of both the historical basis as well as the more recent developments which have allowed for further improvement in the algorithms. The section finishes off with discussing the impact of backtest overfitting and results validation. The Probability of Backtest Overfitting (PBO) and Deflated Sharpe Ratio (DSR), as developed by Bailey et al. [7] and Lopez de Prado and Lewis [81] respectively, are presented as validation techniques for the framework as a whole (Section 2.6).

Section 3 provides the details regarding data processing that takes place prior to training, discussing both the scaling and fluctuation aggregation techniques used. A discussion of Geometric Brownian motion, which is used for the generation of synthetic data, is included with notes around its characteristics and usage in financial prediction models.

Section 4 provides more in-depth details on the algorithms and structures used to implement the framework. The structure of feedforward neural networks is discussed, as well as how they are trained using the backpropagation algorithm, and how that can be applied in a stochastic descent framework (Section 4.2). This section also provides details for how these network weight initializations can impact performance, and how this can be improved with either RBM pre-training (as per Section 4.3) or through newer variance based techniques (Section 4.5) - this includes the structures and training techniques used for the Stacked AutoEncoders (Section 4.4). The Money Management System (MMS) constitutes the implementation of trading decisions and actions based on the network model predictions and is detailed in Section 4.6. The CSCV techniques suggested by Bailey et al. [7] are implemented and used to derive a Probability of Backtest Overfitting (PBO) figure for the full training and testing processes is detailed in Section 4.7. Finally, the implementation of the Optimal Number of Clusters (ONC) and DSR calculations are covered in Section 4.8.

Where Section 4 discusses the functional implementations of each module of the framework, Section 5 is concerned with how these modules fit together to form an end to end system, from the data preparation to the output of a Probability of Backtest Overfitting (PBO) or DSR figure. This includes discussions of various considerations for individual aspects of the framework, as well as decisions around the combinations of these parts with their justifications and relevant advantages or disadvantages. In light of the configurable and modular system developed, potential alternatives and how they might be used are also discussed here.

Section 6 discusses the implementation tools chosen as well as the libraries created in the process of developing the software for the framework. The libraries offer a generic set of tools with highly configurable parameters in order to train and assess neural networks, including an extensive collection of visualizations of results.

Section 7 provides a brief overview of the datasets used for the trials run, including both the synthetic and actual datasets. Visualisations for the individual asset prices are also included here.

Finally, Section 8 discusses the full set of results from the experiments, and offers several key takeaways. It's shown that historical financial data is of limited use in financial model training, and predictions are served best by a

recent cross sectional view on information. Section 8.2 discusses the nature of prediction strategies learnt, showing that they're influenced heavily by the data horizon choices. Further, SAE based feature reduction is shown to be both possible and effective, though with results also being subject to data horizons and recency. Online learning, and consequently network initializations, are shown to be of high importance, the results for which are covered in Section 8.4. The complexity of financial time series, and how it impacts both supervised and unsupervised learning, are discussed in Section 8.3, with comparisons to synthetic data being made in Sections 8.5 and 8.11. The MMS returns are presented in Section 8.8, and validated through the noted methods in Sections 8.9 and 8.10, showing that the framework was able to deliver a profitable and verifiable set of strategies.

2 Literature Review

2.1 Technical Analysis

Technical analysis is a financial analytical practice that makes use of past price data in order to identify market structures, as well as forecast future price movements. The techniques are typically objective methodologies which rely solely on past market data (price and volume). They stand in contrast to fundamental analysis, where experts will consider a companies operations, management and future prospects in order to arrive at an evaluation. The basis of much technical analysis, originally developed through Dow Theory, is the belief that stock market prices will move directionally (upwards, downwards or sideways), and that past movements can be used to determine these trends [88].

One of the primary methods in technical analysis is the use of charts in order to identify price patterns. These charts will be produced using the available market data and a known design, such as the popular candle-bar plot, which can then be compared to historical data to match it to a particular pattern. These patterns are thus indicative that the stock is likely to take on a partigm There is a certain amount of controversy around technical analysis, where many argue that it is contradictory to the random walk and weak form efficient market hypotheses, and as such is not valuable or useful [53]. The argument against this, is that technical analysis does not rely on past action to predict the the future, but is rather a measure of current trading, and how the market has reacted after similar patterns have occurred in the past [69]. Further, even if the analysis is unable to effectively forecast future price trends, it can still be useful to exploit trading opportunities in the market [103].

With the advent of processing power becoming cheaply available, there has been an increase in research to adapt computing techniques to technical analysis. The breadth and superhuman speed in which systems are able to perform technical analysis far outstrips what was possible before, and as such they have become the focus of competitive performance for many market participants [68]. To this end, there has been much research to apply machine learning algorithms to perform pattern recognition on stock price movements.

Financial markets have been shown to be complex and adaptive systems, where the effects of interaction between participants can be highly non-linear [3]. Complex and dynamic systems such as these may often exist at the ‘order-disorder border’ - they will generate certain non-random patterns and internal organisation, which can be assessed and identified, however they will also exhibit a certain amount of randomness in their behaviours, or ‘chaos’ [19]. Further, it’s been shown that there is enough signal to reconstruct the phase space of chaotic systems from singular observations, encouraging that we might be able to perform effective technical analysis in the context of financial markets

[93, 109]. As a result, trying to identify these patterns and structures is a simultaneously reasonable and notoriously difficult goal. While it is often clear in hindsight that the patterns exist, the amount of noise and non-linearity in the system can make prediction challenging. Fittingly then, neural networks have become a popular choice for modelling within financial markets. Due to their structure, they are able to learn non-linear interactions between their inputs and outputs, with even early research showing their ability to achieve statistically significant results, which lends weight to the argument against the efficient market hypothesis [107].

The work presented here fits into the growing body of work which considers mechanistic and brute-force approaches of applying machine learning models to financial market data. In doing so, the financial market complexity in terms of non-linearity, noise and stability are highlighted through both the successes and challenges found in training these machine learning models. These difficult dynamics, and their notable difference when compared to other popular areas of ML research - which are often around Independently and Identically Distributed (IID) datasets - present fundamental problems to be explored, both in terms of prediction efficacy as well as validation. Gebbie and Loonat [49] have explored the application of online learning models in this space in the South African market, showing that direct online learning approaches would be able to identify and exploit trading opportunities on the JSE through assessment of Open High Low Close (OHLC) data. Murphy and Gebbie [89] later explore the use of online learning as applied to optimizing parameters which apply to maximising wealth trading zero-cost portfolio strategies, also in the JSE. They consider validation in terms of statistical arbitrage, as well the non-parametric Probability of Backtest Overfitting (PBO). Similar ideas are explored here, in the use of mechanistic batch and online learning in order to identify patterns in JSE closing data, as well as the use of non-parametric validation techniques for return assessment.

2.2 Neural Networks

A Neural Network (NN) is a learning model which was originally inspired by the biological mechanisms of neurons in brains. The structure is essentially that of a network system, with connected nodes and edges, or neurons and weights in context. The neurons are based on the same idea as synapses as seen in the brain - where a build-up of input results in a firing of output. The input here is determined by the models input (real numbers typically), and processed through the weights and activation functions of the neuron, which then results in an output value either at an intermediate level, or as the models final output. The system learns by considering input samples sequentially, and adjusting the weights between edges to result in more accurate outputs, which may either be classification or regression values.

Structured neural networks that learn to some extent have been around

since the second half of the 21st century [101], though have been through several cycles of popularity. The first versions tended to be very simple with one layer of hidden neurons [67]. It was only later, through the application of the backpropagation algorithm, that they started to become more practical and popular [117].

With the rise in popularity, many different network formations were developed and suggested. One of the initial suggestions was the conceptually simple Feedforward Neural Network (FNN) as described above - an acyclic graph where inputs are processed in a single direction until the output is reached. The other notable earlier model was the Recurrent Neural Network (RNN), which has a cyclic graph instead - this results in a more powerful computational system than the standard FNN, which was shown to be effective quite early on [106]. The Long Short-Term Memory (LSTM) network was another that used recurrent dynamics, though at a neuron level, in that the neuron is responsible for remembering values for an arbitrary time period [63]. Convolutional Neural Networks (CNN) have a non-recurrent structure, but implement separate pooling layers of neurons which consider the adjacent input values for each feature (e.g. pixels next to each other). These have been shown to be incredibly effective at tasks such as image recognition, as elaborated on later.

There are three primary learning paradigms used in neural network training - Supervised Learning (SL), where the network is trained on inputs with known outputs; Unsupervised Learning (UL), where the network is trained to identify unknown structures as an output; and Reinforcement Learning (RL), where environmental reactions are used as inputs to train a network for certain outputs [101]. While all of these configurations and paradigms have their benefits and uses, this paper will largely focus on FNNs and RNNs, trained through SL and UL.

2.2.1 Training and Backpropagation

Historically, the crux of neural networks popularity has often been based on the development of novel training methodologies, and how they have increased performance. In line with this, the Backpropagation (BP) algorithm (as defined in Section 4.2.3) has played a pivotal part: while neural network (or perceptron) models were around long before NN popularity, they were largely deemed ineffective, at least in comparison to other available models of the time [87]. It was only during the 1980s that the BP algorithm was applied to NNs, and the field started to gain in popularity again [73, 116].

Rumelhart et al. [99] showed that the BP algorithm as applied in NNs resulted in useful feature representations occurring in hidden layers and the empirical success that resulted thereof. Shortly after, LeCun et al. [74] applied the BP algorithm to CNNs with adaptive connections. They were able to show

impressive performance for the time in classifying handwritten images, with the images as a direct input (rather than a feature vector).

While many improvements were made during this time via gradient descent modifications, the models were typically of a shallow nature due to problems encountered trying to train deeper networks. Early experiments with deep networks resulted in poor performance due to what is now widely known as the problem of either vanishing or exploding gradients [94]. Essentially, as more layers are added to the network, the backpropagation algorithm (with typical activation function neurons), results in error signals that either shrink or grow out of bounds at an exponential rate. One of the first suggested and primary solutions to the problem is to perform pre-training on the network through unsupervised learning [101], which is discussed more fully in Section 2.3.2. Variance based weight initialization techniques have grown in popularity in recent years, as discussed in Section 2.2.4.

There were also initial concerns that the BP algorithm as applied to high dimensional neural networks would result in the network weights being trapped in local minima if a simple gradient descent was used (e.g. where no small changes to the configuration would reduce the average error rate) [76]. However, empirically, this tends not to be so problematic, and large networks usually reach solutions of equitable performance. More recent research has shown that the solution spaces largely consist of many saddle points, each with varying gradients of the features, but which also tend to have similar values of the objective function [40]. Ge et al. [48] have also shown that it is possible to escape saddle points and offer a guaranteed global convergence in certain non-convex problems.

2.2.2 Activation Functions

One of the upfront configuration choices necessary is the activation function, which allows the mapping of input to output at the neuron level. There have been many suggestions and experiments with different functions, though there are some common features amongst functions which might make them appropriate: Non-linearity allows for neural networks to operate as universal approximators, as shown in [64], continuous differentiability allows for the use of gradient descent and whether the function is monotonic has been shown to indicate whether the solution can be guaranteed to have a unique periodic solution [119]. Lastly, the range of the function (infinite or finite) can impact both the stability and efficiency of the training.

Some of the most popular functions that have been used are the Sigmoid, Tanh, ReLU and Softsign (the equations for which are detailed in Section 4.2.2). There have been various studies showing the effectiveness of the different activations under varying initialization (or pre-training) for weights. Glorot

and Bengio [50] noted that the typical Sigmoid and Tanh functions performed poorly with standard minimization, and result in slower convergence and worse minima, and showed that Softsign with a non-standard initialization resulted in quicker convergence . Further research by Glorot et al. [51] found that the rectifier (ReLU) functions were more effective in deep sparse networks compared to the Tanh function.

2.2.3 Deep Learning

As noted above, most of the earlier work using neural networks relied on shallow models with few layers. However, a resurgence in interest occurred in 2006 after several papers demonstrated the efficacy of unsupervised pre-training of networks prior to supervised training. The effect was substantial enough to allow much deeper layered networks to be trained than before [11, 61].

The essential point behind the unsupervised learning was to initialize the weights in the network to sensible values in light of the problem context. The methods used trained each layer to be able to reconstruct the model of the features in the layer below (to a varying degree of accuracy). Sequentially pre-training and combining layers like this, the process generated a deep neural network with appropriate weights. Once done, a final output layer was added and the entire network could then be fine-tuned through backpropagation, without suffering such performance degradation through vanishing or exploding gradients [61, 97, 59]. This is expanded up further in Section 2.3.2. Roux and Bengio [98] were able to show that within the DBNs produced by Hinton et al. [61], adding hidden nodes resulted in strictly improved modelling capabilities, and they suggested that increasing the number of layers is likely to result in increased representational ability (subject to efficacy of previous layers), thus establishing the argument for deep networks in theory as well as practice .

FNNs had been shown to be effective in modelling high dimensional data even prior to the breakthroughs in deep networks [10], so it fits that the deep networks were shown to be extremely effective in high dimensional data classification. Early implementations resulted in increased efficacy in handwriting recognition, as well as pedestrian recognition [104]. When it came to data types such as sound and images, CNNs were implemented on several occasions with record breaking model performances in recognition, notably in ImageNet and WaveNet [70, 91].

As more research into deep networks was conducted, it became apparent that with large enough datasets, the layerwise pre-training of networks was not actually necessary to achieve high performance standards [70, 51, 17]. When training for long enough, it was reported that the pre-training offered little to no benefit, though these models were typically using datasets far larger than were attempted before (as a result of hardware improvements enabling as

much). While these results did require that certain attention was paid to the initialization, as well as the use of non-linear activation units, it did suggest that pre-training largely acted as a prior which may not be necessary if large enough labelled datasets are available [12]. Naturally, pre-training was still implemented to prevent overfitting in smaller datasets.

2.2.4 Weight Initialization Improvements

One of the more critical innovations to allow effective training of deep networks without using pre-training was the development of more sophisticated techniques for weight initialization. One of the first and most popular of these was presented by Glorot and Bengio [50] for use in Sigmoid based networks, and is commonly referred to as Xavier/Glorot initialization. The technique is layer specific and based on a linear activation hypothesis, such that the initial weights would maintain the same variance for input for information that is passed backwards as in accordance with the nature of the activation function. While the assumption of linearity is not entirely applicable, they point out that at the start of the learning process, it is typically the area of the activations where the gradient is close to 1 which is being explored, thus initially approximating a linear effect. The effect is a technique that increases learning efficacy and optima found [50].

This same methodology was extended for the ReLU activation by He et al. [57], once again based on the linearity hypothesis around the relevant activation function (Parametric Rectified Linear Units in this case). The combination of ReLU activations, which are computationally inexpensive and do not suffer from learning slowdown, as well as an effective weight initialization technique such that pre-training was not necessary, produced a seminal FNN training framework. He et al. [57] were able to achieve state of the art performance and produced the best known error rate at the time on the ImageNet dataset. The efficacy of these techniques has established them as norms in the training of deep neural networks.

2.3 Stacked AutoEncoders

2.3.1 High Dimensional Data Reduction

Machine learning techniques have been shown to be extremely effective at modelling non-linear inputs to outputs - neural networks have even been shown to be universal function approximators in this regard [64]. More traditional statistical models will typically process the available feature data to select the most significant features to be used in the model once its defined - evident in processes such as subset selection [100]. Machine learning techniques are no different in this regard, and feature data will typically be transformed to smaller observations of more significance prior to being used as input to a

model, such as the neural networks described above.

Financial data, in line with the complex and dynamic system that it represents, is often of a very high dimensional nature, which offers opportunities through more sophisticated analysis, but also introduces the curses of dimensionality [41]. The increased dimensionality can result in higher processing complexities when needing to do basic tasks such as estimating a covariance matrix (a commonplace necessity in finance), as well as increase the risk of incorrect assumptions based on spurious variable collinearity [46]. Noise accumulation in high dimensional data can create further problems, resulting in problems performing variable selection and ultimately having a large impact on classification and regression models [45].

Time series data can introduce its own set of challenges - there is often not enough data available to understand and predict the process [44], the time variable dependence creates complexity in how much past data to consider at any point, and the data is typically non-stationary [72]. Thus, high dimensional time series data (which many financial problems focus on), require careful consideration on how to handle their inputs and analysis.

Deep learning techniques are a natural choice in this context, and much research has been done to show their (varying) efficacy on time series data. The most successful of these models have been ones which modify deep learning techniques to incorporate the temporal aspect of the data (e.g. Conditional restricted Boltzmann machines or Recurrent Neural Networks), rather than static, and those which have performed feature selection processes rather than operating on the raw data (e.g. AutoEncoders) [72].

Two of the seminal pieces of research that have lead to the resurgence in machine learning and deep learning were the algorithms for training deep belief networks [61], as well as the usage of Stacked AutoEncoders [97, 11].

2.3.2 Deep Belief Networks

AutoEncoders were suggested by Hinton and Salakhutdinov [59] as a method of transforming high dimensional data to lower dimensional input vectors, in order to alleviate some of the problems detailed above, and increase performance of deep belief networks.

One of the more prominent classical techniques for dimension reduction is Principal Components Analysis (PCA), which uses linear algebra to find the directions of greatest variance, and represent the observation samples features along each of these directions, thus maximising the variational representation. Hinton et al. show that AutoEncoders are a non-linear generalization of PCA. The structure and training algorithms of the AutoEncoder show it to be a specialised neural network - there is a multilayer encoder network which is

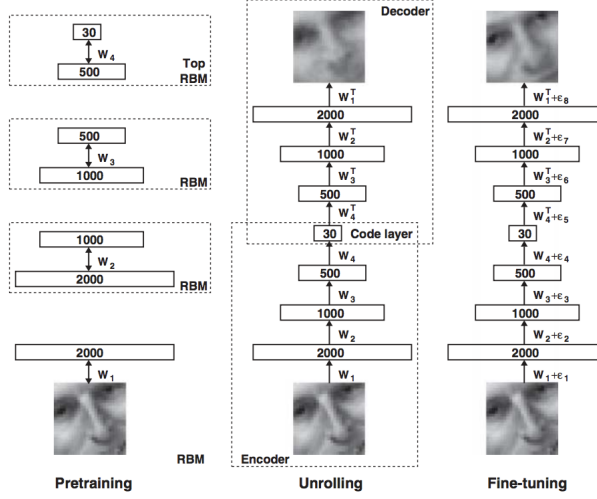


Figure 1: The AutoEncoder training steps [59]

able to transform to a lower dimension, and a symmetrical decoder network to recover the data from the code as represented in Figure 1. As with neural networks, the gradient weights can be trained through the feedforward and backpropagation algorithms.

The primary challenge presented here was the initial weighting of the networks - with large initial weights the AutoEncoder will often find a poor local minima, and with small initial weights the gradients are too small to effectively train deep layered networks. The critical suggestion by Hinton [60] was to used layered restricted Boltzmann machines (RBM) in order to initialise the weights. For each layer of the desired AutoEncoder, a RBM is formed and trained with the previous layer (or RBM). Once all the layers have been trained in this way, they are mirrored to form the decoder network. This then forms the initial weights to be fine tuned further, as per the ‘Fine-tuning’ step in Figure 1. They showed the deep AutoEncoder networks were significantly more effective than PCA or shallow AutoEncoders on multiple dataset types.

2.3.3 Stacked Denoising AutoEncoders

The second important piece of work was the development of a Denoising AutoEncoder (DAE), by Vincent et al. [113]. One of the problems identified in the DBN model described in Section 2.3.2 (and those similar), is that if the encoder dimensions were too high, it is likely that the encoder would learn a trivial encoding - essentially creating a “copy the input” model. The one way of tackling this issue is to constrain the representation with bottlenecks and sparse AutoEncoder layers, which can be seen in Figure 1.

Vincent et al. [113] explore a very different approach to the problem, which was to develop an implementation of AutoEncoder which focused on partially corrupting the input, and so force the network to denoise it. The theory here is based on two ideas - the first, is that a higher dimensional representation should be robust to partial corruption of the input data; and the second is that the denoising process will force model focus to shift to extracting useful features from the input.

The algorithms and structures are largely the same as described for DBNs above, with the key difference being that the model is trained to reconstruct the original input, but only using a corrupted version of the input (where noise has been added to it), and so is forced to learn smarter feature mappings and extractions. The DAE suggested then is a stochastic variant of the AutoEncoder, which has the benefit of being able to implement higher dimensional representations without risking training of a trivial identity mapping. Notably, in the Stacked Denoising AutoEncoder (SDAE) formation, only the initial input is corrupted (as opposed to the input from layer to layer). It was shown that the SDAE model outperformed previous AE and DBN networks on numerous benchmark datasets [113].

2.3.4 Pre-training

The methods described above follow a similar approach: greedy layer-wise unsupervised pre-training in order to determine initial weights, followed by supervised fine tuning to arrive at the final model. It is shown numerous times, that the pretraining process can result in significant performance gains [113]. However it is not immediately apparent, given the nature of backpropagation algorithms and the like, why this is the case. Erhan et al. [43] performed extensive empirical simulations in order to suggest an explanation to the mechanism of pre-training.

While their results were not entirely conclusive, they did lend themselves to a reasonable hypothesis: the unsupervised pre-training results in a form of regularization on the model - variance is minimized, and the bias introduced acts as a prior to direct the model configuration towards a sample space that is effective for the unsupervised learning generalization optimisations.

2.3.5 Time Series Applications

The AutoEncoder papers reviewed so far in this section derive their results primarily from classification problems, and so do not necessarily account for the problems involved with time series as described in Section 2.3.1. Due to the inherent difficulties with predictions in the financial system, it can sometimes be unclear if the shortcoming in results is due to this system complexity or if the methodologies used are unsuited for the purpose. In light of this it is worth pointing out that Stacked AutoEncoder (SAE) implementations have

been shown to be effective in many time series systems.

Yisheng et al. [120] implemented a deep learning SAE model using the methods described in Section 2.3.3 in order to predict traffic flow at various time intervals (15, 30, 45 and 60 minutes) - a problem not so structurally dissimilar from what will be considered in this paper. They were able to show that the deep SAE was able to offer prediction results which were both objectively good and also persistently outperformed the comparison models used (backpropagation neural network, random walk forecast, support vector machine and a radial basis function neural network).

In a review of unsupervised feature learning and deep learning methods on time series, Langkvist et al. [72] noted that the use of AutoEncoders, either as a technique in themselves, or as an auxiliary technique to models such as convolutional neural networks, were able to offer performance increases in areas such as video analysis, motion capture data and bacteria identification.

2.3.6 Financial Applications

There have of course also been successful applications of stacked AutoEncoders and deep learning models in finance as well. Takeuchi [110] performed some earlier work showing the use of AutoEncoders when applied to a momentum trading strategy. They implemented an RBM pre-trained DBN as per Section 2.3.2, and assessed the networks classification performance for ordinary shares on NYSE, AMEX and Nasdaq. This showed that using a DBN network resulted in significant performance increases compared to the standard momentum strategy.

Zhao et al. [122] used SDAEs and combined them with the bootstrap aggregation ensemble method (bagging) in a study of predicting the crude oil price. They compared the proposed model to a variety of benchmarks, including standard SAE, bagged and standard feedforward networks and Support Vector Regression (SVR) models. The results indicated that the SAE models were more accurate, with the bagged SAE model performing the best, though at a significant increase in computational costs in comparison to standard SAE.

While much of the financial literature has focused on the use of RBM based models, AutoEncoders and SAEs have recently been gaining popularity in performing feature reduction. Troiano et al. [111] specifically investigate the use of different feature reduction models for trend prediction in finance. In line with being primarily interested in the effect of feature reduction techniques, rather than the classification performance itself, only a Support Vector Machine (SVM) model was used to test results. Using various periods from historical S&P 500 data, they were able to show that AE outperformed the RBM model significantly in numerous accuracy measures, and was able to do so at a fraction of the training time.

Bao et al. [8] note that the research has been lacking with regards to whether SAEs should be used for financial prediction models or not. They suggest a novel model which combines Wavelet Transformation, SAEs and a LSTM network. Using data from several financial exchanges (considering a range of developed and undeveloped markets), they assess the models applicability to OHLC prediction. Comparing the model to configurations without the SAE layers, and a RNN model as benchmark, they showed that the inclusion of SAEs resulted in less volatility and greater accuracy, which in turn offered higher profitabilities in a buy-and-hold trading strategy.

More novel AutoEncoder applications have also been attempted, with Hsu [65] suggesting the use of a Recurrent AutoEncoder for multidimensional time series prediction. There is a clear pattern through the literature that the use of AEs and SAEs both by themselves and when used as an assisting technique result in more accurate prediction results and less computationally expensive training.

2.4 Online Learning Algorithms and Gradient Descent

Most classic machine learning algorithms operate under the assumption that, for all intents and purposes, the full dataset has been collected and that the amount of training data for the model is both finite and immediately available. However, as the growth of information grows in an exponential fashion, there are numerous areas where the expected training data for the model will continue to grow. In these cases it would be disadvantageous to go through the full training and validation process again in order to incorporate the newly available data.

Online algorithms are designed to offset these issues by adjusting the batch training technique to rather repetitively draw on single samples from the data on which the models parameters can be adjusted. The benefit is that they are able to quickly process a large number of observations and readjust the model, though the downfall is that they are not always able to optimize the cost function to the same extent as offline batch algorithms [1].

Bottou and Lecun [13] argue that as the size of the dataset grows significantly, online algorithms advantages result in them outperforming offline models, despite any initial drawbacks. Previous research had shown that online algorithms typically perform as fast as batch algorithms during the search phase of parameter optimization, but that final phase convergence tended to fluctuate around the optima due to the noise present in single sample gradients [75, 14]. Bottou and Lecun [13] showed that it is actually more practical to

consider the convergence towards the parameters of the optima, rather than the optima itself (as defined by the cost function) - the difference between the learning speed and optimization speed, respectively.

Online learning methods are thus well suited to financial market modelling using neural networks. They allow effective and efficient incremental updates as more recent (and relevant) data becomes available. Further, the increased learning speed over optima convergence makes them a fitting choice when data is non-IID and constantly changing.

2.5 Gradient Learning Improvements

2.5.1 Gradient Adjustments and Regularization

One of the earlier improvements to convergence rates was the Momentum algorithm, as developed by Tseng [112]. As noted, stochastic descent often introduces significant oscillation around an optima, which slows down convergence. Momentum reduces this by decreasing movement in directions of high curvature, and increasing movement towards directions consistent with previous gradients (this is achieved through combining gradient movements in opposite directions).

There have been several attempts to introduce effective regularization into the SGD process. Bartlett et al. [9] presented Adaptive Online Gradient Descent, which implements an adaptive step size through a λ penalty on the learning rate, which was shown to be nearly optimal in a strong sense. Langford et al. demonstrated a variation named Truncated Gradient, which introduced an enforced weight sparsity parameter. The weight sparsity is able to achieve equitable effects to L_1 regularization (similar to Lasso Regression). They were able to show that implementation performed effective feature reduction, while having little effect on performance [71]. Other approaches, such as AdaGrad, aim to improve the robustness of gradient training by adjusting the updates to parameters according to frequency - e.g. larger updates to infrequent parameters, and smaller updates to frequent parameters [42, 121].

2.5.2 Dropout

One of the instrumental improvements in further achievements, was to modify the backpropagation algorithm using the “dropout” technique, as suggested by Hinton et al. [62]. When training of large networks is attempted on small datasets, it often results in overfitting and poor results on out of sample data. Dropout helps resolve this by randomly excluding a certain percentage (usually 0.5) of feature detectors on each training iteration. The effect is to stop co-adaptations of feature detectors, and by rather training each neuron in a wide variety of internal configurations, it forces them to take on more use-

fully generalizable characteristics (it was noted that this is not a dissimilar technique to ensemble methods, or bagging). The authors were able to show that the method resulting in significant improvements on benchmark data sets (e.g. MNIST, CIFAR-10), and that a simpler model using dropout was able to achieve near comparable performance for the ImageNet dataset.

Goodfellow et al. [52] used the dropout technique as the basis for their “maxout” activation function technique, which leverages and improves on dropout’s fast optimisation and accuracy through averaging characteristics. The maxout model was shown to achieve state of the art performance on benchmark datasets, as well as have a strong theoretical grounding. Further work was done by Wang and Manning [114], which improved on the dropout (and potentially maxout) techniques through fast sampling, resulting in an order of magnitude speed-up in training.

2.5.3 Learning Rate Schedules

Several more recent approaches look towards learning rate adjustment schedules rather than strategies to alter the weight update, as with momentum and the like. A constant learning rate often suffers from one of two problems - if set too high, it can cause divergent behaviour in the loss function, though if set too low, it can result in slow learning or an inability to escape saddle points effectively. Finding an optimal learning rate requires some degree of testing, though even then a singular value may fail to achieve the same degree of efficacy as a range of values explored throughout the solution space.

Learning rate scheduling has been proposed as a solution to this problem. These methods implement an repetitive cycle for the learning rate, such that it is set through a range of values between a minima and maxima, being adjusted slightly with each new epoch. Smith [108] suggests using the Cyclical Learning Rate (CLR) to achieve this, and points out that part of the benefit in learning rate schedules is the ability to jump out of sharp optima points which may not generalise well to unseen data. It’s shown that this implementation can have significant performance effects in reaching either the same optima in fewer epochs or a better overall optima, including when used in conjunction with other learning optimizations noted in Section 2.5. These results were shown against standard datasets such as CIFAR-10, CIFAR-100 and ImageNet [108].

Similarly, Loshchilov and Hutter [82], expand on this and present Stochastic Gradient Descent with Warm Restarts. The approach is implemented similarly, but rather follows an asymmetric cycle from a maximum to a minimum, and then starting once again at the maximum once the set number of epochs has passed. They too note the increased performance on CIFAR-10 and CIFAR-100 datasets in reaching optima far quicker, as well as noting the efficacy of the learning rate schedule even without implementing the restarts.

2.6 Backtesting and Model Validation

Financial academic literature is currently facing a problem in terms of validation and verification of results. Trading strategy profitability has typically been proven using historical simulations, or “backtests”. However, the recent advances in technology and algorithms available to construct these strategies have resulted in researchers being able to test a number of variations that is factors above what used to be possible. This has made it increasingly difficult to control for spurious results. The problem is so extensive that some meta-research papers suggest that most published research findings are false [66].

The standard way of implementing backtests is to split the data into two portions: an In Sample (IS) portion which is used to train the model, and an Out of Sample (OOS) portion which is used to test the model and validate results. If millions of different model configurations are tested, then it is only a matter of time before a false positive result occurs which shows high performance both IS and OOS (i.e. overfitting) [7, 85].

The nature of financial data makes it difficult to resolve these issues effectively. There is a low signal-to-noise ratio in a dynamic and adaptive system, and only one true data sequence. Traditional hypothesis testing frameworks (e.g. Neyman-Pearson) are not sufficient in this context, and more sophisticated techniques are necessary.

Overfitting is not a novel issue. This has been tackled in various literature areas, including machine learning. However, in that context, the frameworks are often not suited to the buy/sell with random frequency structure of investment strategies. They also do not account for overfitting outside of the output parameters, or take into consideration the number of trials attempted.

One of the common approaches to avoid backtest overfitting is the hold-out strategy, where a certain portion of the dataset is reserved for testing true OOS performance. Numerous problems have been pointed out with this approach, including that the data is often used regardless, or that awareness of the movements in the data may, consciously or otherwise, influence strategy and test design by the researchers [102]. For small samples, a hold-out strategy may be too short to be conclusive [115], and even for large samples it results in the most recent data (which is arguably the most pertinent) not being used for model selection [56, 7].

There have been some suggestions to resolve the problem that is occurring in the literature as a result of this - some work suggesting new frameworks, which this section will cover, and others which focus on the review process or how data and replication procedures are made available [78]. The points made with regard to the review and data processes are important, but do not aid

with more effective model training for the researcher up front and so are not covered here.

2.6.1 Sharpe Ratio Assessment Methodologies

The Sharpe Ratio (SR), as introduced by Sharpe [105] in earlier literature, has become the favoured choice as a widely usable investment portfolio performance measure [4]. The measure, indicating the amount of return relative to risk that a portfolio offers, makes for a sensible choice in that any portfolio which maximizes this can be shown to lie on Markowitz's efficient frontier. In line with its popularity, there has been extensive research around its distributional properties. Lo [77] shows that the estimated SR of a portfolio's returns has been shown to follow a normal distribution, regardless of whether the underlying returns are themselves normally distributed or not. Further work by Christie [16] and Opdyke [92] derived a limiting distribution, assuming only stationary and ergodic returns.

The Sharpe Ratio, and indeed most standard performance measures, are based on the assumption that the returns used are the result of a single trial. In consideration of the issues laid out above, it then becomes a misrepresentative performance measure. Bailey and Lopez de Prado [4] expanded on the work by Christie [16] and Opdyke [92] and developed the Probabilistic Sharpe Ratio (PSR) in order to estimate the likelihood that an observed best estimated \widehat{SR} exceeds a provided benchmark SR^* , which might be expected from variance in the trials.

It is worth emphasising the distinction in investment strategies between a Family Wise Error Rate (FWER), which is the probability that one or more false positives occur, and a False Discovery Rate (FDR), which is the ratio of false positives to predicted positives. Where an FDR based approach may be applicable to a manufacturing process where there is an acceptable defect rate, investment strategy generations will tend to rely on the single best approach produced. Necessarily then, the FWER must be controlled for. Further work by Bailey and Lopez de Prado [5] developed the False Strategy Theorem (FST) with this in mind, allowing the assessment of whether a presented strategy is a false positive or not.

This allowed the development of the Deflated Sharpe Ratio (DSR) which calculates the likelihood that the true SR is positive under consideration of numerous trials being tested [5]. The DSR can be estimated using the PSR methodology as $\widehat{PSR}[SR^*]$ where the benchmark SR^* (SR) is no longer user defined, but rather calculated based on the False Strategy Theorem. That said, the calculation of SR^* requires both the variance of trial SR values the number of independent trials, which are usually unknown on accounts of being meta-research variables which cannot be estimated from the selected strategy. It is not typical for researchers to track and report on these variables, and even

if they were to, the trials would not typically be independent, thus further complicating the practical realities around calculating SR^* . Lopez de Prado and Lewis [81] provide critical work to this end with the Optimal Number Clusters (ONC) algorithm. They present a modified K-means methodology of clustering strategies and trial results, such that the dependent returns are categorised into subgroups with high intra-cluster correlations and low inter-cluster correlations. This clustering allows an estimation then of both the variance and number of trials, which in turn allows the DSR to be calculated. With this as a confidence level, one can accept or reject the notion that the observed \widehat{SR} is positive.

The approach developed by Lopez de Prado and Lewis [81] (of combining PSR, FST, DSR and ONC) relies on several principles which may differ from prior methods suggested (such as those by Harvey and Liu [55]). The first is that returns do not always follow a normal distribution, which is supported by empirical evidence, and so their method rather takes into account the skewness and kurtosis of observed returns. The second is that Extreme Value Theory is a more appropriate technique than something such as Sidak's correction, due to the incorporation of return variance when a non-normal distribution is present. The third is that they do not assume a constant average correlation across trials, noting that there is often a hierarchical structure amongst returns where there may be highly correlated clusters of strategies. Failing to take this into account would then bias the expected number of independent trials and so the false positive probability.

2.6.2 Generalised Assessment Methodologies

There has been work by several authors to try and lay out alternative techniques to try and avert backtest overfitting. The Model Confidence Set (MCS), as developed by Hansen et al. [54], starts with a collection of models or configurations, and removes models iteratively according to a defined loss function. The confidence set is defined by the remaining models once a non-rejection takes place within the process, and these models are considered to be statistically similar within a certain confidence range. MCS is thus able to facilitate equitable model selection. However, Aparicio and Lopez de Prado [2], showed that while MCS is a potential strategy, in practice it is ineffective due to the inordinate requirement of signal-to-noise necessary to identify true superior models, as well as a lack of penalization over the number of trials attempted.

Bailey et al. [7] have developed a more robust approach to backtesting and how overfitting during strategy selection might be avoided, called Combinatorially Symmetric Cross-Validation (CSCV). Their research defines backtest overfitting as having occurred when the strategy selection which maximizes IS performance systematically underperforms median OOS in comparison to

the remaining configurations. They use this definition to develop a framework which measures the probability of such an event occurring, where the sample space is the combined pairs of IS and OOS performance of the available configurations. The Probability of Backtest Overfitting (PBO) is then established as the likelihood of a configuration underperforming the median IS while outperforming IS.

The CSCV methodology provides several important benefits over traditional testing frameworks, including the usual K-fold cross validation used in machine learning. By recombining the slices of available data, both the training and testing sets are of equal size, which is particularly advantageous when comparing financial statistics such as the Sharpe Ratio, which are susceptible to sample size. Additionally, the symmetry of the set combinations in CSCV ensure that performance degradation is only as a result of overfitting, and not arbitrary differences in data sets. It is pointed out that while CSCV and PBO should be used to evaluate the quality of a strategy, they should not be the function on which strategy selection relies, which in itself would result in overfitting. In this sense, the methodology helps assess overfitting, but not necessarily avoid it. Another of the noted limitations of the framework is that a high PBO indicates overfitting within the group of N strategies, which is not necessarily indicative that none of the strategies are skilful - it could be that all of them are.

2.6.3 Test Data Length

When using SR estimations, where it is possible that where the true SR mean is zero, we may still (with enough configurations attempted) find an SR measurement which optimises IS performance. This is shown by Bailey et al. [6], who propose the non-null probability of selecting an IS strategy with null expected performance OOS. Notably, typical methods such as hold-out once again fail, as the number of configurations attempted are not recorded. They add a further derivation, which is the Minimum Backtest Length (MinBTL), a statistic which highlights the relationships between: selecting a strategy with a higher IS SR than expected OOS, the number of strategies tested, and the number of years tested. The equation shows that as the number of strategies tested increases, the minimum back test length must also increase in order to contain the likelihood of overfitting to IS SR.

As shown extensively throughout ML literature, increased model complexity and number of parameters is one of the primary causes of overfitting. In context of the MinBTL formula, model complexity affects the number of configurations that are available and which may be tested, which in turn will increase likelihood of overfitting. A lack of consideration, or reporting, of the number of trials makes the potential for overfitting difficult to assess.

Bailey et al. [6] expanded on this view with assessing the impact of presenting overfit models as correct. They were able to show that in lieu of any compensation effects (i.e. a series following a Gaussian random walk), there is no reason for overfitting to result in negative performance. However, where compensation effects apply (e.g. economic/investment cycles, bubble bursts, major corrections etc.), then the inclusion of memory in a strategy is likely to be detrimental to OOS performance if overfitting isn't controlled for.

3 Data Processing and Generation

3.1 Data Processing

The datasets used go through several transformations throughout the training and prediction process:

1. The raw data is log differenced and aggregated to rolling windows,
2. The transformed data is split into Training and Prediction subsets,
3. The predicted outputs have the scaling and log differencing reversed in order to reconstruct the actual price points.

3.1.1 Log Difference Transformation and Aggregation

All datasets are transformed into log feature fluctuation values, and are then aggregated to include fluctuations over rolling window periods. The log feature fluctuation for measured prices \tilde{p} at timepoint t is calculated using (1):

$$\Delta p_i = \ln(\tilde{p}_i) - \ln(\tilde{p}_{i-1}) \quad (1)$$

This log feature fluctuation, is processed for each asset's closing price and for each time point (from the previous time point). The log fluctuations have the benefit of taking compound effects into account in a systematic way and are symmetric in terms of gains and losses. Further, the log transformation provides an ergodic time series which is indicative what will happen to \tilde{p} over time, and has been shown to be the correct optimization choice [90].

The datasets are then expanded with the rolling window summations both in the past, for input, and in the future, for predicted output. A typical example would be past data aggregation windows of 1, 5 and 20, and a future prediction point of 5. These are calculated as summations of the log differences, such that for d days:

$$\bar{p}_{(d,t)} = \sum_{i=t-d}^t \Delta p_i \quad (2)$$

$$p_{(t,d)}^+ = \sum_{i=t+1}^{t+d} \Delta p_i \quad (3)$$

Only data points with a full set of features are used for training and prediction later on in the framework.

3.1.2 Data Scaling

Once the log difference data has been aggregated using equations 2 and 3, the datasets are either standardized or normalized to allow for better learning. Typical implementations of these methods are detailed below:

3.1.2.1 Standardization

$$\mathbf{z}_i = \frac{(\mathbf{p}_i - \bar{\mathbf{p}})}{\sigma_p} \quad (4)$$

3.1.2.2 Normalization

$$\mathbf{n}_i = \frac{\mathbf{p}_i - \min_{\mathbf{p}}}{\max_{\mathbf{p}} - \min_{\mathbf{p}}} \quad (5)$$

The framework presented here only uses the suggested variations, dubbed “Limited Standardization” and “Limited Normalization”, which are used when the data is split up into the Training and Prediction sets. In this case all the data needs to be scaled, but the variance or range should not be travelling from the Prediction set to the Training set through the use of aggregated measures such as $\bar{\mathbf{p}}$. Thus, if the data is split at point t out of n data points, the scaling would be implemented as follows:

3.1.2.3 Limited Standardization

$$\mathbf{q}_{(i,t)} = \frac{(\mathbf{p}_i - \bar{\mathbf{p}}_{1:t})}{\sigma_{p_{1:t}}}, \forall i \in (1, n) \quad (6)$$

3.1.2.4 Limited Normalization

$$\mathbf{v}_{(i,t)} = \frac{\mathbf{p}_i - \min_{\mathbf{p}_{1,\dots,p_t}}}{\max_{\mathbf{p}_{1,\dots,p_t}} - \min_{\mathbf{p}_{1,\dots,p_t}}}, \forall i \in (1, n) \quad (7)$$

This log-differenced, aggregated and scaled data is then used as the input for the neural network models.

3.1.3 Reverse Data Scaling

The predicted data points are transformed back into actual prices for returns analysis. The first step is to reverse the scaling that is done in Section 3.1.2 in order to retrieve the log difference fluctuations. The reverse scaling equations are for a dataset of n observations, which has been split at point t .

3.1.3.1 Reverse Standardization

$$\mathbf{z}_i^* = \mathbf{z}_i \cdot \sigma_p + \bar{\mathbf{p}} \quad (8)$$

3.1.3.2 Reverse Normalization

$$\mathbf{n}_i^* = \mathbf{n}_i \cdot \left(\max_{\mathbf{p}} - \min_{\mathbf{p}} \right) + \min_{\mathbf{p}} \quad (9)$$

3.1.3.3 Reverse Limited Standardization

$$\mathbf{q}_i^* = \mathbf{q}_i \cdot \sigma_{p_{1:t}} + \bar{\mathbf{p}}_{1:t}, \forall i \in (1, n) \quad (10)$$

3.1.3.4 Reverse Limited Normalization

$$\mathbf{v}_i^* = \mathbf{v}_i \cdot \left(\max_{p_1, \dots, p_t} - \min_{p_1, \dots, p_t} \right) + \min_{p_1, \dots, p_t}, \forall i \in (1, n) \quad (11)$$

3.1.4 Price Reconstruction

The predicted log fluctuations produced in Section 3.1.3 are used to reconstruct the predicted prices.

$$\mathbf{p}^r_i = \tilde{\mathbf{p}}_{i-d} \cdot e^{\hat{p}_i} \quad (12)$$

where:

- $\tilde{\mathbf{p}}$ = original asset prices,
- \hat{p} = predicted log fluctuation,
- i = price timepoint, and
- d = price fluctuation prediction horizon.

These reconstructed prices are then used to assess model returns later in the Money Management Strategy (Section 4.6).

3.1.5 Decorrelation

The data processing does not incorporate any sort of decorrelation processes or data “whitening” transformations, thus keeping all correlation relationships between asset price fluctuations intact.

3.2 Synthetic Data Generation

Synthetic data generation is implemented using Geometric Brownian Motion (GBM) as described in Algorithm 1, which allows the stocks simulations to be implemented with a drift (μ) and variance (σ) for each stock. The GBM simulation has the benefit of generating prices in a random walk, such that future movements are independent of past prices and so suitable for emulating an efficient financial market. The implications of using such data are discussed more fully in Section 8.5. Each dataset was generated with a random seed

(using a Mersenne Twister pseudorandom number generator).

Algorithm 1: Geometric Brownian Motion Simulation

```

Input:  $\sigma, \mu, \tilde{p}_0, n$ 
 $t = \frac{1}{n};$ 
 $\tilde{\mathbf{p}}^s = [\tilde{p}_0];$ 
foreach  $i$  in  $1:n$  do
     $z = \text{random}() \sim \mathcal{N}(0, 1);$ 
     $\tilde{p}_i^s = \tilde{p}_{i-1}^s \cdot e^{(\mu - \frac{\sigma^2}{2})t + \sigma\sqrt{t}z};$ 
     $\tilde{\mathbf{p}}^s = [\tilde{\mathbf{p}}^s, \tilde{p}_i^s];$ 
end
Result:  $\tilde{\mathbf{p}}^s$ 
```

3.2.1 GBM Data Distributions

An important aspect of GBM generated data is that the price changes follow a Log-Normal distribution. If this data is then processed as per the steps above in Section 3.1, then after taking the log differenced values using equation (1), the values will follow a Normal distribution. Once scaled using standardization or normalization, these values will become centred and possibly be following a standard normal distribution. However, due to the effect of the limited scaling techniques used, only the Training dataset will be consistent in following this distribution, with the Prediction dataset having an increasing number of outliers as the timepoint moves further away from the Training set demarcations. These issues have notable impacts throughout the results, and are discussed more in Section 8.

3.3 Price Considerations

The “Actual10” dataset, as described in Section 7.1.1, is a price relative dataset. It should be noted that this does not account for inflation, which arguably mask the effective training of SAE and predictive networks more difficult. However, not being able to fully account for inflation would be an issue in any forward looking predictive model, and so it seems sensible to keep it this way in our current dataset. It is also not expected to have a material impact on short term predictions, though it does make comparisons across time periods (i.e. IS and OOS) more difficult. Additionally, the dataset is price relative starting at 1.0, and so only price changes from the start onwards are accounted for and impact P&L, rather than the initial starting prices which might have then caused some imbalances. This does not have a large impact on the process, but does mean the P&L figures quotes in the results section are of unit measures, rather than any particular currency.

4 Models and Algorithms

4.1 Process Overview

The implementation focuses on bringing together several ideas: data reduction, deep learning with pre-training/weight initialization, online learning and backtest overfitting validation for the purposes of stock price prediction. The process implementation is discussed fully in Section 5.1, but can be summarised as the following:

1. The dataset is split into 2 subsets: the Training portion, and the Prediction portion.
2. The Training set is used to train the SAE and predictive FFN using the SGD algorithm. These networks are constructed with pre-training or weight initialization techniques.
3. Once the SGD training is complete for the predictive network, the same Training dataset is used to generate the IS predictions to be used for the CSCV process.
4. The Prediction set of data is used to continue training the network in an online manner using OGD.
5. The predictions made during steps 3 and 4 are descaled and prices are reconstructed.
6. These reconstructed price predictions are used by the MMS to calculate returns and P&L.
7. The returns and P&L calculated by the MMS are used by the CSCV process, to estimate the PBO or DSR figures.

The rest of this section will detail the algorithms used to train the relevant FFN, RBM and SAE networks, as well as the trading strategy and CSCV & PBO testing procedures.

4.2 Feedforward Neural Networks

Constructing Feedforward Neural Networks (FFN) in the form of multilayer perceptrons is a well established network technique, providing effective non-linear representations for both shallow and deep structures [101]. Specifically, a FFN is made up of several non-cyclical layers: the first and last are the input and output layers, respectively, and any inbetween are referred to as 'hidden' layers. Each layer is made up of nodes which are fully connected to the nodes in the previous and following layers, but does not have connections to nodes within the layer - information only travels forward. Each node has an activation function, which acts on the weighted input from the previous layers' nodes.

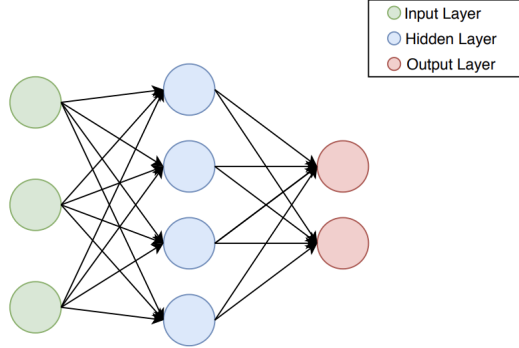


Figure 2: An example diagram of a Feedforward Neural Network with 1 hidden layer

4.2.1 Notation and Network Representation

For the purposes of this section, the following notation will be used:

- 1 A network N will be constructed with L layers, each with e nodes
- 2 The weights from the j^{th} node in the ℓ^{th} layer to the k^{th} node in the $(\ell - 1)^{th}$ layer are represented by \mathbf{w}_{jk}^ℓ
- 3 The bias for the j^{th} node in layer ℓ is represented by \mathbf{w}_{0j}^ℓ
- 4 The output for the j^{th} node in layer ℓ is

$$\mathbf{a}_j^\ell = \theta(\mathbf{z}_j), \quad (13)$$

for an activation function θ (with inverse θ') and weighted input z .

- 5 The weighted input for the j^{th} neuron in layer ℓ is

$$\mathbf{z}_j^\ell = \sum_{i=1}^{e^{\ell-1}} \mathbf{a}_i^{\ell-1} \mathbf{w}_{ij} + \mathbf{w}_{0j}^\ell \quad (14)$$

These definitions allow an input into the network to be propagated through it, having the original values processed through the weights and activations functions, and have an output in the form of the network's last layer.

4.2.2 Activation Functions

As noted in Section 2.2.2, there are 3 primary characteristics of concern for activation functions: non-linearity, continuous differentiability and monotonicity. While many different functions have been suggested and used, several of the more popular were implemented here.

4.2.2.1 Sigmoid

The sigmoid, or logistic, function is one of the most popular and widely used activation functions historically, and is defined as

$$\theta(x) = \frac{1}{1 + e^{-x}} \quad (15)$$

$$\theta'(x) = \theta(x)(1 - \theta(x)) \quad (16)$$

The Sigmoid function is in the range [0,1], making it a suitable choice for problems requiring a probabilistic output. The slope of the function curve is both a boon and a drawback: it allows for fast learning initially, but results in learning slowdown later (often causing what is referred to as node “saturation”). The exponent calculation is also computationally expensive, relatively speaking.

4.2.2.2 ReLU

The Rectified Linear Unit (ReLU) is a newer activation function which has been shown to be effective in deep learning networks. It is defined as

$$\theta(x) = \max(0, x) \quad (17)$$

$$(18)$$

$$\theta'(x) = \begin{cases} 1, & \text{if } x \geq 0 \\ 0, & \text{otherwise} \end{cases}$$

The function has the benefits of quick learning which doesn't saturate, as well as being computationally cheap. The downside is that the non-gradient for the negative range of the function can result in 'dead' nodes, which stop updating with the learning process.

4.2.2.3 Leaky ReLU

The Leaky ReLU resolves the dying ReLU problem by adding a small gradient to the negative range of the function. This results in a slow learning being applied to “dead” ReLU’s, which may in turn result in them being used again if necessary. The choice of 0.01 as the negative range gradient in equations (19) and (20) has been shown to be generally effective [84], though further work might investigate different parameter values for this.

$$(19)$$

$$\theta(x) = \begin{cases} x, & \text{if } x \geq 0 \\ 0.01x, & \text{otherwise} \end{cases}$$

(20)

$$\theta'(x) = \begin{cases} 1, & \text{if } x \geq 0 \\ 0.01, & \text{otherwise} \end{cases}$$

4.2.2.4 Linear Activation

Linear activations don't transform the input, and have a constant gradient, which can be useful for key layers where no loss in error signal is desired, such as the output or encoding layers.

$$\theta(x) = x \quad (21)$$

$$\theta'(x) = 1 \quad (22)$$

4.2.3 Backpropagation

The backpropagation algorithm, as discussed in Section 2.2.1, has allowed for effective training of FNNs for given data. The algorithm relies on incremental improvements of the model, as defined by decreasing the cost function. A common choice for cost (C) is Mean Squared Errors (MSE):

$$C = \frac{1}{2} \|\mathbf{y} - \mathbf{a}^L\|^2. \quad (23)$$

The conceptual steps for the backpropagation (fully detailed in Algorithm 2) are:

1. **Forward Pass:** The samples are propagated through the network, in order to generate the output \mathbf{a}^L .

Vectorization is typically used to calculate the results for multiple samples at once, though conceptually each sample is used as input for the first layer, and subsequent layers use the weighted output from the previous layer passed through the activation function as input.

Equation 14 is used to calculate the weighted output and the equations defined in Section 4.2.2 are used for the activation functions.

- 2. Calculate Cost:** The cost between the training output \mathbf{y} and the model output \mathbf{a}^L is calculated.

Using a cost function such as MSE (equation (23)), the rate of change for the error in the output layer by the rate of change in the activation function in the last layer, L , is calculated. This rate of change for the error for the j^{th} node, δ_j , is expressed as:

$$\delta_j^L = \frac{\partial C}{\partial \mathbf{a}_j^L} \theta'(\mathbf{z}_j^L). \quad (24)$$

The vectorized version of this is often used, and expressed in equation (25). $\nabla_a C$ is a vector of components which are the partial derivatives, such that they represent the rate of change of cost C relative to the activation functions' outputs.

$$\delta^L = \nabla_a C \otimes \theta'(\mathbf{z}^L), \quad (25)$$

where \otimes is the Hadamard (or element-wise) matrix product.

If using quadratic cost, as per equation (23), then the term $\frac{\partial C}{\partial a_j^L}$ can be reduced to $(a^L - y)$. The equation for the output layer error rate of change is then:

$$\delta^L = (\mathbf{a}^L - \mathbf{y}) \otimes \theta'(\mathbf{z}^L). \quad (26)$$

3. Backwards Pass:

- (a) **Calculate Errors For Previous Layers:** The activation values are propagated back through the network to calculate the delta values at each layer.

This uses the same rationale as equation (24), but rather uses $(w^{\ell+1})^T$ by the next layers error in order to get an indication of how the error rate and how it moves backwards through the network.

$$\delta^\ell = ((\mathbf{w}^{\ell+1})^T \delta^{\ell+1}) \otimes \theta'(\mathbf{z}^\ell). \quad (27)$$

- (b) **Adjust Network Weights:** Network weights are adjusted in proportion to the error observed and chosen learning rate.

Each weights output error and input activation are multiplied to find the weights gradient, which is then reduced by a factor of the learning rate η . This adjustment value is subtracted from the current network weights:

$$\mathbf{w}^\ell \rightarrow \mathbf{w}^\ell - \eta \delta^\ell (\mathbf{a}^{\ell-1})^T, \quad (28)$$

where η , the learning rate, is a configured parameter.

Choices regarding the learning rates are discussed in Section 4.2.6 and the full algorithm is presented below in Algorithm 2.

Algorithm 2: Backpropagation

Input: Neural Network N , with randomly initialized weights \mathbf{w} , L layers, and activation functions θ and learning rate η
Data: Testing set with inputs \mathbf{x} , and outputs \mathbf{y}

```

repeat
    Select a sample  $x_s$  from  $x$ ;
    // Perform the Forward Pass, to calculate the network output,  $y_s$ ,
    // for input sample  $x_s$ 
     $a_0 = x_s$ ;
    foreach  $\ell$  in  $1:L$  do
        foreach  $j$  in  $1:e^\ell$  do
             $\mathbf{z}_j^\ell = \sum_{i=1}^{e^{\ell-1}} \mathbf{a}_i^{\ell-1} \mathbf{w}_{ij} + \mathbf{w}_{0j}$ ;
             $\mathbf{a}_j^\ell = \theta(\mathbf{z}_j^\ell)$ ;
        end
    end
    // Calculate the error term (aka cost), as
     $\delta^L = (\mathbf{a}^L - \mathbf{y}) \otimes \theta'(\mathbf{z}^L)$ ;

    // Perform the Backward Pass, to propagate the errors back and
    // update the network accordingly
    foreach  $\ell$  in  $(L-1):1$  do
        // Calculate the delta values
         $\delta^\ell = ((\mathbf{w}^{\ell+1})^T \delta^{\ell+1}) \otimes \theta'(\mathbf{z}^\ell)$ ;
        // Update the weights
         $\mathbf{w}^\ell \rightarrow \mathbf{w}^\ell - \eta \delta^\ell (\mathbf{a}^{\ell-1})^T$ ;
    end
until no new samples can be drawn from  $x$ ;
Result: Updated Network  $N$ 

```

4.2.4 Gradient Descent Algorithms

The backpropagation algorithm is defined at a single sample level, and the learning from a dataset is usually repeated for a number of “epochs”. As noted though, implementation is often implemented using a vectorized version of the algorithm which either samples the entire dataset at once (batch), or a subset of samples (mini-batch). The latter is the Stochastic Gradient Descent (SGD), as discussed in Section 2.4, which has been shown to increase the speed and stability at which the backpropagation algorithm can converge to a minima in terms of cost. The algorithm runs backpropagation over the entire dataset for the number of epochs, and updates the network incrementally through the epoch. The stopping condition for the algorithm is usually defined as either

a particular number of epochs being reached, or cost no longer decreasing for some number of epochs (i.e. a minima has been reached).

The changes to the initial backprop algorithm, detailed in Algorithm 2, are relatively minor:

- 1 Selection is now performed such that at each epoch m , s new samples are from x , forming the subset x_s .
- 2 The weight update is now performed such that it represents an aggregate update according the m samples that were selected:

$$\mathbf{w}^\ell \rightarrow \mathbf{w}^\ell - \frac{\eta}{m} \sum_x \delta^{x,\ell} (\mathbf{a}^{x,\ell-1})^T, \quad (29)$$

where

1. w^ℓ is the ℓ^{th} layer's weights,
2. η is the configured learning rate parameters,
3. m is the size of the mini-batch,
4. δ is the rate of change in the error (calculated using equation (27)), and
5. a is the output of the activation function for the weighted input (calculated using equation (13)).

Online Gradient Descent Where SGD is appropriate and effective for scenarios where the entire dataset is available, Online Gradient Descent (OGD) is applicable for when the model is learning in an online fashion. In this case, the backpropagation is run as defined above in Algorithm 2 but with no repetition (i.e. only 1 epoch).

4.2.5 Regularization

Regularization is a commonly used technique in machine learning used to reduce a model's capacity to overfit to the data, and in so doing reduces the variance in the model results. One of the typical methods, “L2” (or “weight decay”), is implemented by adding an extra term to the cost function which is itself a function of the weights in the model. This extra term forces the learning process to favour smaller weights, and only allows large weights to occur if they are able to offer an appropriate increase in performance. The modified cost function is calculated as:

$$\mathbf{C} = \frac{1}{2n} \sum_x \|\mathbf{y} - \mathbf{a}^L\|^2 + \frac{\lambda}{2n} \sum_w \mathbf{w}^2, \quad (30)$$

where

1. n is the dataset sample size,
2. y is the input data,

3. a is the output of the activation function in the L^{th} layer (calculated using equation (13)),
4. λ is the configured regularization rate, and
5. w is a layer's weights.

The additional term is scaled by the configurable regularization parameter, λ , which if small approximates the original cost function or if large will increase the degree of regularization used.

In order to implement this in backpropagation, the weight update rule is changed to the following (while biases remain the same):

$$\mathbf{w} \rightarrow \mathbf{w} - \eta \frac{\partial \mathbf{C}_0}{\partial \mathbf{w}} - \frac{\eta \lambda}{n} \mathbf{w} \quad (31)$$

For SGD, this can be simplified to the following:

$$\mathbf{w} \rightarrow \left(1 - \frac{\eta \lambda}{n}\right) \mathbf{w} - \frac{\eta}{m} \sum_x \frac{\partial \mathbf{C}_x}{\partial \mathbf{w}} \quad (32)$$

4.2.6 Learning Rate Schedule

Learning rates schedules are implemented to allow for a more dynamic exploration of the possible solution space, and allow fine tuning around an optima. With a constant learning rate implementation, one has to choose between a larger learning rate which allows faster progress but less optimisation, or a smaller learning rate which learns slower but is more effective at optimising (by avoiding the learning algorithm from bouncing around a minima valley). Learning rate schedules aim to get the best of both scenarios by cycling through a minimum and maximum range across epochs.

The learning rate schedule is specified to cycle through from the minimum value to the maximum value every T epochs, from η_{\min} to η_{\max} . Thus for the current epoch i , the learning rate is calculated as:

$$\eta_i = \eta_{\min} + \frac{1}{2} (\eta_{\max} - \eta_{\min}) \left(1 + \cos\left(\frac{i}{T}\pi\right)\right). \quad (33)$$

This is the Cyclical Learning Rates approach, though using sinusoidal form rather than linear [108]. For a minimum learning rate of 0.1, a maximum of 1.0 and an epoch cycle of 100, it will produce learning rates as displayed in Figure 3 below.

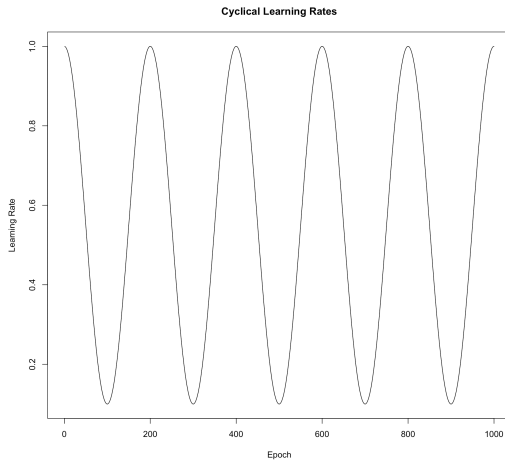


Figure 3: Learning rates calculated over 1000 epochs with $\eta_{\min} = 0.1$ to $\eta_{\max} = 1.0$ and $i = 100$

4.2.7 Dropout

Input layer dropout has been implemented in order to perform regularization on the data features. The methodology used will set a percentage of the features for each sample to 0 during the SGD training process. While the percentage stays the same throughout the testing process, the features selected for each sample are reselected every time it is used (i.e. for subsequent epochs). Conceptually, the dropout as applied to the input layer may result in the network learning relations between assets and possible patterns that would improve predictive efficacy.

4.3 Restricted Boltzmann Machines

Restricted Boltzmann machines (RBM) are generative networks which can be trained to learn probability distributions over a dataset. They are structurally different from a FFN in that they have a recurrent weight structure and stochastic unit determination. Specifically, a typical RBM has one visible layer (input/output), and one hidden layer, and the values in the hidden layer will take on a binary value with a probabilistic likelihood.

Thus, the input and output have the same structure, and the processing from the hidden layer creates the generative process learned by the RBM. The hidden units correspond to feature detection of the visible unit data structures, and the learning process of the network results in effective parameter estimation.

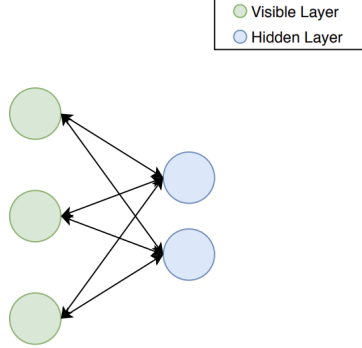


Figure 4: An example diagram of a restricted Boltzmann machine network

RBM input processing goes through the following steps:

1. An input sample, \mathbf{y} , is processed from the visible layer to the hidden layer using typical feedforward functions.
2. Each node in the hidden layer takes on a value of 1 with a probability of its activation function output, or else is equal to 0.
3. The visible layer nodes are reconstructed to provide $\hat{\mathbf{y}}$, using the hidden layer values as the input.

4.3.1 RBM Stochastic Descent

Hinton [58] shows that the joint configuration (\mathbf{v}, \mathbf{h}) of the visible and hidden units has an energy given by :

$$E(\mathbf{v}, \mathbf{h}) = - \sum_{i \in \text{visible}} \mathbf{a}_i \mathbf{v}_i - \sum_{j \in \text{hidden}} \mathbf{b}_j \mathbf{h}_j - \sum_{i,j} \mathbf{v}_i \mathbf{h}_j \mathbf{w}_{ij} \quad (34)$$

, where

1. \mathbf{v} and \mathbf{h} are the binary state vectors of the visible and hidden units respectively,
2. \mathbf{a} and \mathbf{b} are the bias value vectors for the visible and hidden units respectively, and
3. \mathbf{w} is the weights vector for the 2 visible and hidden layers.

It can be shown, that network weights can be adjusted to change the probabilities assigned to a particular training sample . The derivations of equation (34) show that performing a stochastic descent for the log probability of the data can be implemented through the following weight adjustment:

$$\Delta \mathbf{w}_{ij} = \eta (\langle \mathbf{v}_i \mathbf{h}_j \rangle_{\text{data}} - \langle \mathbf{v}_i \mathbf{h}_j \rangle_{\text{model}}) \quad (35)$$

The angular brackets here indicate expectations under the distribution specified by the following subscript. Due to the probabilistic nature of RBMs, the [0,1] ranged Sigmoid activation function is typically used. Thus, for hidden nodes and a data sample v , it is easy to get unbiased sampling of $\langle v_i h_j \rangle_{data}$

$$P(\mathbf{h}_j = 1) = \sigma(\mathbf{w}_{0j} + \sum_{i=1} \mathbf{v}_i \mathbf{w}_{ij}) \quad (36)$$

Similarly, the visible states (or reconstruction), can then be calculated as

$$P(\mathbf{v}_i = 1) = \sigma(\mathbf{w}_{0i} + \sum_{j=1} \mathbf{h}_j \mathbf{w}_{ij}) \quad (37)$$

Getting an unbiased sample of $\langle v_i h_j \rangle$ proves more problematic, and so the model reconstructions via Gibbs sampling are used instead (this is expanded on below), resulting in the weight updates of

$$\Delta \mathbf{w}_{ij} = \eta (\langle \mathbf{v}_i \mathbf{h}_j \rangle_{data} - \langle \mathbf{v}_i \mathbf{h}_j \rangle_{reconstruction}) \quad (38)$$

While it's important for the hidden units to take on a binary value (and so avoid communicating real values rather than learning structure), the visible units may be chosen to take on the probability values, rather than the stochastic samples, particularly if real valued output is necessary.

4.3.2 Contrastive Divergence

The process of sampling and resampling may be run for many iterations between the two layers before finishing on an output - this potentially long running and stochastic process results in the generative aspect of the network, and constitutes a Gibbs sampling chain. Multiple sampling steps in this chain is known as Contrastive Divergence, or CD- n , where n represents the number of steps, and which allows for effective parameter estimation. CD-1 is detailed in Algorithm 3.

Algorithm 3: CD-1

Input: RBM Network N , with visible nodes \mathbf{v} and hidden nodes \mathbf{h} and weight distribution \mathbf{w} (representing $\langle vh \rangle$)
Data: Training sample dataset D

```

foreach  $\mathbf{V}^D$  in  $D$  do
    // Sample  $\mathbf{H}^D$  from  $P(\mathbf{H}^D|\mathbf{V}^D)$ 
    foreach  $n$  in  $(1:j)$  do
        |  $P(\mathbf{H}_n^D = 1) = \sigma(\mathbf{w}_{0j} + \sum_{i=1} \mathbf{V}_i^D \mathbf{w}_{in})$ 
    end

    // Sample  $\mathbf{V}$  from  $P(\mathbf{V}|\mathbf{H}^D)$ 
    foreach  $n$  in  $(1:i)$  do
        |  $P(\mathbf{V}_n = 1) = \sigma(\mathbf{w}_{0i} + \sum_{j=1} \mathbf{H}_j^D \mathbf{w}_{ij})$ 
    end

    // Sample  $\mathbf{H}$  from  $P(\mathbf{H}|\mathbf{V})$ 
    foreach  $n$  in  $(1:j)$  do
        |  $P(\mathbf{H}_n = 1) = \sigma(\mathbf{w}_{0j} + \sum_{i=1} \mathbf{V}_i \mathbf{w}_{in})$ 
    end

    // Calculate Change in Weights Using Reconstructed Distribution
    //  $\Delta\mathbf{w}_{ij} = \eta(\langle \mathbf{v}_i \mathbf{h}_j \rangle_{data} - \langle \mathbf{v}_i \mathbf{h}_j \rangle_{reconstruction})$ 
     $\Delta\mathbf{w} = \eta([\mathbf{V}^D \mathbf{H}^{DT}] - [\mathbf{V} \mathbf{H}^T])$ 

    // Update the weights
     $\mathbf{w} \rightarrow \mathbf{w} - \Delta\mathbf{w}$ 
end
Result: Network  $N$  with weights  $\mathbf{w}$  updated for dataset  $D$ 

```

There's no upper bound on the iterations used for CD, and running for many can prove more effective for certain purposes. In this case however, where RBMs are used for the purposes of weight initialization, CD-1 is usually deemed sufficient.

4.3.3 CD-1 and SGD

In the same way that the backpropagation learning algorithm in Section 4.2.3 can be implemented in a mini-batch SGD process for FFNs, so can the CD learning algorithm for RBMs. The framework is kept the same, with the implementation of epochs and weight updates based on stochastically chosen minibatches, but the calculation used to update the weights is CD-1 instead.

4.4 Stacked AutoEncoders

As noted in Section 2.3, the use of Stacked AutoEncoders (SAE) have resulted in significant improvements in deep learning networks, and allowed effective reduction of high dimensional data. A single layer AutoEncoder is a specialized type of FNN with 3 layers: one input, one hidden, and one output. The network is trained (using backpropagation as per Section 4.2.3) to reconstruct the input, so the input and output layers have the same structure, and the hidden layer needs to have fewer nodes than the input. This forces the hidden layer to learn effective features of the data, and reduce the dimensional representation.

Stacked AutoEncoders follow a similar structure, but with multiple hidden layers. The only strict requirement of the hidden layers is that the middle one, which will be used as the encoder layer, still has fewer nodes than the input. This structure can still be trained using backpropagation, but with more layers, it is likely to begin suffering from the vanishing or exploding gradient problem. As noted, the work by Hinton et al. for initialization of weights helps resolve this.

4.4.1 Sigmoid Based Greedy Layerwise SAE Training

The steps for implementing the SAE training suggested by Hinton and Salakhutdinov [59] are detailed in Algorithm 4.

Algorithm 4: SAE Training - Sigmoid Greedy Layerwise

Input: Network structure N , which conforms to the requirements of an SAE with L layers; Input dataset X .

1. **Train First Layer:** For the first hidden layer, train as you would for an RBM with 2 layers - with the input layer, and the first layer as the hidden layer, using CD-1 and SGD.
2. **Train Subsequent Layers:** For each layer ℓ in $(2, L/2)$:
 - (a) Process data X through the previously trained layers using the forward propagation as defined in Section 4.2.1.
 - (b) This processed data then forms the input to the ℓ^{th} layer, which can be trained once again using CD-1 and SGD as if it were two layers.
3. **Mirror Network:** Once all the layers up until the encoder layer have been trained in this greedy layerwise fashion, mirror the weights and layers structures after the encoder to create a fully L layered FFN with pre-trained weights.
4. **Train Full AutoEncoder:** This network can then be trained using the backpropagation and SGD algorithms on dataset X , where cost of reproducing the network input is minimised.
5. **Split to Encoder:** Once a minima or acceptable level of reconstruction has been reached, the network can be truncated as the encoder layer, and so the first $L/2$ layers are used as the SAE.

Result: Trained SAE network.

Notably, this weight initialization will only be effective if the RBM and SAE networks use the same activation function, which due to the RBM implementation, needs to be a function that can output a probabilistic value in $[0,1]$.

4.4.2 ReLU based SAE Training

ReLU activations differ from Sigmoid in that they are not fitting for probability estimations, which makes the algorithm suggest by Hinton et al. unsuitable. The process used here relies on effective weight initialization, and is a simplification of the greedy layerwise trianing (Section 4.4.1), as detailed in Algorithm 5.

Algorithm 5: SAE Training - ReLU Backpropagation

Input: Network structure N , which conforms to the requirements of an SAE with L layers; Input dataset X .

1. **Initialize Network Weights:** Use an effective weight initialization for all L layers, such as the Xavier or He Initializations (discussed fully in Section 4.5).
2. **Train Full AutoEncoder:** This network can then be trained using the backpropagation and SGD algorithms for dataset X , where cost of reproducing the network input is minimised.
3. **Split to Encoder:** Once a minima or acceptable level of reconstruction has been reached, the network can be truncated as the encoder layer, and so the first $L/2$ layers are used as the SAE.

Result: Trained SAE network.

4.4.3 Denoising AutoEncoders

As noted in Section 2.3.3, denoising can be used as an optimization technique for AutoEncoders in order to improve general performance and reconstruction. The methodology works by corrupting the input data for training, but using the non-corrupted data as the expected output sample. In doing so, this forces the AutoEncoder to learn more fundamental representations of the data rather than fitting to sample noise, hence “denoising”. Two of the more typical techniques for achieving this have been implemented, as detailed below. In both cases, the noise is reapplied each time training samples are chosen.

4.4.3.1 Additive Gaussian Noise

With Gaussian noise, samples are corrupted such that a degree of variance is added to the input according to a parameterized Gaussian distribution. In this case, the distribution variance is a configurable training parameter.

$$\tilde{\mathbf{x}}|\mathbf{x} \sim \mathcal{N}(\mathbf{x}, \sigma^2 I). \quad (39)$$

4.4.3.2 Masking Noise

With masking noise, a fraction of the features in the data are set to 0, thus masking them for that sample. The percentage of features chosen is a configurable training parameter.

4.5 Variance Based Weight Initializations

Recent research by He et al. [57] has shown that weights can be initialized to maintain expected variance between the input and output layers. These methodologies have the immediate advantages of simpler implementation, as well as faster computation (as no pre-training is required). They also allow for effective weight initialization of non-probabilistic activation functions, such as ReLU. Whether they result in better reconstructions or predictions is less clear (especially as the linearity assumption would prove faulty), and so the methods are tested here as well.

A common initialization heuristic is to use a uniform, and but not layer agnostic, initialization such as equation (40) below. While simple enough, it's been shown that this does not always lead to the best training results, and can be outperformed by variance based initializations [50].

$$\mathbf{w} \sim U\left[-\frac{1}{\sqrt{n}}, \frac{1}{\sqrt{n}}\right], \quad (40)$$

where n is the number of nodes in the layer.

4.5.1 Initialization Rationale

The variance balancing methodology is based on balancing the variance of a linear network. For input X , with n components and linear neurons with weights W , and output Y :

$$\mathbf{Y} = \mathbf{W}_1 \mathbf{X}_1 + \mathbf{W}_2 \mathbf{X}_2 + \dots + \mathbf{X}_n \mathbf{W}_n. \quad (41)$$

It can thus be shown, that for *IID* samples with mean 0:

$$\mathbf{Var}(\mathbf{Y}) = n \mathbf{Var}(\mathbf{W}_i) \mathbf{Var}(\mathbf{X}_i). \quad (42)$$

For the variance of both input X and output Y to be balanced on the forward and backward propagation, then it is necessary for

$$\mathbf{Var}(\mathbf{W}_i) = \frac{1}{n_{in}} = \frac{1}{n_{out}}. \quad (43)$$

In the instance where there are not an equal number of nodes in the two layers, the average can be taken, such that

$$\mathbf{Var}(\mathbf{W}_i) = \frac{2}{n_{in} + n_{out}}. \quad (44)$$

4.5.2 Initializations

4.5.2.1 “Xavier” Initialization

Considering that $\mathbf{Var}(U(-a, a)) = a^2/3$, then ensuring balance variance for weights as per equation (44) provides us with the Xavier Glorot initialization

[50] which can be used for Sigmoid activations, and is defined as follows

$$\mathbf{w}_{ij} \sim U(-r, r), r = \sqrt{\frac{6}{n_i + n_j}}, \quad (45)$$

where n is the number of nodes in the i^{th} or j^{th} layer.

4.5.2.2 “He” Initialization

The initialization for ReLU is different on accounts of the function being equal to zero for half it’s potential input range - in this case it makes sense to double the weight variance, and so the He [57] initialization is used:

$$\mathbf{w}_{ij} \sim U(-r, r), r = \sqrt{\frac{6}{n_i}}. \quad (46)$$

4.5.2.3 “He-Adjusted” Initialization

An adjusted initialization is presented here, dubbed “He-Adjusted”, where the ReLU initialization uses a mean of the input and output layers in order to scale the weight variance. For networks with constant layer sizes, the initialization is the same as He, though for SAE networks which have layer size changes by definition, the He-Adjusted initialization will result in more appropriately sized weights:

$$\mathbf{w}_{ij} \sim U(-r, r), r = \sqrt{\frac{6}{(n_i + n_j)/2}}. \quad (47)$$

4.6 Money Management Strategy and Returns

In line with the general approach here, the Money Management Strategy (MMS) has been designed to be relatively simple, such that the results are more indicative of the underlying modelling rather than intricate trading strategies.

The MMS follows an arithmetic long strategy of buying any asset for which the predicted $t + D$ price is above the current price, and selling the stock at $t + D$. Trading costs have been included at 10% capital costs per annum for borrowing to purchase, and 0.45% for transaction costs as per [49]. This model does not take liquidity affects into account, though these can be accounted for in the costs. Results are compared to a benchmark model which has exact knowledge of the price in D days, which represents an upper bound on performance. This MMS implementation does not make any attempt to account for volume in the trades, and only trades one asset unit at a time.

4.6.1 Input Variables

The MMS takes the following values as input for each time point t and prediction point D

1. $\tilde{\mathbf{p}}_t$, the closing price at time t ,
2. $\tilde{\mathbf{p}}_{t+D}$, the closing price in D days, and
3. $\hat{\mathbf{p}}_{t+D}$, the predicted closing price in D days.

The naming conventions for the variables which are then calculated are as follows:

1. s represents a trading signal indicating whether a trade should occur on a given day,
2. c represents the purchasing cost for an asset,
3. k represents the capital cost for purchasing an asset (i.e. the borrowing and trading costs),
4. f represents the full cost of purchasing an asset (i.e. $c + k$),
5. o represents the nominal P&L observed from trading an asset, and
6. r represents the return rate for trading an asset (with costs accounted for)

Capitalised variations represent the same variables, but aggregated across all assets.

4.6.2 Calculated Asset Variables

Thus, for each asset at each time point, the following values are calculated:

1. A trading signal indicating whether a trade will take place on t :

(48)

$$\mathbf{s}_t = \begin{cases} 1, & \text{if } \hat{\mathbf{p}}_{t+5} > \mathbf{p}_t \\ 0, & \text{otherwise} \end{cases}$$

2. A trading signal indicating whether a trade will take place on t in the benchmark model:

(49)

$$\mathbf{s}_t^b = \begin{cases} 1, & \text{if } \mathbf{p}_{t+5} > \mathbf{p}_t \\ 0, & \text{otherwise} \end{cases}$$

3. The cost incurred in buying the asset at time t :

$$\mathbf{c}_t = \tilde{\mathbf{p}}_t \cdot \mathbf{s}_t. \quad (50)$$

4. The cost incurred in the benchmark model at t :

$$\mathbf{c}_t^b = \tilde{\mathbf{p}}_t \cdot \mathbf{s}_t^b. \quad (51)$$

5. The possible capital and transaction costs:

$$\mathbf{k}_t = \tilde{\mathbf{p}}_t \cdot (0.1/365 \cdot D) + \tilde{\mathbf{p}}_t \cdot (0.45/100). \quad (52)$$

6. The full cost of trading the asset at t in the predictive model:

$$\mathbf{f}_t = (\tilde{\mathbf{p}}_t + \mathbf{k}_t) \cdot \mathbf{s}_t. \quad (53)$$

7. The full cost of trading the asset at t in the benchmark model:

$$\mathbf{f}_t^b = (\tilde{\mathbf{p}}_t + \mathbf{k}_t) \cdot \mathbf{s}_t^b. \quad (54)$$

8. The nominal observed P&L at $t + D$:

$$\tilde{\mathbf{o}}_{t+D} = (\tilde{\mathbf{p}}_{t+D} - \tilde{\mathbf{p}}_t) \cdot \mathbf{s}_t. \quad (55)$$

9. The nominal expected P&L at $t + D$:

$$\hat{\mathbf{o}}_{t+D} = (\hat{\mathbf{p}}_{t+D} - \hat{\mathbf{p}}_t) \cdot \mathbf{s}_t. \quad (56)$$

10. The nominal benchmark P&L at $t + D$:

$$\mathbf{o}_{t+D}^b = (\tilde{\mathbf{p}}_{t+D} - \tilde{\mathbf{p}}_t) \cdot \mathbf{s}_t^b. \quad (57)$$

11. The fullcost observed return rate at $t + D$:

$$\tilde{\mathbf{r}}_{t+D} = \frac{(\tilde{\mathbf{o}}_{t+D} - \mathbf{f}_t)}{\mathbf{f}_t}. \quad (58)$$

12. The fullcost expected return rate at $t + D$:

$$\hat{\mathbf{r}}_{t+D} = \frac{(\hat{\mathbf{o}}_{t+D} - \mathbf{f}_t)}{\mathbf{f}_t}. \quad (59)$$

13. The fullcost benchmark return rate at $t + D$:

$$\tilde{\mathbf{r}}_{t+D}^b = \frac{(\tilde{\mathbf{o}}_{t+D}^b - \mathbf{f}_t^b)}{\mathbf{f}_t^b}. \quad (60)$$

4.6.3 Calculated Strategy Variables

The MMS is then implemented using these calculated values which are aggregated at each time point t for all assets, a , as follows:

1. The nominal expected P&L for $t + D$ from all assets traded at t :

$$\hat{\mathbf{O}}_{t+D} = \sum_{a \in \text{assets}} \hat{\mathbf{o}}_{a,t+D}. \quad (61)$$

2. The nominal observed P&L for $t + D$ from all assets traded at t :

$$\tilde{\mathbf{O}}_{t+D} = \sum_{a \in \text{assets}} \tilde{\mathbf{o}}_{a,t+D}. \quad (62)$$

3. The nominal benchmark P&L for $t + D$ from all assets traded at t :

$$\mathbf{O}_{t+D}^b = \sum_{a \in \text{assets}} \mathbf{o}_{a,t+D}^b. \quad (63)$$

4. The cost of all trades at t :

$$\mathbf{C}_t = \sum_{a \in \text{assets}} \mathbf{c}_{a,t}. \quad (64)$$

5. The cost of all trades at t in the benchmark model:

$$\mathbf{C}_t^b = \sum_{a \in \text{assets}} \mathbf{c}_{a,t}^b. \quad (65)$$

6. The cost of all trades at t including transaction costs:

$$\mathbf{F}_t = \sum_{a \in \text{assets}} \mathbf{f}_{a,t}. \quad (66)$$

7. The cost of all trades at t , including transaction costs, in the benchmark model:

$$\mathbf{F}_{p,t}^b = \sum_{a \in \text{assets}} \mathbf{f}_{a,t}^b. \quad (67)$$

8. The fullcost observed return rate at $t + D$:

$$\tilde{\mathbf{R}}_{t+D} = \frac{(\tilde{\mathbf{O}}_{t+D} - \mathbf{F}_t)}{\mathbf{F}_t}. \quad (68)$$

9. The fullcost expected return rate at $t + D$:

$$\hat{\mathbf{R}}_{t+D} = \frac{(\hat{\mathbf{O}}_{t+D} - \mathbf{F}_t)}{\mathbf{F}_t}. \quad (69)$$

10. The fullcost benchmark return rate at $t + D$:

$$\tilde{\mathbf{R}}_{t+D}^b = \frac{(\tilde{\mathbf{O}}_{t+D}^b - \mathbf{F}_t^b)}{\mathbf{F}_t^b}. \quad (70)$$

11. The Sharpe Ratio [77]:

$$\text{SR} = \frac{\mathbb{E}(\tilde{\mathbf{R}})}{\sqrt{\text{Var}(\tilde{\mathbf{R}})}}. \quad (71)$$

4.7 Combinatorially Symmetric Cross-Validation and Probability of Backtest Overfitting

The combinatorially symmetric cross-validation (CSCV) method developed by Bailey et al. [7], as discussed in Section 2.6, can be used to assess the likelihood of backtest overfitting through comparison of IS and OOS return metrics. As discussed more extensively in Section 2.6, their research defines backtest overfitting as having occurred when the strategy selection which maximizes IS performance systematically underperforms median OOS in comparison to the remaining configurations. The N configurations are assessed according to a fixed performance measure, such that $\mathbf{R} = (R_1, R_2, \dots, R_N)$ and $\bar{\mathbf{R}} = (\bar{R}_1, \bar{R}_2, \dots, \bar{R}_N)$ represent the IS and OOS performance of each configuration, respectively.

The crux of the framework lies in comparing the ranking of a selected strategy, and so Ω is used to represent ranking space consisting of the $N!$ permutations of $(1, 2, \dots, N)$ indicating the ranking of the N strategies. The random vectors r and \bar{r} are used to denote the IS and OOS ranking of the configurations making up \mathbf{R} and $\bar{\mathbf{R}}$. Lastly a subset of Ω is defined, such that $\Omega_n^* = \{f \in \Omega | f_n = N\}$ - this encapsulates the highest ranking configurations.

The definition of backtest overfitting (where a strategy with optimal IS performance has an expected ranking below the median OOS) is given by:

$$\sum_{n=1}^N \mathbb{E}[\bar{r}_n | r \in \Omega_n^*] \mathbf{P}[r \in \Omega_n^*] \leq \frac{N}{2}. \quad (72)$$

Equation 72 allows the Probability of Backtest Overfitting (PBO) to be calculated using the Bayesian formula, such that:

$$\text{PBO} = \sum_{n=1}^N \mathbf{P}[\bar{r} < \frac{N}{2} | r \in \Omega_n^*] \mathbf{P}[r \in \Omega_n^*]. \quad (73)$$

Notably, the above definitions consider IS as the data made available to the strategy selection, rather than the models calibration (e.g. the full IS dataset, rather than, for example, the number of days used in a moving average). This allows the model-free and non-parametric nature of the definition.

They further developed the CSCV framework as a methodology to reliably estimate the probability used in PBO, which allows a concrete application of

the concept. The CSCV framework does not require using the typical hold-out strategy (and thus avoids credibility issues), and is ultimately able to provide a bootstrapped distribution of OOS performance. The full methodology is shown in Algorithm 6, as originally presented by Bailey et al. [7].

Algorithm 6: CSCV

Input: N configuration trials over T time periods with P&L

1. **Generate P&L Matrix:** Generate a $T \times N$ performance series matrix, M , representing the profits and losses by the N configuration trials over T time periods.
2. **Define P&L Submatrices:** Partition the M matrix by rows into S submatrices, each of even size $(\frac{T}{S} \times N)$.
3. **Define P&L Submatrix Combinations:** Generate the combinations C_S of M_S , in groups of size $\frac{S}{2}$, for total $\binom{S}{S/2}$ of combinations.
4. **Process Combinations:** For each combination in $c \in C_S$:
 - (a) **Define IS Set:** Form a training set J by joined $\frac{S}{2}$ M_S submatrices, in their original order. J is a matrix of order $(\frac{T}{S}) (\frac{S}{2}) N$.
 - (b) **Define OOS Set:** Form the test set \bar{J} as the complement of J in M , once again in the original order.
 - (c) **IS Performance Stats:** Form a vector of R^c of performance statistics of order N , where the N th component R_n^c of R^c reports the performance associated with the n^{th} column of J .
 - (d) **OOS Performance Stats:** Repeat [c] for \bar{J} to derive \bar{R}^c and \bar{r}^c .
 - (e) **Find Best IS Strategy:** Determine the element n^* such that $R_n^c \in \Omega_n^*$ - i.e. n^* is the best performing strategy IS.
 - (f) **Calculate Relative Rank of OOS Strategy:** Define the relative rank of $\bar{r}_{n^*}^c$ by $\bar{\omega}_c := \frac{\bar{r}_{n^*}^c}{N+1} \in (0, 1)$. This is the relative rank of the OOS performance associated with the strategy chosen IS, which should systematically outperform OOS if no backtest overfitting has taken place.
 - (g) **Calculate Logit Value:** Define the logit $\lambda_c = \ln \frac{\bar{\omega}_c}{(1-\bar{\omega}_c)}$. High values here indicate consistency between IS and OOS performances (and so low overfitting).
5. **Measure Overfitting:** The logit values can now be used to compute the distribution ranks of OOS, by collecting all λ_c for $c \in C_S$. The relative frequency for λ occurring across all C_S is:

$$f(\lambda) = \sum_{c \in C_S} \frac{\chi_\lambda(\lambda_c)}{\#(C_S)}, \quad (74)$$

where χ is the characterization function and $\#(C_S)$ is the number of elements in C_S , and so $\int_{-\infty}^{\infty} f(\lambda) d\lambda = 1$.

Result: Logit distribution.

The CSCV framework and results thus allows the consideration of several notable statistics. First and foremost, the PBO may now be estimated using the CSCV method and using an integral over the $f(\lambda)$ function as defined above which offers a rate at which the best IS strategies underperform the median of OOS trials. The PBO is estimated using

$$\Phi = \int_{-\infty}^0 f(\lambda) d\lambda. \quad (75)$$

If $\Phi \approx 0$, it is evidence of no significant overfitting (inversely, $\Phi \approx 1$ would be a sign of probable overfitting). Critically then, a PBO measure may be used in a standard hypothesis test to determine if a model should be rejected or not. This can be extended, as shown by Bailey et al. [7], to show the relationship between overfitting and performance degradation of a strategy. It becomes clear that with models overfitting to backtest data noise, there comes a point where seeking increased IS performance is detrimental to the goal of improving OOS performance.

4.8 Deflated Sharpe Ratio

The crux of the DSR assessment lies on the acknowledgement that a given set of SR estimates will have a greater maximum than zero, even if the true SR is zero, i.e testing the null hypothesis of $H_0 : SR = 0$.

In order to reject this, the observed SR must exceed the expected SR after controlling for the number of trials. Using the work noted in Section 2.6.1, Lopez de Prado and Lewis [81] combine several ideas allowing the assessment of the Sharpe Ratio under multiple trials. The Optimal Number of Clusters (ONC) algorithm is used to cluster the trials into hierarchical independent trial groups (Section 4.8.1). These clusterings can then be used to estimate the trial set variance and number of trials, which can in turn be used to estimate the maximum likely Sharpe Ratio expected under the False Strategy Theorem (Section 4.8.3). The Deflated Sharpe Ratio can be calculated by using this as the benchmark for the Probabilistic Sharpe Ratio, which gives a likelihood of whether the best observed \widehat{SR} is a false positive or not (Sections 4.8.2, 4.8). These methods are explained in full detail below.

4.8.1 Optimal Number of Clusters Algorithm

The primary contribution by Prado and Lewis is the Optimal Number of Clusters (ONC) approach to estimating the number of independent trials, such that the correct variances between strategies can be calculated. The methodology aims to partition a series of returns into clusters with higher intra-cluster correlations, and low inter-cluster correlations.

The initial data, N strategies each with their own return series \mathbf{r} , go through the following steps for pre-processing:

1. **Construct the Correlation Matrix:** ρ is constructed, An $N \times N$ correlation matrix, such that each element at ρ_{ij} represents the correlation between \mathbf{r}_i and \mathbf{r}_j .
2. **Construct the Distance Matrix:** A proper distance matrix is calculated with which the clustering can be done. The proper distance satisfies the necessity that higher correlations will have closer distances, as well as the classical axioms of non-negativity, identity, symmetry and sub-additivity.

$$\mathbf{D}_{ij} = \sqrt{\frac{1}{2}(1 - \rho_{ij})}. \quad (76)$$

3. **Calculate Global Distance Matrix:** The ONC algorithm works on a distance of distances matrix, such that the distances incorporate information about the entire set of returns, which in turn reduces noise and increases the robustness of the clustering [79]. The distance matrix $\tilde{\mathbf{D}}$ is then calculated such that:

$$\tilde{\mathbf{D}}_{ij} = \sqrt{\sum_k (\mathbf{D}_{ik} - \mathbf{D}_{jk})^2}. \quad (77)$$

Using the distance matrix $\tilde{\mathbf{D}}$, a modified K-means clustering algorithm is run, which addresses 2 concerns with a typical K-means implementation: the number of clusters needs to be set prior to running, and the random initialization can lead to similarly random efficacy.

The first problem is addressed using an objective function which can then be optimised. The silhouette score, introduced by Peter [96] is used as base to measure the quality of an individual strategy's assigned cluster.

$$\mathbf{S}_i = \frac{b_i - a_i}{\max(a_i, b_i)}. \quad (78)$$

where a_i is the average distance between i and all other nodes in the same cluster, b_i is the smallest average distance between i and all the nodes in any other cluster. \mathbf{S}_i then ranges between -1 (poor fit) and 1 (good fit), and incorporates a measure of both inter-cluster and intra-cluster quality. This allows the definition of the objective function to be used, where for a given cluster:

$$\mathbf{q} = \frac{\mathbb{E}[\mathbf{S}_i]}{\sqrt{\text{Var}[\mathbf{S}_i]}}. \quad (79)$$

The initialization problem is, in part, addressed through the use of nested clustering. Typical K-means clustering is run for $k = 2, \dots, N-1$ clusters, for which each clustering is evaluated according to \mathbf{q} (equation (79)). This process is itself repeated a number of times, thus obtaining the results for different

random initializations. Naturally, the clustering results with the highest \mathbf{q} are used for the steps that follow.

A final modification is made in order to address lower quality clusters that may have occurred as a result of the initial clustering capturing larger and broader clusters, but missing smaller and more distinct ones. In order to assess this, any cluster k where $\mathbf{q}_k < \bar{\mathbf{q}}$ has its components aggregated into a partition, K_1 , with the remaining components in K_0 . The components in K_1 are then run through the full ONC algorithm. This recursive approach may produce a better clustering, and so the $\bar{\mathbf{q}}$ for the cluster before and after the recursive step are compared. If the new clustering is better, then the new clusters for K_1 are combined with the original K_0 clusters. If not, then the original clustering is used as the final result. These clusterings will be used below, where both the number and variances thereof will be used.

4.8.2 Sharpe Ratio Normality and Probabilistic Sharpe Ratio

While it has often been assumed in the past that strategy returns will follow a Normal distribution, it has been shown empirically that they often do not [15], which may in turn lead to an underestimation of false positive probability. Under the assumption of *IID* and non-normal returns, Mertens [86] was able to show the asymptotic distribution of \widehat{SR} for a strategy with returns $r_t, t = 1, \dots, T$, as

$$(\widehat{SR} - SR) \xrightarrow{a} \mathcal{N} \left[0, \frac{1 + \frac{1}{2}SR^2 - \gamma_3 SR + \frac{\gamma_4 - 3}{4}SR^2}{T} \right] \quad (80)$$

where

1. γ_3 is the skewness of r_t , and
2. γ_4 is the kurtosis of r_t .

Christie [16] and Opdyke [92] showed that this holds under the more general assumption of returns being stationary and ergodic, but not necessarily *IID*. Thus, \widehat{SR} follows a Normal distribution, with a variance that depends on the skewness and kurtosis of returns, which in turn allows the metric to be expressed in a probabilistic space. Bailey and Lopez did so, producing the Probabilistic Sharp Ratio (PSR) measure, an adjusted \widehat{SR} , removing the inflationary effect of short series with skewed and/or fat-tailed returns.

$$\widehat{PSR}[SR^*] = Z \left[\frac{(\widehat{SR} - SR^*) \sqrt{T-1}}{\sqrt{1 - \hat{\gamma}_3 \widehat{SR} + \frac{\hat{\gamma}_4 - 1}{4} \widehat{SR}^2}} \right], \quad (81)$$

where

1. T is the number of observed returns,
2. \widehat{SR} is the non-annualized estimate of SR, computed on the same frequency as the T observations,

3. SR^* is the user provided benchmark,
4. $Z[.]$ is the CDF of the standard Normal distribution,
5. $\hat{\gamma}_3$ is the skewness of r_t , and
6. $\hat{\gamma}_4$ is the kurtosis of r_t .

This PSR calculation then gives the probability that the observed $\widehat{\text{SR}}$ exceeds SR^* . Expectedly then, PSR will increase with $\widehat{\text{SR}}$, T and $\hat{\gamma}_3$, but decrease with $\hat{\gamma}_4$.

4.8.3 False Strategy Theorem

Bailey and Lopez de Prado [5] provided a proof for the following statement, allowing for PSR to be properly adjusted for multiple trials:

$$\mathbb{E} \left[\max_k \{\widehat{\text{SR}}_k\} \right] \left(V \left[\{\widehat{\text{SR}}_k\} \right] \right)^{-1/2} \approx (1 - \gamma) Z^{-1} \left[1 - \frac{1}{K} \right] + \gamma Z^{-1} \left[1 - \frac{1}{Ke} \right], \quad (82)$$

where

1. $\widehat{\text{SR}}_k \sim \mathcal{N} \left[0, V \left[\{\widehat{\text{SR}}_k\} \right] \right]$,
2. $Z^{-1}[.]$ is the inverse CDF of the standard Normal distribution,
3. e is Euler's number, and
4. γ is the Euler-Mascheroni constant.

The critical takeaway from this, is that unless $\max_k \{\widehat{\text{SR}}_k\} > \mathbb{E} \left[\max_k \{\widehat{\text{SR}}_k\} \right]$, then it is likely that $\max_k \{\widehat{\text{SR}}_k\}$ represents a false positive trial.

Prado and Lewis use the Probabilistic Sharpe Ratio and the False Strategy Theorem (FST) to define the Deflated Sharpe Ratio (DSR) as $\widehat{PSR}[\text{SR}^*]$: the probability that the true SR exceeds SR^* , which no longer needs to be user defined. Following from the FST statement in equation (82),

4.8.4 Deflated Sharpe Ratio

$$\text{SR}^* = \sqrt{V \left[\{\widehat{\text{SR}}_k\} \right]} \left((1 - \gamma) Z^{-1} \left[1 - \frac{1}{K} \right] + \gamma Z^{-1} \left[1 - \frac{1}{Ke} \right] \right), \quad (83)$$

where

1. $V \left[\{\widehat{\text{SR}}_k\} \right]$ is the variance across trials' estimated SR,
2. K is the number of independent trials,
3. $Z[.]$ is the CDF of the standard Normal Distribution, and
4. γ is the Euler-Mascheroni constant.

For any set of trials with strategy returns, it is expected that there will be some maximum \widehat{SR} that is more than zero, even if the true SR is zero. This maximum can be defined using equation (83) for SR^* . The PSR from equation (81) can then be used to assess if the observed SR is statistically significantly larger than the expected maximum, and in doing so possibly reject the null hypothesis that $H_0 : SR = 0$. Thus, DSR gives us a confidence level as to whether the observed SR is legitimate and not just a false positive.

4.8.4.1 Estimating $\mathbb{E}[K]$ and $\text{Var}[\widehat{SR}_k]$

The results from the ONC algorithm, having already determined $\mathbb{E}[K]$ by clustering the trials into K clusters, can then be used to estimate the variance of the cluster sharpe ratios. In order to do so, a single time series return needs to be constructed for the strategies in each cluster. The minimum variance allocation from Lopez de Prado [79] is used in order to choose the best weightings and reduce the effects of strategies with large variances.

For each cluster k , where $k = 1, \dots, K$, with components C_k , the weightings for each component can be calculated using equation (84):

$$\mathbf{w}_k = \frac{\Sigma_k^{-1} \mathbf{1}}{\mathbf{1}' \Sigma_k^{-1} \mathbf{1}}, \quad (84)$$

where Σ_k is the covariance matrix for the components of C_k .

Using these weights, the cluster return time series can then be calculated using equation (85):

$$\mathbf{S}_{k,t} = \sum_{i \in C_k} \mathbf{w}_{k,i} \mathbf{r}_{i,t}, \quad (85)$$

where $r_{i,t}$ is the return series for component i .

With a single time series for each cluster k , \widehat{SR}_k can be calculated normally (as per equation (71)), and then annualized using equation (86). In this paper, all strategies have the same trading frequency of $\frac{T_k}{Years_k}$ (as per the MMS presented in Section 4.6), though other implementations may need to adjust the frequency for each cluster. The annualized Sharpe Ratio (aSR) is calculated as:

$$\widehat{aSR}_k = \frac{\mathbb{E}[\{S_{k,t}\}] \text{ Frequency}_k}{\sqrt{\text{Var}[\{S_{k,t}\}] \text{ Frequency}_k}} = \widehat{SR}_k \sqrt{\text{Frequency}_k}. \quad (86)$$

These annualized sharpe ratios for each cluster can now be used to calculate

the inter-cluster variance using equation (87), with their frequency adjusted to match the SR* presented for DSR in equation (83):

$$\mathbb{E} \left[\text{Var} \left[\left\{ \widehat{\text{SR}}_k \right\} \right] \right] = \frac{\text{Var} \left[\left\{ \widehat{\text{aSR}}_k \right\} \right]}{\text{Frequency}_{k^*}}. \quad (87)$$

The results from equation (87) and K can then be plugged into equation (83) in order to calculate SR*, the expected maximum SR from the set of trials. This SR* with the observed maximum $\widehat{\text{SR}}$ can then be plugged into equation (81) to calculate PSR, and assess the likelihood of the observed $\widehat{\text{SR}}$ being a false positive.

5 Framework Implementation

5.1 Full Framework Process

Having covered the technical implementations in Sections 3 and 4, a full overview of the end to end experimental process can be detailed and discussed. The process here rests on two key principles: implementing a generalised version of a system which could offer exploration of more complex techniques, and ensuring an effective modularisation of steps such that the process can be reconfigured accordingly while maintaining its integrity. In doing so, a separable system is created which brings together data reduction, deep learning with pre-training/weight initialization, online learning and back test overfitting validation.

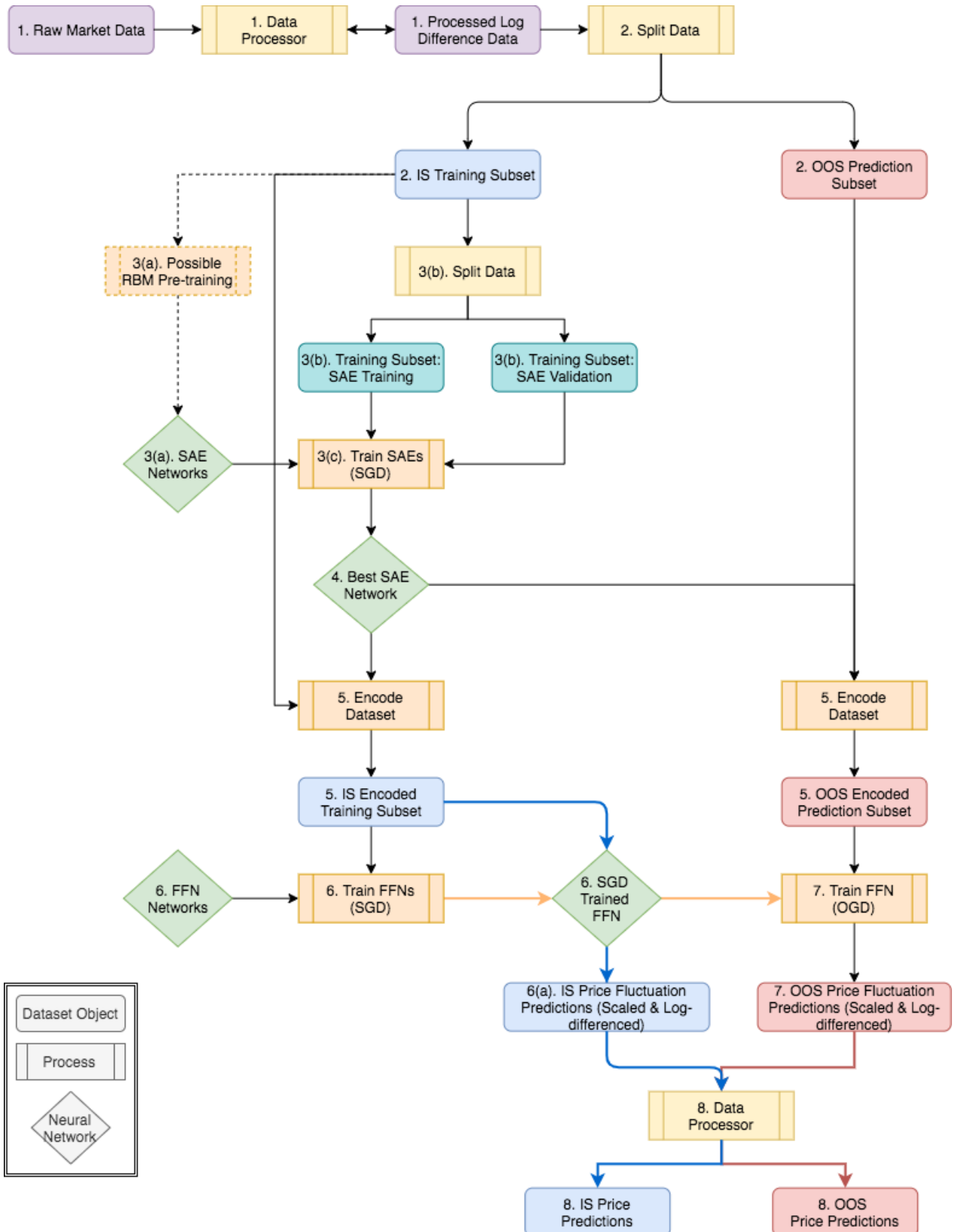
The steps below detail the conceptual stages for the full end to end process. These are also shown visually in Figure 5, with the diagram numbers corresponding to stages or items produced by each of the steps below.

1. **Process Data:** The raw market data, $\tilde{\mathbf{P}}$ from the JSE (see Section 7.1.1), goes through data processing, as per the steps below in Section 5.6, to form \mathbf{L} (a log differenced and aggregated time series).
2. **Split Data:** \mathbf{L} is split to form the Training and Prediction datasets, \mathbf{L}^I and \mathbf{L}^O .
3. **Train SAE Networks:**
 - (a) Either RBM pre-training or variance based techniques are used to initialize the network weights (see Sections 4.3 and 4.5, respectively).
 - (b) \mathbf{L}^I is split into two datasets: \mathbf{S}^T and \mathbf{S}^V , used to train and validate the SAE networks, respectively.
 - (c) The networks are trained using SGD (see Section 4.2.3) and \mathbf{S}^T , and validated using the MSE score on \mathbf{S}^V .
4. **Select Best SAE Network(s):** The network MSE scores can be used to select the best SAE networks to be used for the following steps. Only the best need be selected out of each configuration category that is desired to be carried forward (e.g. 1 for each configuration of data horizon aggregations used).
5. **Encode Datasets:** The Training and Prediction datasets, \mathbf{L}^I and \mathbf{L}^O , are encoded using the SAE networks to form \mathbf{E}^I and \mathbf{E}^O .
6. **Train Predictive Network on IS Data:** The predictive network is initialized using variance based techniques, and trained using SGD on \mathbf{E}^I .
 - (a) After training, \mathbf{E}^I is used to generate and record the IS predictions, $\hat{\mathbf{L}}^I$.
7. **Train Predictive Network on OOS Data:** The predictive network is trained on \mathbf{E}^O using OGD (see section 4.2.4). The predicted outputs from the training, denoted $\hat{\mathbf{L}}^O$, are also recorded.

8. **Reconstruct Price Predictions:** Price prediction sets $\hat{\mathbf{L}}^I$ and $\hat{\mathbf{L}}^O$ are processed to reconstruct actual timepoint prices using the steps in Section 3.1.4, denoted $\hat{\mathbf{P}}^I$ and $\hat{\mathbf{P}}^O$, respectively.
9. **Calculate MMS Variables:** $\hat{\mathbf{P}}^I$ and $\hat{\mathbf{P}}^O$ are used by the MMS to calculate variable at each time point, as per Section 4.6. One of the primary calculations is the daily return rates, which can be used to calculate the Sharpe Ratio.
10. **Calculate CSCV and PBO:** The CSCV algorithm is run using both the $\hat{\mathbf{P}}^I$ and $\hat{\mathbf{P}}^O$ MMS rates in order to calculate a PBO score, as detailed in Section 4.7.
11. **Calculate DSR:** The CSCV algorithm is run using $\hat{\mathbf{P}}^O$ MMS rates to calculate a DSR score, as detailed in Section 4.8.

5.2 Process Diagram

The flow diagram below provides a graphical representation of this process described above in Section 5.1 (the MMS calculations and CSCV process are not included). The process may be repeated accordingly in terms of SAE structures that are desired for testing, such that the “Best SAE Network” is different for different encoding layer sizes, or data aggregations used (as was the case in many of the experiments which will be discussed in Section 8).

**Figure 5:** Overall Process Flow

The flow diagram here offers a visual representation of the process set out in Section 5.1, with the numbers corresponding to the steps of the process.

5.3 Parameter Space Exploration

The parameter space is explored using a phased gridsearch approach. For each stage, the relevant parameters are specified as a set of values (or one, if so chosen), and all sets are then used to generate the full combinatorial space, such that each possible combination of the specified parameters is tested.

1. **Stage 1:** The data configuration (i.e. data windows, prediction point, scaling, data split points) as well as the SAE configuration (network size, learning rates, learning optimization parameters, SGD epochs) are set in Stage 1 and used to train the SAE networks.
2. **Stage 2:** The preferred SAEs are chosen from Stage 1 manually, and determine the data configuration used for Stage 2. These are then used to encode the datasets, which will be used for FFN training. The FFN SGD and OGD parameters are set in this stage (network size, learning rates, SGD epochs etc.), and will be combined combinatorially with the SAEs that were chosen for testing as well.

5.4 Reproducibility

Reproducible results were ensured with the use of set random data seeds and a Mersenne Twister pseudorandom number generator. Each SAE training process is initialized with a dataseed which is recorded in the `dataset_config` schema (see Section 6 for more details). These are propagated through to the FFN training, such that any of the results presented could be reproduced using the data seeds and configurations noted in Appendix 11.3 (which are all detailed in the relevant figure captions as well).

5.5 Synthetic Data

The use of synthetic GBM generated data offers a way of exploring the parameter space without running configuration experiments on the actual data which might then raise the probability of backtest overfitting. The synthetic data has enough similarity that it can allow a broad exploration to get ideas of optimization usage and parameter choices. This is an appealing option in light of the concerns around increasing the number of particularly poor performing networks when it comes to calculating PBO, as discussed in Section 8.9. That said, there are characteristic differences between GBM generated data and actual financial time series. With these in mind, the results section will make comparisons of the two in order to offer a sufficient understanding for when synthetic data can be relied upon to guide future training.

The process for generating synthetic data is detailed in Algorithm 1 (Section 3).

5.6 Data Preparation

The fulldataset goes through several steps of pre-processing - these are covered in more detail in Section 3.1, though the steps are included here:

1. The data is processed into day to day log fluctuations (see equation (1)).
2. At each time point, rolling historic fluctuation summations are calculated (e.g. the past 1, 7 and 30 days, see equation (2)).
3. At each time point, rolling future fluctuation summations are calculated (e.g. the next 5 days, see equation (3)).
4. The dataset is truncated to only include points with all aggregations or predictions available.
5. The dataset undergoes scaling - the different functions are detailed in Section 3.1.2, though Limited Normalization (as per equation (7)) was used for most of the results produced.

5.6.1 Data Window Aggregations

The time aggregations were chosen according to domain knowledge - it's expected that prices may move in daily, weekly, fortnightly, monthly and quarterly patterns as trading is actioned by day traders such as speculators to institutional investors such as mutual funds. Indeed, it can be shown that markets can be modelled such that they are hierarchical in space and time, with actors at different hierarchical levels within the market interacting under different causitive structures [118]. The effect is such that price trends and patterns can be expected to exist in time at multiple levels, with price being set as an emergent property of these hierarchies. Taking this into account, variations of 1, 5, 10, 20 and 60 working days were considered throughout the configuration tests, in the following combinations:

1. Horizon Tuple 1: [1, 5, 20]
2. Horizon Tuple 2: [5, 20, 60]
3. Horizon Tuple 3: [10, 20, 60]

The calculations for the aggregated values can be seen in equations (2) and (3).

5.6.2 Point Predictions

Various configurations were tested in terms of the historic summations used, while the fluctuation predictions were set at 5 days. It's worth noting that the prediction horizon is configurable, and in the case of implementing a more complex trading strategy, one would likely choose to predict multiple points across the horizon in order to develop a distribution. In this case, the MMS was kept purposefully simple, and so didn't warrant the more intensive implementation.

One point of concern is that point predictions at 5 days in advance could open the process up to aliasing error, as it is unlikely to be predicting at the Nyquist frequency, and may end up fitting to the band ripple rather than the underlying signal. Conversely, 1 day predictions for closing price might offer a high degree of accuracy, but are not practical for trading due to market auction and bidding structures. The system implementation veered on the side of practicality in this case, and was configured for longer term predictions despite the risk of aliasing. While some of the configurations were run with 2 day predictions, it was seen that once costs were considered it was difficult for even the benchmark to produce desired P&L figures and so a 5 day prediction was implemented in subsequent tests.

5.6.3 Scaling

When testing the two limited scaling methodologies, standardization and normalization, it was found that the results for standardizing tended to be notably worse than normalization (discussed in Section 8.6). It's possible that outliers in price fluctuations and changing variance through time (which is not captured effectively through the limited variation) resulted in a less informative representation and worse performance of the FNN models which can be prone to error maximisation. As a result of this, the limited normalization process was used for most of the tests run. It's worth noting that an implementation which incorporates processing of the data through the Error Function in order to reduce the impact of outliers would likely prove a worthwhile endeavour, and could be easily swapped in due to the systems modularity.

The implementation for “Limited Normalization” can be seen in equation (5).

5.7 Data Segregation

Once processed, the dataset is split into 2 portions:

1. Training: The first set is used for the SAE training, as well as the initial SGD training on the predictive FFN network. This is the IS dataset and is used as what would typically be the historical training set.
2. Prediction: The second set is used only for the OGD training in order to generate returns from the predictive network. This is the OOS dataset and is used as what would typically be the testing / validation set.

The predictions from both the Training and the Prediction sets are used by Bailey’s CSCV method to assess overfitting (the use of the CSCV technique negates the need for a hold-out portion of the dataset [7]), however only the OOS prediction returns are used in order to assess DSR or model P&L figures and performance.

In this case, a simple split point of 60:40 was chosen for the Training and Prediction sets, respectively. In a more restrictive case, where there is less data

to work with, it would be advised to consider a method such as MinBTL as developed by Bailey et al. [6] and the estimated number of configurations to be tested in order to decide an appropriate split point.

5.8 Unsupervised Learning: SAE Training

The Training dataset is used to train the AutoEncoder network using either RBM pretraining or weight initialization algorithms and SGD training, as defined in Section 4.4. The Training portion of the dataset, as noted in Section 5.7, is itself split up into a training and validation set for the SAE. The efficacy of the SAE on the validation set is required in order to determine which networks to choose for subsequent steps in the process. The full testing process here will rely on a generated set of best SAE networks at each encoding layer size, to be used for FFN training and prediction (chosen by a minimum MSE score). The benefit of the modularised system is emphasised here, as the SAE training will not suffer from limitations due to backtesting considerations: any amount of configurations or processes can be tested for feature extraction without concern.

Once the SAE networks have been defined and chosen, they can be used to reprocess both the Training and Prediction datasets such that the input is encoded, and the output is as before. These encoded datasets can then be used for the following steps in the process.

In a productionized system, where data is updated daily, there would be a set period after which the SAE network would be retrained to reflect more recent data. This step wasn't deemed necessary at the outset of developing this process, but results detailed in Section 8.2 suggest that it is an important implementation step.

5.9 Supervised Learning: Prediction Network Training

Typically, the SAE and predictive network might be presented as one and the same, however in the process presented we are able to separate the two and optimise for feature extraction prior to training for predictions. Having done so, the datasets can have their input encoded, but retain the same output. The predictive network is then trained using the Training set, as detailed in Section 4.2.3. There's no requirement to validate this part of the training, so the dataset is not split into subportions as it was for SAE training.

Once the predictive network is trained, the OGD process (as per Section 4.2.4) is run through the encoded Prediction dataset in order to generate the predictions for the assets prices that the model produces - thus emulating what

would have occurred in a live environment.

5.10 Price Reconstruction

In the interest of more interpretable results for figures such as P&L, the prices fluctuations for both IS and OOS predictions are re-scaled back to their original price fluctuation predictions using the reverse scaling detailed in Section 3.1.3. These prices are then reconstructed using equation (12), such that they represent a predicted future price of the asset which can then be used by the MMS. It's worth noting that the price reconstruction applies the predicted fluctuation to the known original price, such that it would represent a system that is run daily, rather than a system that is making rolling predictions over a period of time.

5.11 Money Management Strategy

The MMS, as described in Section 4.6, takes a proof of concept approach to the system being investigated. It is a simple long strategy with a set liquidation point, and no notable refinement. The naive approach is taken purposefully here, so as not to bias the perspective of the system as a whole by the effects of an impactful trading strategy. A more effective trading strategy would incorporate a shorting side as well, though ultimately this isn't necessary in order to obtain a necessary indication of efficacy for the system (and conceptually, a consistently losing long strategy would be of interest in any case).

It is important, in the interest of effective optimization and development, that the pattern recognition in the prediction portion of the system is not tightly coupled with making it profitable. With this in mind, the modularity of the system is continued, with a distinct separation between the prediction signal and the MMS implementation which relies only on the predicted prices of each stock for a time point. The comparisons for the MMS are made against a benchmark of the same MMS, but with perfect information. This allows an indication for how effective the prediction system is (and need be) in order to generate comparable returns.

An effective production trading strategy would be likely to include stop losses or pyramiding stop losses for effective P&L optimization. An ideal implementation, and possible area for further work, would include an MMS strategy where the bands for this are defined using a machine learning technique (rather than being chosen from domain knowledge or heuristics).

The calculated variables used by the MMS are fully detailed in Section 4.6.

5.12 Probability of Backtest Overfitting

The CSCV and PBO parts of the system are essentially just an implementation of Algorithm 6 detailed in Section 4.7, though with a somewhat novel application to the predictive network and MMS combination. The CSCV process uses the IS and OOS returns from the MMS, which in turn used the prices from the predictions network, which then constitutes the M matrix used by the algorithm. Conceptually, the whole system comes into place here, as the results from the CSCV process are now indicative of not only backtest overfitting in the trading strategy, but also in the prediction network and without having to consider the impact of the many configuration tests for feature extraction.

5.13 Deflated Sharpe Ratio

The DSR calculations are a straight forward implementation of the process described in Section 4.8, with only minor changes from the authors recommendations. Unlike the CSCV process, the DSR calculation only uses returns generated from the predictive model and MMS on OOS data. As with the CSCV & PBO calculations, the DSR now offers an effective assessment of the experimentations results and their legitimacy. The value of a modularised approach is highlighted again, where the DSR process is not coupled to any aspect of the neural network training.

6 Software Libraries and Development

A significant aspect of this dissertation was the implementation of software libraries that fulfilled the criteria of generalised training of neural networks, an implementation of the full process as described later in Section 4.1, the creation and management of database records for analysis and an extensive set of diagnostic tools in order to assess performance. This section details the implementation choices as well as the final libraries which were produced.

6.1 Programming Languages

The libraries developed were primarily written in Julia, a relatively new scientific computing language (initially developed in 2009) [37, 18]. The main motivation, both for Julia as a language as well as choosing it for this task, is its efficiency and speed. Julia was created with high performance tasks in mind, and with its use of a Just-In-Time (JIT) compiler, can approach similar benchmarks to C [95]. This stands in stark contrast to some of the more popular analytical languages used, such as R or Python, which often suffer from performance issues. In the context of a project which required extensive processing power, it was natural to prioritize this computational efficiency.

Julia's focus on technical computing is emphasised with its built in support for mathematical and statistical work, composable functional base and dynamic and optional typing schemes. Its ability to fulfil general purpose programming, familiar syntax (which also works effectively for mathematical commands) and its interactive (REPL) command line also make it a practical choice for the task at hand [95].

SQLite was chosen as the database management language. Relational schemas were a fitting choice for the nature of the data being captured, and SQLite offers a fast, effective and free implementation of SQL.

6.2 Data Generation & Processing

Data processing libraries were implemented to offer configurable processing for the steps outline in Section 3. The `DataGenerator` module [27] implements Geometric Brownian Motion (GBM) generation for a set number of steps and assets with their mean and variances specified.

The `DataProcessor` module [28] offers a more extensive set of operations in order to implement the processing laid out in Section 3.1. The different scaling techniques (Normalize, Standardize, Limited-Normalize and Limited-Standardize) are implemented, as well as the methods to reverse scaling and reconstruct price predictions to the original format. The log differencing, aggregation of past and future horizons as well as dataset partitioning is also

made available here, as per methodologies in Section 3. The module also includes dataset encoding through SAE networks, and adding Gaussian noise for the purposes of denoising training, as per Section 4.4.3.

6.3 Network Training

Neural networks were implemented with highly configurable training, such that the parameters are easily specified within Julia types [39] and then passed onto the training functions. The parameters are grouped accordingly to the different aspects of the training that they pertain to.

The network structures are easily configurable in terms of layers and layer sizes, as well as having the activation functions specified at each layer (i.e. Linear, Sigmoid, ReLU, LeakyReLU, Softmax, Tanh as described in Section 4.2.2) [20]. The network weight initialization is also specifiable, with the noted initializations in Section 4.5 available: Normal Random, Xavier, He, He-Adj [34].

The Stochastic Gradient Descent (SGD) and Contrastive Divergence-1 (CD-1) learning algorithms, as per Sections 4.2.3 and 4.3.2, can be specified according to minimum and maximum learning rates, and learning rate epoch cycles (as per the learning rate scheduling in Section 4.2.6). Training length can be specified in terms of maximum training epochs or a custom stopping function, which may rely on the Cost function hitting a particular point (with Mean Squared Error, Cross Entropy Error, Log Likelihood Error being made available [24]). Learning optimization hyperparameters for L1 Regularization or Denoising are also set here (implemented as per Sections 4.2.5 and 4.4.3). Dataset usage in terms of training / testing splits can also be specified accordingly.

The Online Gradient Descent (OGD) training parameters, as per OGD learning in Section 4.2.3, are specifiable through the learning rate and cost functions available.

The `NetworkTrainer` module [35] then offers 3 primary methods, given the relevant parameter configurations and dataset:

1. Train a Feedforward Neural Network, using variance based weight initializations.
2. Train an SAE, using variance based weight initializations.
3. Train an SAE, using RBM based pre-training for weight initialization.

These functions are supported by the following learning algorithm modules: SGD [38], RBM [36] and `GradientFunctions` [33].

6.4 Process Implementation

The process implementation, as described in detail in Section 4.1, is largely implemented in the `ExperimentProcess` module [31].

The `RunSAEConfigurationTest` method uses the `SAEExperimentConfig` Type to wrap up all necessary configurations and with a passed dataset runs through the following steps:

1. Either generate or process the raw dataset, according to the specified configuration.
2. Train the SAE, either by RBM or variance based weight initializations.
3. Pass back the SAE with original and reconstructed testing datasets.
4. Store the SAE as a bson object to be used later.

The `RunFFNConfigurationTest` method similarly uses the `FFNExperimentConfig` Type and a passed dataset to run through the following steps:

1. Either generate or process the raw dataset, according to the specified configuration.
2. Encode the datasets for the different steps of the process using the specified SAE.
3. Train the FFN using variance based weight initialization and SGD.
4. Use the FFN to generate predictions for IS data, reconstruct them and record them in the database.
5. Train the FFN using OGD on OOS data.
6. Use the FFN to generate predictions for OOS data, reconstruct them and record them in the database.

Two further modules allow the exploration of the configuration space, such that diagnostics can be performed on different aspects of the training. The `ConfigTestsFFN` [22] and `ConfigTestsSAE` [23] modules make use of the `ConfigGenerator` module [32] in order to generate a full grid configuration space for a given range of values for any chosen parameters, as per Section 5.3. Each of these combination configuration sets is then run as per the processes detailed above, with the various results recorded as usual.

6.5 Process Reproducibility

As noted in Section 5.4, it was ensured that the full process and results were reproducible. A Mersenne Twister pseudorandom number generator was set with a particular seed, which is recorded in the `dataset_config` schema in the database. This seed is propagated through from the SAE training process to the FFN training process. Consequently, any configuration set with the same parameters and random seed can be used to reproduce the results presented in this paper and otherwise.

6.6 Database Implementation

As noted, the database platform chosen was SQLite, with Julia modules handling the creation and management. The `DatabaseCreator` module [29] creates the database with the schemas noted in Table 1.

| Schema Name | Description |
|-------------------------|--|
| configuration_run | The primary record for any experiment process |
| dataset_config | The dataset configuration that may relate to an experiment |
| network_parameters | The network configuration for an experiment |
| training_parameters | The SGD/RBM/CD training configuration for an experiment |
| epoch_records | Details relating to ongoing training performance for the duration of an experiment |
| backtest_results | Predictions for IS data |
| prediction_results | Predictions for OOS data |
| cscv_returns | MMS level returns by timestep for an experiment |
| cscv_cost_returns | MMS level returns by timestep for an experiment with cost accounted for |
| config_oos_pl | The total OOS Profit & Loss for an experiment |
| config_oos_pl_cost | The total OOS Profit & Loss for an experiment, with cost accounted for |
| config_oos_sharpe_ratio | The OOS Sharpe Ratio for an experiment |
| config_confusion | The percentages of correct trades made for an experiment |

Table 1: Database Schema Descriptions

The `DatabaseOps` module [30] handles the creation of records for these schemas, as well as the writing and reading of bson files which are used to store actual networks.

6.7 Diagnostic Libraries

The diagnostic implementations were focused on 2 primary themes: Exploratory Data Analysis (EDA) through the use of visualizations of network results

through configuration spaces, and formalised testing in the form of PBO and DSR.

The EDA makes use of the PlotlyJS library [83], and allows the net performance of any set of networks to be plotted along a particular dimension in their configuration space. In the case of a set of SAE networks, this would typically be the MSE scores, and in the case of predictive FFN networks, this would typically be the P&L values generated from the MMS. A full list of diagnostic charts can be viewed in Appendix 11.4.

The CSCV and PBO methodologies can be found in the `CSCV` module [21], which encapsulates the generation and assessment of the logit distributions, as well as the PBO calculation.

6.7.1 DSR Libraries

Unlike the rest of the framework implementation, the DSR process was written in Python [47]. This was done so the code provided by Lopez de Prado and Lewis [81] for the ONC algorithm (see Section 4.8.1) could be used. The `DSR_PradoLewis` module [80] contains all the python code used which was presented in [81]. Modules `DSR_dataproc` [25] and `DSR_proc` [26] contain the code for returns processing and DSR calculations, respectively.

7 Datasets Used

7.1 Actual Datasets

Several datasets have been used using JSE closing price relative data for 2003-2018. They were processed following the steps set out in Section 3 and with a 60/40 split on the Training/Prediction datasets.

7.1.1 “Actual10”

This is the primary closing price dataset that has been used through out the experiment process, which focused on choosing more prominent stocks from multiple sectors. The price fluctuations can be seen in Figure 6.

| Code | Company | Sector |
|------|----------------------------------|------------------------|
| AGL | Anglo American | Resources |
| BIL | BHP Billington | Resources |
| IMP | Impala Platinum Holdings | Resources |
| FSR | FirstRand Limited | Finance |
| SBK | Standard Bank | Finance |
| REM | Remgro Limited | Finance |
| INP | Investec | Finance |
| SNH | Steinhoff International Holdings | Retail |
| MTN | MTN | Communication Services |
| DDT | Dimension Data | Tech |

Table 2: Assets in the “Actual10” dataset, from 2003-2018.

7.1.2 “Scaling10”

This dataset was used specifically to test scaling techniques, and consisted of the following JSE closing price relatives: ACL, AGL, AMS, AOD, BAW, BIL, BVT, CFR, CRH, DDT. The price fluctuations can be seen in Figure 7.

7.1.3 “AGL” and “AGL&ACL”

The AGL and ACL data from JSE closing price relatives was used for some limited framework testing. The price fluctuations can be seen in Figure 8.

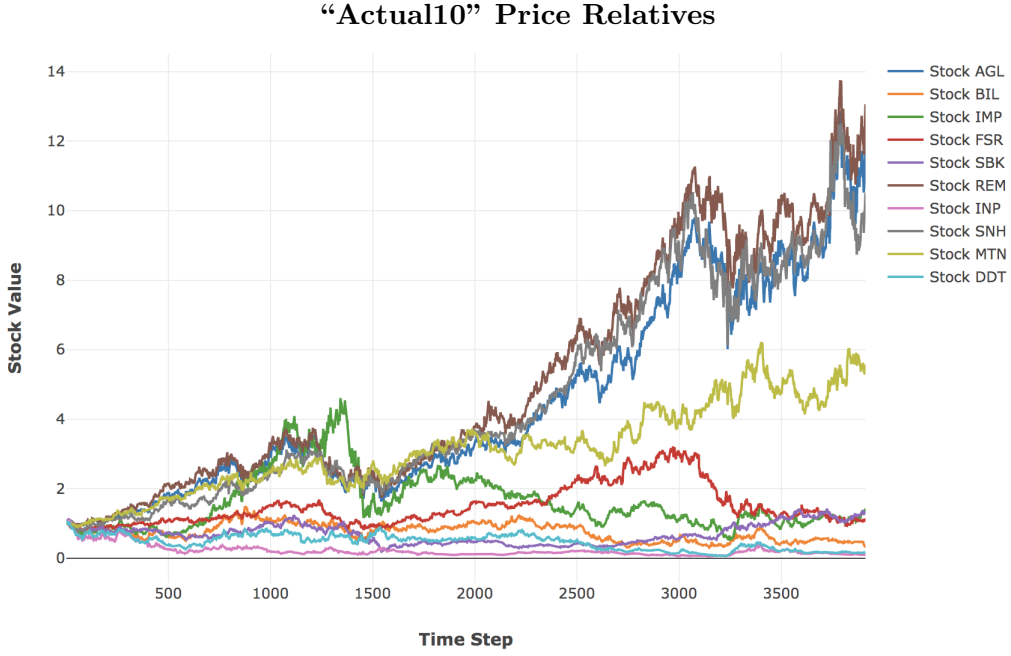


Figure 6: The primary dataset for actual price relatives is displayed here, as noted in Table 2. There is a varied collection of behaviours amongst assets, with upwards, downwards and sideways trends over the full period, as well as assets with very high and low variances. The dataset contains assets from most major sectors, and show some strong correlations amongst groups of assets (e.g. AGL, REM and SNH).

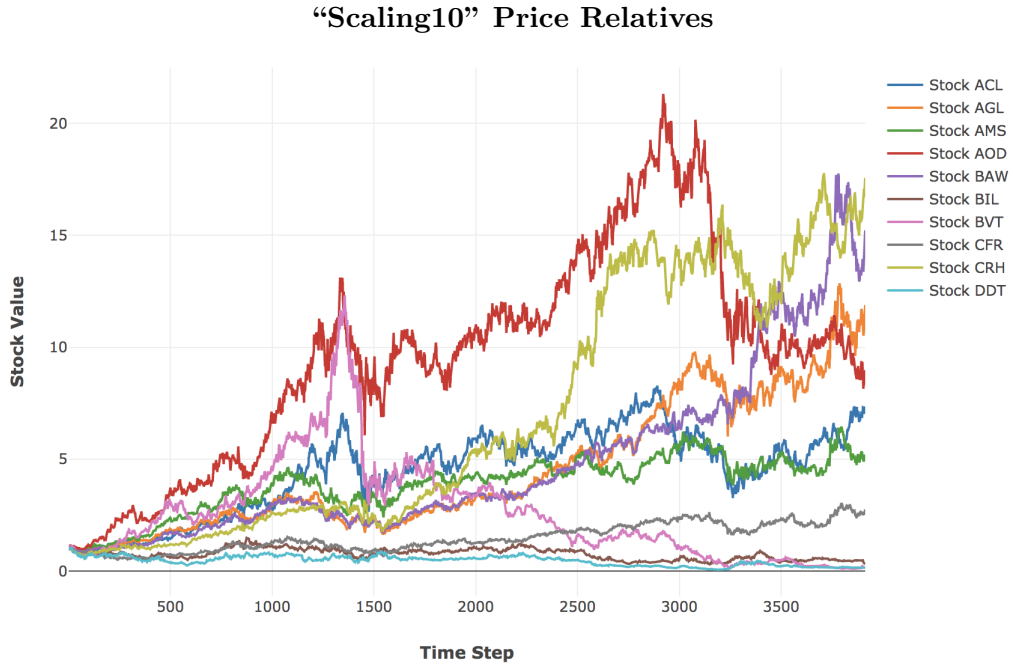


Figure 7: The figure here shows the price relatives for the “Scaling10” Dataset as detailed in Section 7.1.2. The group of assets show a wide variety of behaviours, which was appropriate for the testing of training techniques on SAE networks. These results can be seen in Section 8.7.2.

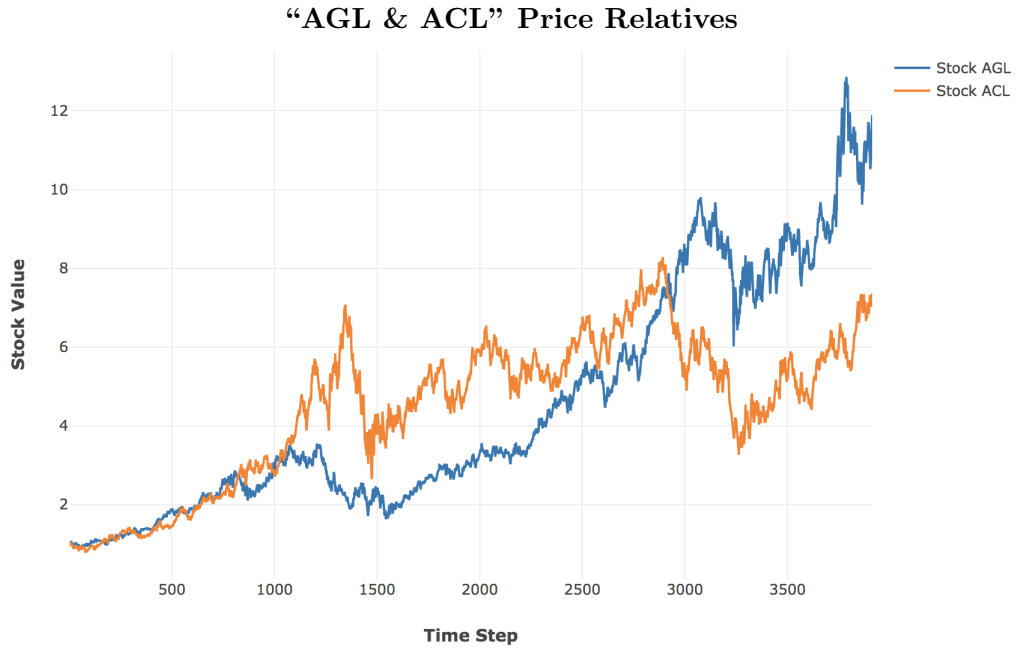


Figure 8: The figure here shows price relatives for AGL and ACL which make up the “AGL” and ‘AGL&ACL’ datasets (7.1.3, 7.1.3), which were used for some limited testing.

7.2 Synthetic Datasets

Data was generated and scaled, as per the methods detailed in Sections 3.2 and 3.1.2. The sets were generated with the following configurations, each for 5000 timesteps and with a 60/40 split on the Training and Prediction sets.

7.2.1 “Synthetic6”

The Synthetic6 dataset was configured to represent a combination of upwards, downwards and sideways Trends, each with high and low variance variations.

7.2.2 “Synthetic10”

The Synthetic10 dataset was configured to represent a wide array of behaviours, including very high (positive and negative) mean stocks, as well as much lower mean stocks (which may be more representative of typical behaviour). These were chosen to make sure the network learning is able to differentiate and correctly learn across different asset categories.

| Trend Category | Variance Category | Trend Mean | Variance |
|-----------------|-------------------|------------|----------|
| Strong Upward | High | 0.9 | 0.5 |
| Strong Upward | Low | 0.9 | 0.2 |
| Upward | High | 0.05 | 0.4 |
| Upward | Low | 0.05 | 0.1 |
| Strong Downward | High | -0.8 | 0.55 |
| Strong Downward | Low | -0.8 | 0.15 |

Table 3: Assets in the “Synthetic6” dataset, as detailed in Section 7.2.1.

| Trend Category | Variance Category | Trend Mean | Variance |
|-----------------|-------------------|------------|----------|
| Strong Upward | High | 0.9 | 0.5 |
| Strong Upward | Low | 0.7 | 0.2 |
| Upward | High | 0.05 | 0.5 |
| Upward | High | 0.05 | 0.4 |
| Upward | Low | 0.04 | 0.1 |
| Sideways | Low | 0.02 | 0.15 |
| Sideways | Low | 0.01 | 0.05 |
| Downwards | Low | -0.1 | 0.2 |
| Strong Downward | Low | -0.4 | 0.15 |
| Strong Downward | High | -0.8 | 0.55 |

Table 4: Assets in the “Synthetic10” dataset, as detailed in Section 7.2.2.

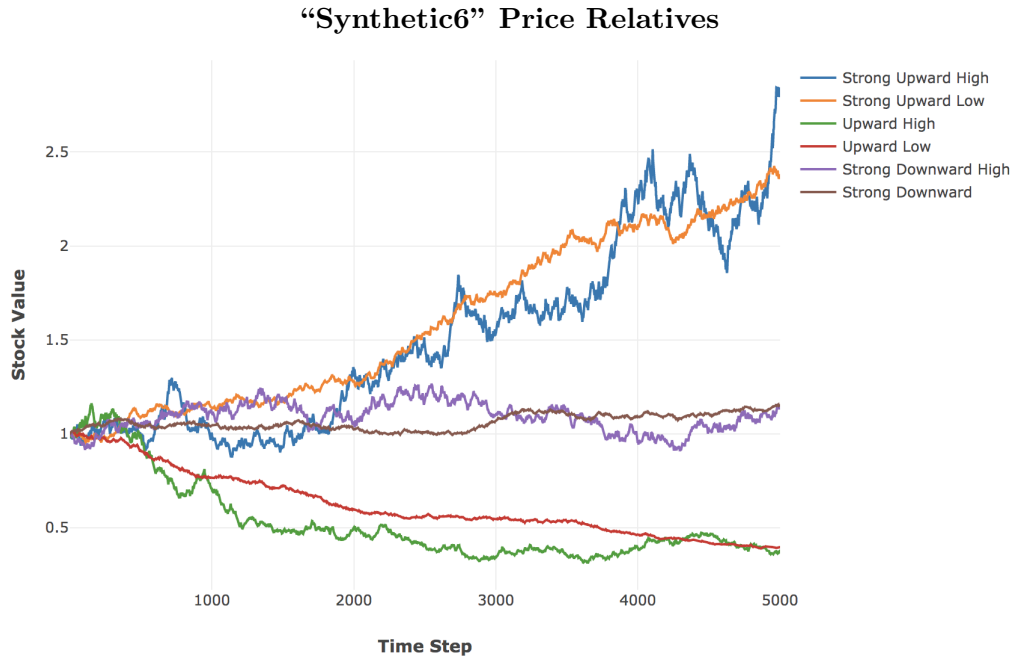


Figure 9: This figure show the price relatives for the Synthetic6 dataset (Section 7.2.1), generated for 5000 days and with the attributes in Table 3. Assets were generated for high and low variances with upwards, downwards and sideways trends.

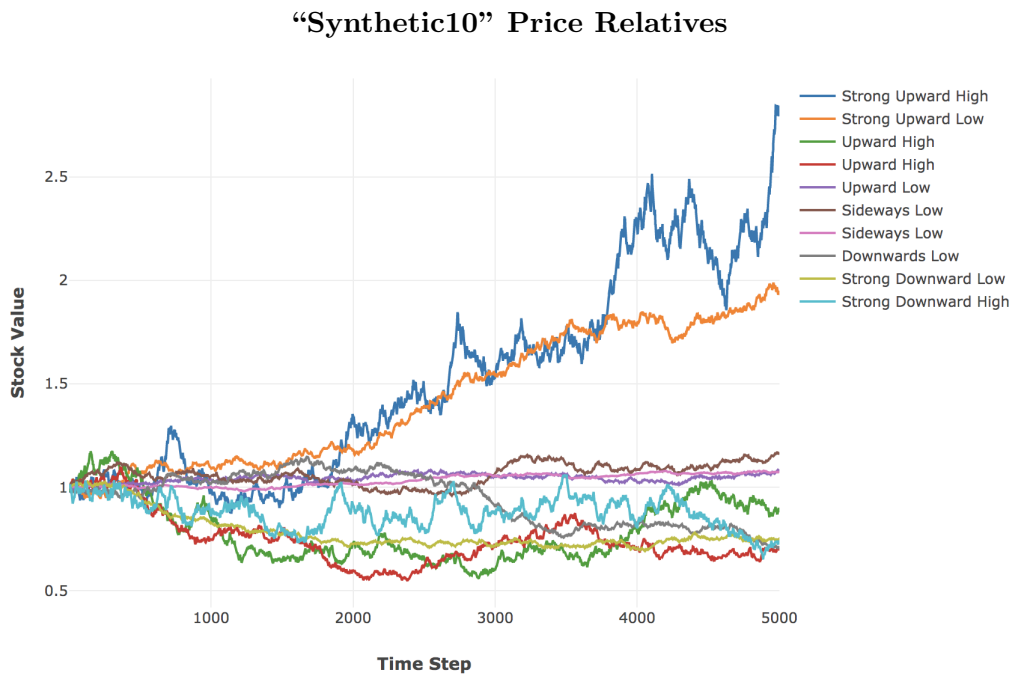


Figure 10: This figure show the price relatives for the Synthetic10 dataset (Section 7.2.2), generated for 5000 days and with the attributes in Table 4. A wide range of means and variances were chosen, such that the data might be representative of an non-synthetic dataset.

8 Results

8.1 Introduction

This section offers a full discussion of the results seen at all stages in the framework, providing numerous takeaways both in terms of technical training as well developing a perspective on the phenomenology of financial markets, and how these influence mechanistic learning approaches to pattern prediction.

Section 8.2 discusses the primary determinants of OOS P&L seen in actual data results, covering data horizon aggregations, SAE feature reduction and the OGD learning phase. It's shown that data horizon aggregations form the primary determinant of the prediction strategies learnt, and that SAE networks learn different classes of features according to the encoding size (which may differ in suitability for different prediction strategies). These are both considered in the context of the online OOS learning, which proves to be critical in effective learning. This is expanded on in Section 8.3, which shows the negligible impact of extensive training on historical data, noting that reducing training epochs and datasets has limited effect, and that the online learning phase is most impactful for OOS P&L.

Section 8.4 discusses network weight initialization techniques, noting their importance in context of financial time series where the value of extensive batch training has been shown to be of limited value (or even detrimental to performance).

Section 8.5 discusses the nature of Synthetic data, and how it differs in the key OOS determinants. The fundamental differences in data distributions result in P&L performing better over longer data horizons (which is not definitive in actual data), and less complex features being learnt in SAE networks.

The complexity of actual financial time series is discussed further in Section 8.6, where results for data scaling and SGD learning optimizations are shown to be affected by the unstable nature of dynamics in financial markets.

Section 8.7 gives an overview of the more typical network training components such as layer sizes and activation functions.

The financial returns and Sharpe ratios from the prediction networks, as used by the MMS, are discussed in Section 8.8 with overall distributions shown with the relative benchmark. These results are validated, showing a low likelihood of backtest overfitting in Section 8.9, and showing a confidently positive Deflated Sharpe Ratio in Section 8.10.

Lastly, Section 8.11 summarises the results presented for synthetic data throughout the framework, and notes it's limited value in assessing behaviours

for actual data.

8.1.1 Technical Notes

While the predictive networks are trained using an MSE loss function, the performance will mostly be reported on according to the P&L they were able to achieve through the MMS. Looking at Figure 11, we can see that while there is a strong correlation between predictive accuracy and P&L achieved, it is not absolute and there are many “worse” configurations according to OGD MSE which have higher P&L. This is due in part to OGD’s potential to oscillate wildly in the beginning of training while it adjusts, and also representative of lower variance models being able to achieve competitive P&L. Also, in consideration of the task at hand, P&L is the primary metric of interest and so is a sensible analysis choice. It is worth noting though that this P&L is a relative unit measurement, rather than a particular currency (as noted in Section 3.3), and that the MMS, as described in Section 4.6, only trades 1 stock unit at a time, and so any P&L figures are relative indications rather than absolute limits. It is also usually reported without capital and trading costs (as per equation (52)) applied, though these costs are taken into account for the PBO and DSR validations.

The results for synthetic data are compared against actual data when appropriate, such that it might guide when synthetic data can and should be used for parameter space exploration (as discussed in Section 5.5). These results are discussed more completely in Sections 8.5 and 8.11.

Sample sizes for some configurations may differ greatly across results (particularly as results are aggregated across training sets and phases), though these are noted in the figures as well as the configurations in the appendix.

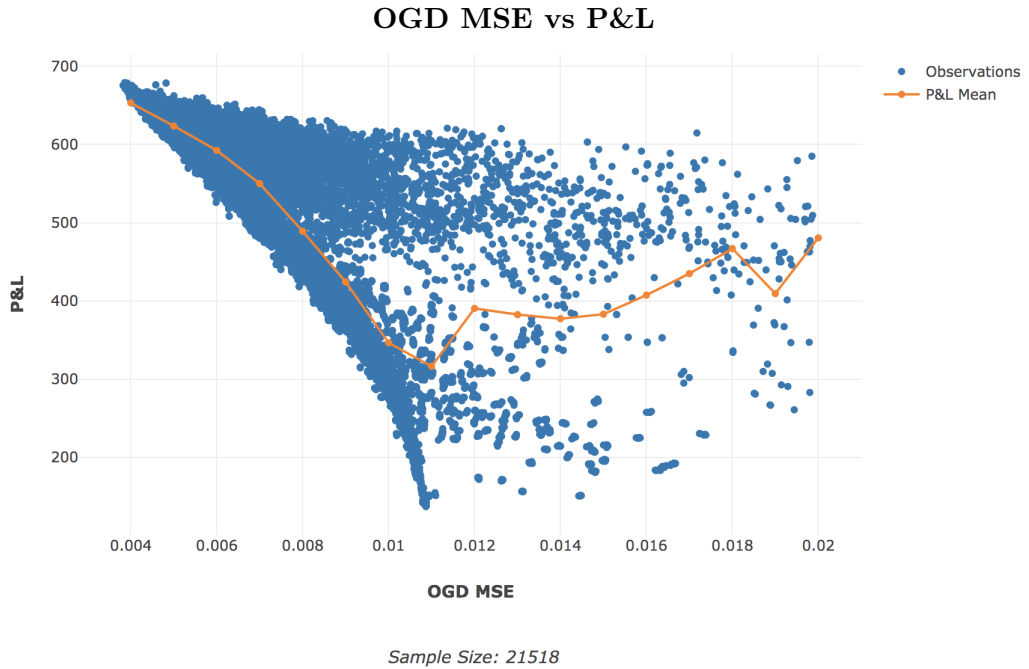


Figure 11: The figure here shows the paired OGD MSE score and OOS P&L achieved for the trials run. There is a very strong correlation with $\rho = -0.74$, indicating the relationship of P&L increasing as OGD MSE decreases (or, predictive accuracy increases). As can be seen however, there are still many configurations which outperform in P&L despite having a worse OGD MSE score (reasons are noted above in Section 8.1). As a result, and with the end goal in mind, P&L is chosen as the reporting primary assessment metric for the analyses on predictive networks.

8.2 Primary Determinants of OOS P&L

The initial expectations of the process implemented was that the IS batch training using SGD for the predictive network would have a significant influence on priming the network through the use of historical data, and in doing so affect OOS P&L performance. The results however, indicate that the effects of IS training has relatively limited effect, highlighting the complexity and dynamic nature of financial time series, where past relations and behaviours are not necessarily indicative of present state. These issues are discussed more extensively in Section 8.3, however the follow through is that the primary determinants of OOS P&L are those which are present in the OGD learning phase: the OGD learning rate, the data horizon aggregations and the SAE feature reduction.

8.2.1 Effects of Data Horizon Aggregations

Input data was scaled to 3 different configurations in order to assess the effects of shorter and longer configurations on both SAE MSE performance, as well as the predictive P&L results. The configurations tested (in trading day window periods) were:

- Horizon Tuple 1. [1, 5, 20]
- Horizon Tuple 2. [5, 20, 60]
- Horizon Tuple 3. [10, 20, 60]

By way of example using the 3rd configuration: the implementation of this is such that at each time point considered by a network the log difference changes for the past 10, 20 and 60 days are available for each asset. This is described more extensively in Section 3.

The predictive strategies learnt by the networks were determined by the data horizon aggregation chosen: predictions using short term fluctuations (with horizons of [1, 5, 20] days) and predictions using long term trends (with horizons of [5, 20, 60] or [10, 20, 60]). The differentiation between these groups is shown more robustly in Section 8.10, where it is shown to be the primary clustering attribute for trade correlations. It's shown that using short term fluctuations is a less reliable strategy, with higher variance in the returns delivered, but it is also able to deliver the highest P&L when compared to the longer term strategies. This can be seen more fully in Figure 13.

The horizons are also shown to have notable impacts on the ability of the SAE network to reconstruct them. Lower variance in the shorter horizon aggregations result in easier replication, while longer horizons are more difficult (as indicated through MSE scores). These characteristics can be seen in Figure 12.

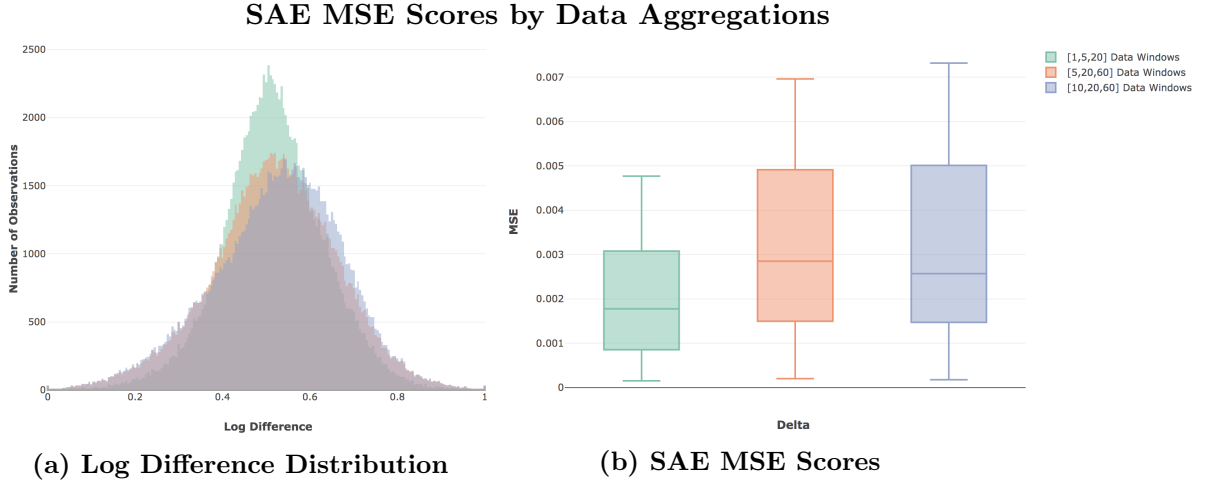


Figure 12: Dataset: Actual10 dataset (7.1.1), Configuration 12 (11.3.12)

Figure (a) shows the distribution of values to be replicated by the SAE for actual data. Variances are quite different across the configurations ($\sigma_{[1,5,20]} = 0.118$, $\sigma_{[5,20,60]} = 0.146$, $\sigma_{[10,20,60]} = 0.150$). Smaller data windows are less likely to capture larger fundamental price changes, thus leading to these lower variances. This in turn, makes for easier replication for the SAE networks due to less variety in the sample set, which is seen in Figure (b) with the noticeably better performance in the [1, 5, 20] configuration.

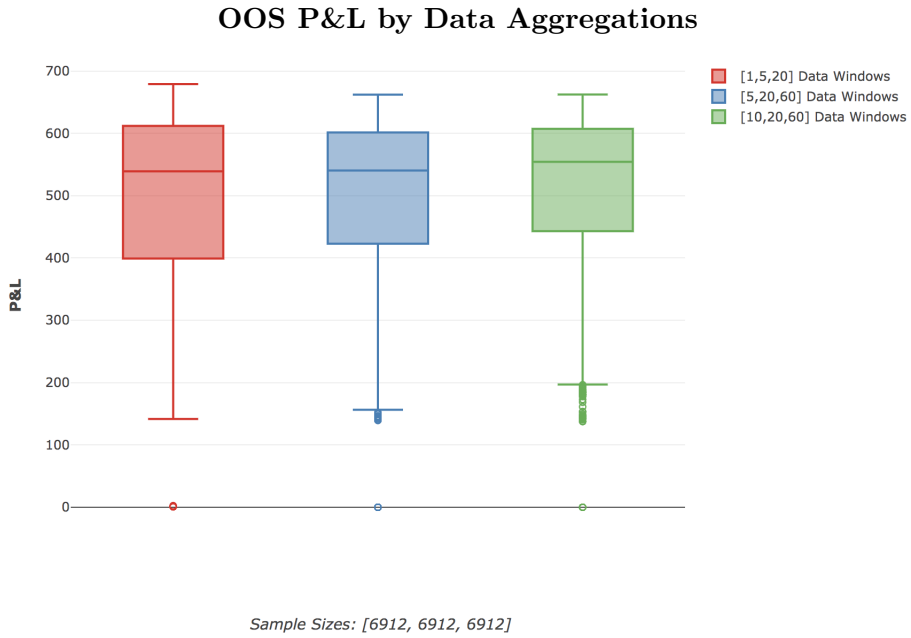


Figure 13: Dataset: Actual10 dataset (7.1.1), Configuration 13 (11.3.13)

The OOS P&L by data horizon configurations show a more complex view than the SAE performance. At a mean level, predictive performance is increasing as the span of the windows increase, but with a decrease in the lower and upper bounds. The highest P&L occurs for the shortest window configuration ([1, 5, 20]). This is a clear view on a consistent dynamic in the results: focusing on short term fluctuations for predictions has a higher risk and reward, whereas focusing on longer term trends with the longer horizons offers a more reliable, though less profitable, return.

8.2.2 OGD Learning Rate

The OGD learning rate has the most distinctive impact on P&L performance, as can be seen in Figure 14. The large differences between rates further highlights the unstable nature of financial systems. If dynamics were consistent across time, we would not expect to see such large changes in OOS performance due to larger learning rates. That we do shows how the networks ability to adapt to more recent information is critical in determining performance.

The effect of the OGD learning rate on networks can once again be separated by the prediction strategy, with lower and higher learning rates performing better for different strategies, which can be seen in Figure 15.

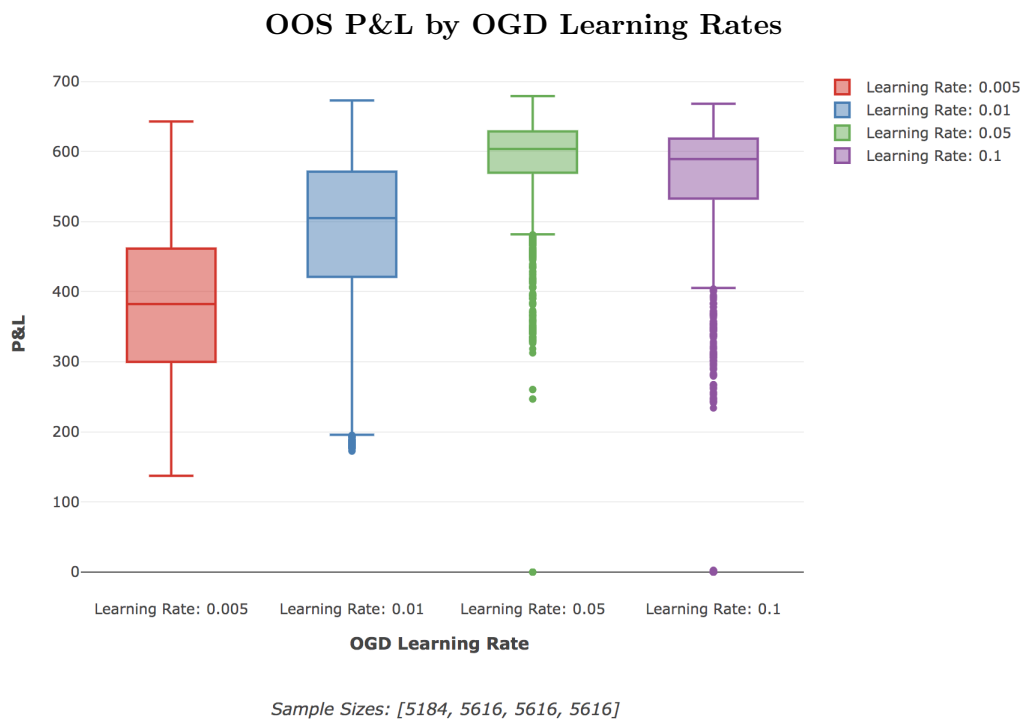


Figure 14: Dataset: Actual10 dataset (7.1.1), Configuration 13 (11.3.13)

The OOS P&L performance for OGD learning rates is expectedly non-linear, with performance increasing significantly from 0.001 up until 0.05 where the network, and degrading thereafter as the network overcorrects to noise and short term changes picked up in the online learning period. The higher learning rates, with networks more able to adapt to changing signal dynamics also result in significantly lower variance in the P&L delivered.

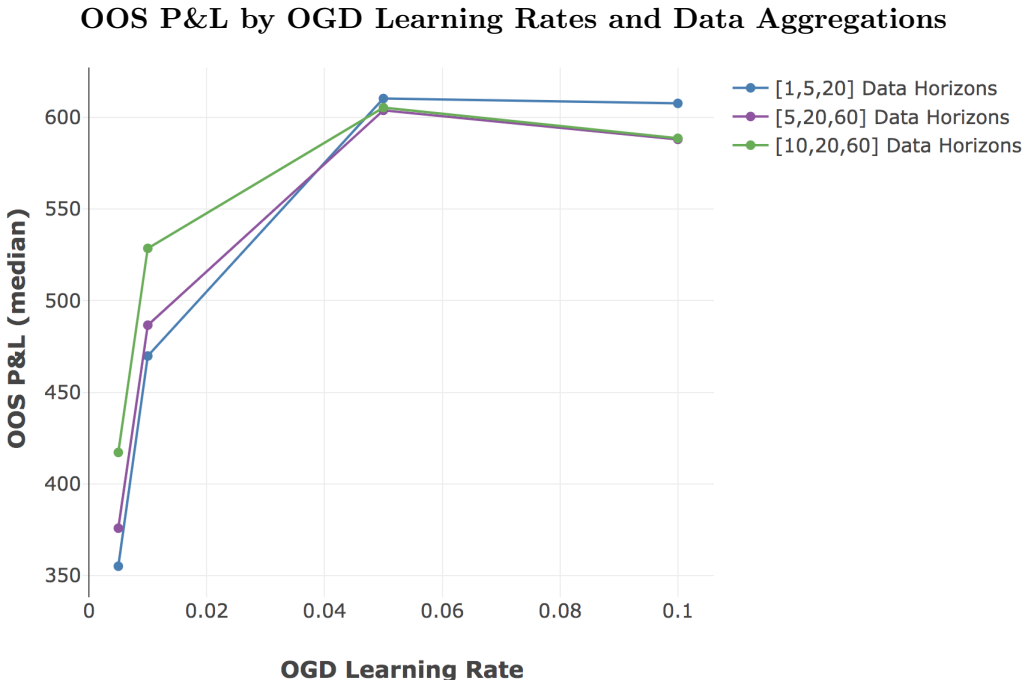


Figure 15: Dataset: Actual10 dataset (7.1.1), Configuration 13 (11.3.13)

The median OOS P&L by learning rate and data aggregation highlights the nature of the different prediction strategies. At lower learning rates, networks using long term changes and trends perform better as they benefit from smaller adjustments from one observation to the next. At high learning rates, networks using short term fluctuations perform better as they are able to more quickly adapt to changing dynamics and signals.

8.2.3 Feature Selection

Feature selection through SAE dimensional reduction proves to be both possible and effective, though with complex behaviours and analyses. An important aspect to note is that the SAE networks were only trained on the first portion of IS data, and not updated afterwards. In light of changing dynamics in financial markets then, an effective SAE feature reduction in this process is an optimization that may be limited to a certain time period and may not generalise well in a different context (i.e. OOS). Inspection of the nature of features learnt is somewhat difficult, though results suggest that the features can generally be categorised into 2 groups: larger encodings (25, 20, 15) which perform the equivalent of denoising or smoothing, and smaller encodings (10, 5) which perform more robust feature selection of legitimate properties ¹.

While the OOS performance of the larger encoding sizes behave expectedly for the most part, the SAEs with encoding sizes of 5 and 10 are more inconsistent. In line with the view of changing dynamics within financial markets over time, it would seem that the SAEs with encoding of 10 have overfit to

¹Input data was 10 assets with 3 horizon aggregations each, resulting in an input size of 30 at each timestep

some particular features. These appear to perform well for strategies focusing on long term trends, but are seemingly pathological for the strategies focusing on short term fluctuations. The SAEs with encoding size of 5 results in more dependable performance, presumably because the small encoding layer acts as a form of regularization and so forces the SAE to learn more consistently generalisable features. These dynamics are explored more in Figures 18 and 17.

The most noteworthy results are the SAE networks with encoding size of 5 which have learnt generalisable features for 10 assets, each with 3 data aggregations. Their performances are often on par or better than the higher encoding sizes, or no encoding at all, as can be seen in Figure 17a. The performance of these SAE networks, with an 83% reduction in input data, are clear evidence of the efficacy and potential of feature selection in financial times series.

IS SAE Performance for MSE and P&L by Encoding Size

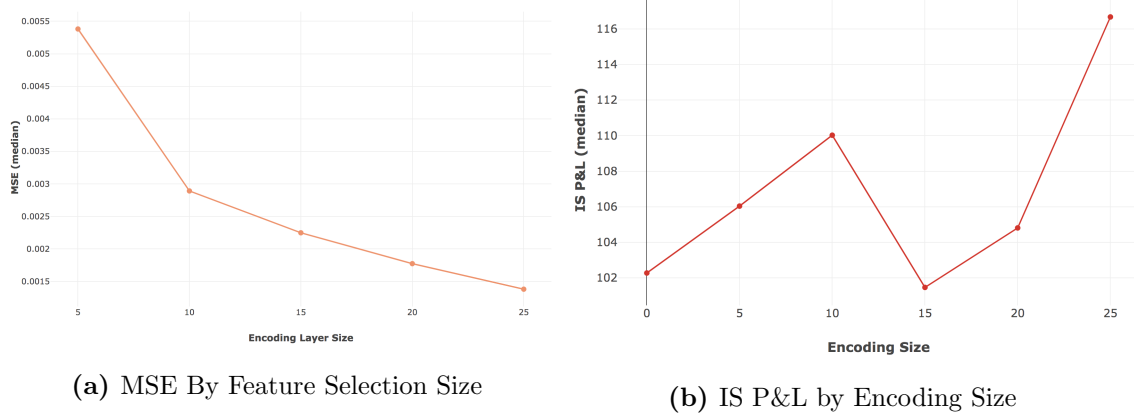


Figure 16: Dataset: Actual10 dataset (7.1.1), Configurations 11 and 12 (11.3.11, 11.3.12)
 Figure (a) shows the MSE scores at different encoding sizes, and while feature selection and reduction is possible through the SAE networks, the ability to reproduce input precisely does decrease monotonically with the encoding layer size. Figure (b) shows the IS P&L for the same groups, and provides a different assessment, showing a clear increase in P&L at the 5 and 10 encoding sizes ('0' indicates no feature reduction was done). This is indicative of the 2 different type of features being learnt: sizes 15, 20 and 25 are essentially denoising the data and so reproductive MSE is correlated to P&L performance; conversely, at sizes 5 and 10 the SAE begins learning more fundamental features of the data, at which point the relative reproductive MSE score is not a clear indicator for P&L performance trends.

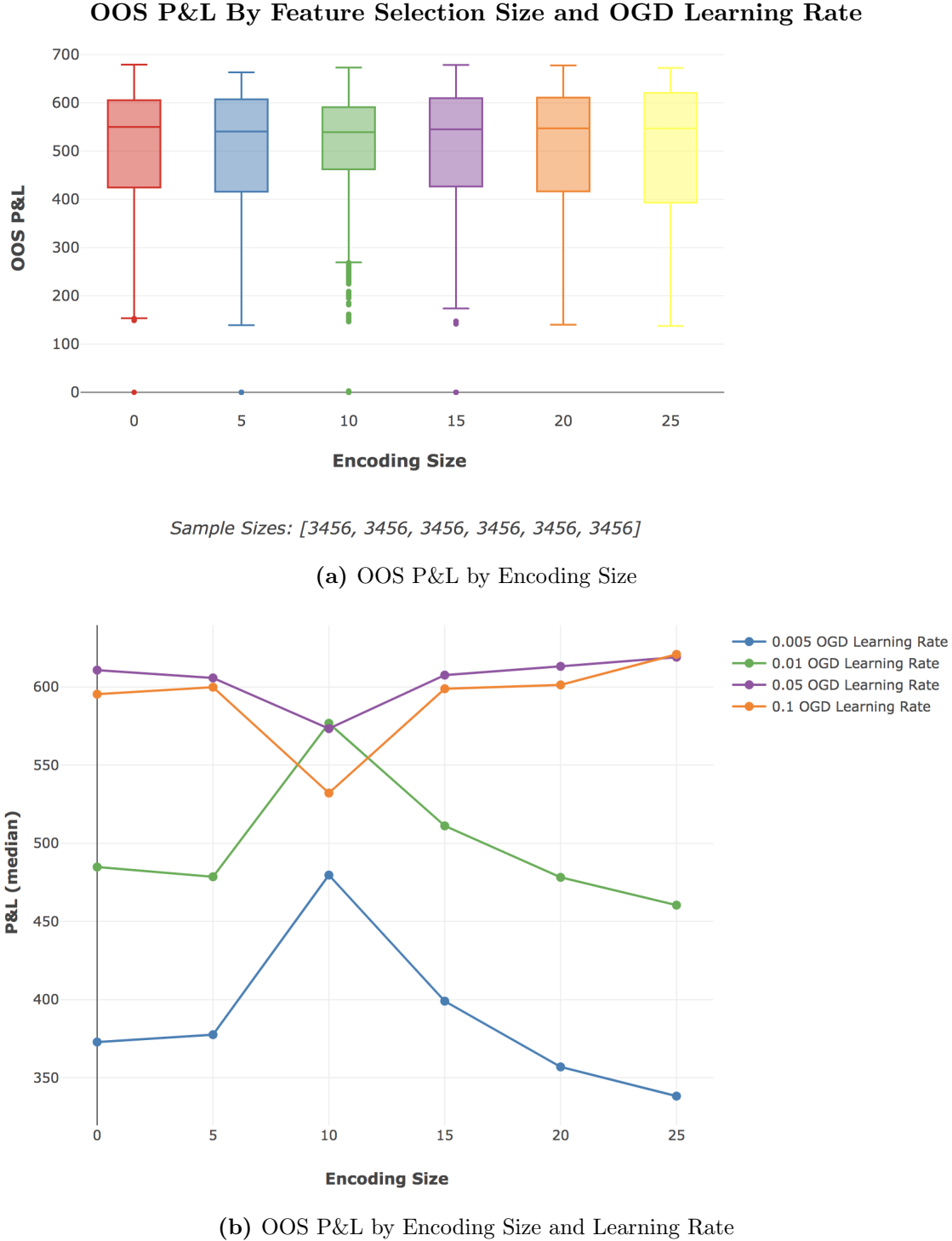


Figure 17: Dataset: Actual10 dataset (7.1.1), Configuration 11 (11.3.11)

Figure (a) shows the OOS P&L performance for all encoding sizes, with an encoding of 0 indicating no feature reduction being performed. It is interesting to note that at their best, almost all encodings were able to offer equitable performance. There is however a general variance reduction from 25 to 15, with 10 and 5 behaving somewhat differently. Figure (b) gives us far more insight into the dynamics causing the changing P&L. The lower learning rates (0.005, 0.01) perform best with strategies using long term trend pricing (as seen in Figure 15). The 10 feature encoding appears to have optimised specifically for this perspective, causing outperformance at the lower learning rates and causing detrimental performance at higher learning rates, which perform best with short term fluctuation strategies. The 15 to 25 encodings show a general association to the short term strategies, where higher encodings and higher learning rates offer the best performance. Notably, the 5 feature encoding offers the most consistent performance across learning rates, further emphasising the learning of generalisable features. These dynamics are explored further in Figure 18.

OOS P&L By Feature Selection Size, OGD Learning Rate and Data Horizons

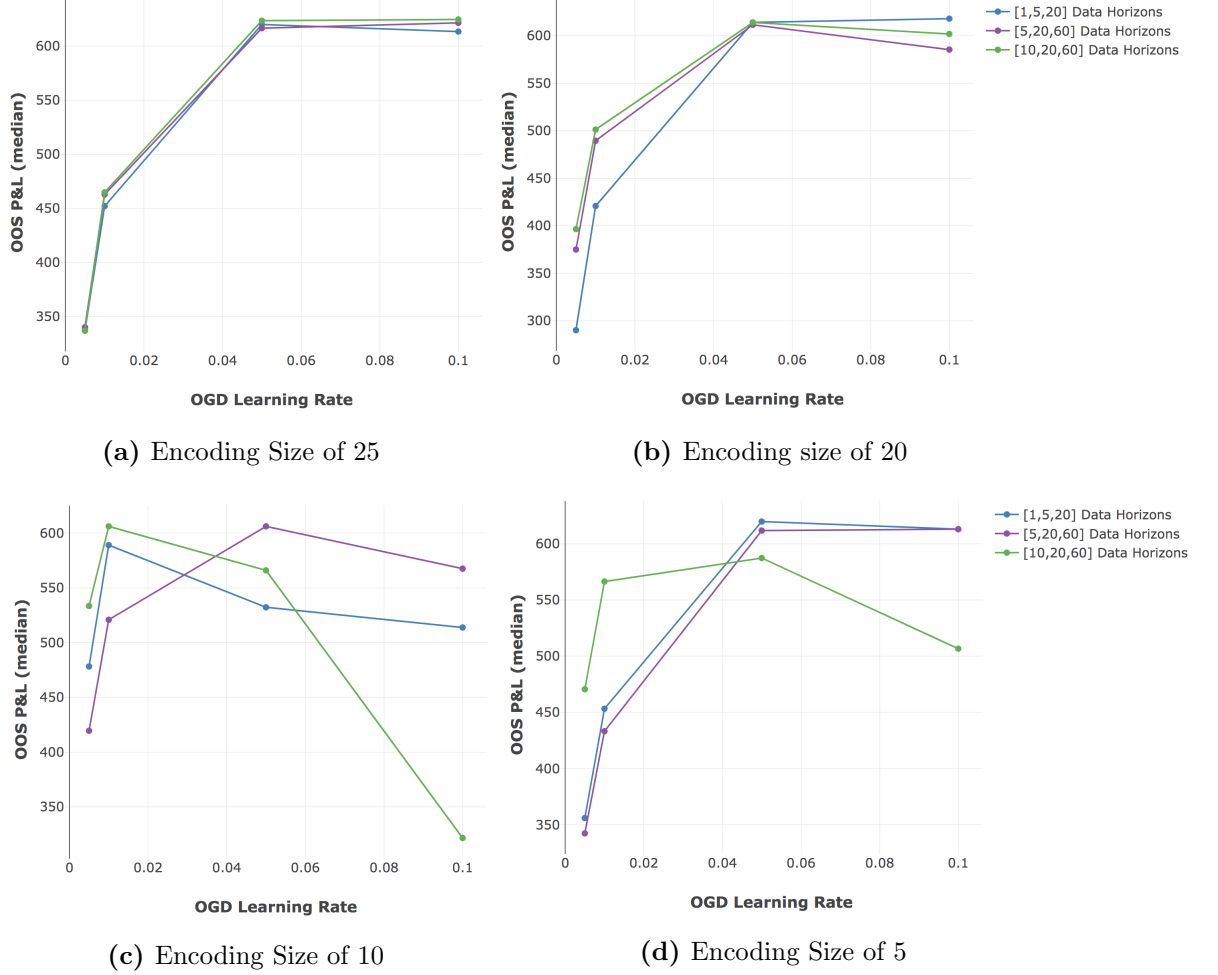


Figure 18: Dataset: Actual10 dataset (7.1.1), Configuration 11 (11.3.11)

The 4 plots above offer a cohesive view of all 3 primary determinants of OOS P&L. At encoding sizes of 25 and 20, which are largely smoothing the input, the feature reduction has less material impact and so the relation between data horizons and learning rates are more prominent. Longer horizons deliver higher P&L with lower learning rates (and so smaller adjustments), while short term horizons outperform with large learning rates (and so an ability to adapt quickly). The SAEs with encoding size 10 show the most inconsistent behaviour, clearly having overfit to the long term features. This results in high performance with the low learning rates and longer horizons, and extremely poor performance with higher learning rates and longer horizons. The encoding size 5 offers a more robust feature selection, resulting in the best of longer horizons at low learning rates, and the best of shorter horizons at larger learning rates.

8.3 Value of Historical Signal

Experimental trials were run to test the hypothesis that the amount of historical IS data available is of limited use, and that the real value is in broader current and cross sectional data. This idea is in line with the understanding that financial markets are inherently complex, adaptive and dynamic, as discussed more broadly in Section 2.1. With this in mind, and especially so in light of a fundamentally changing macroeconomic landscape, there is limited reason to believe that the functions and relations that may have governed the asset prices 10-15 years ago would still be in effect today. The P&L results shown in Figures 19 and 20 validate this and show that extensive training on past data may be akin to pre-training network weights at best, and counterproductive in overfitting to dynamics that no longer exist at worst. These findings fall in line with those found in Section 8.2, which highlighted the efficacy of prediction strategies using shorter data aggregation horizons over those using longer horizons.

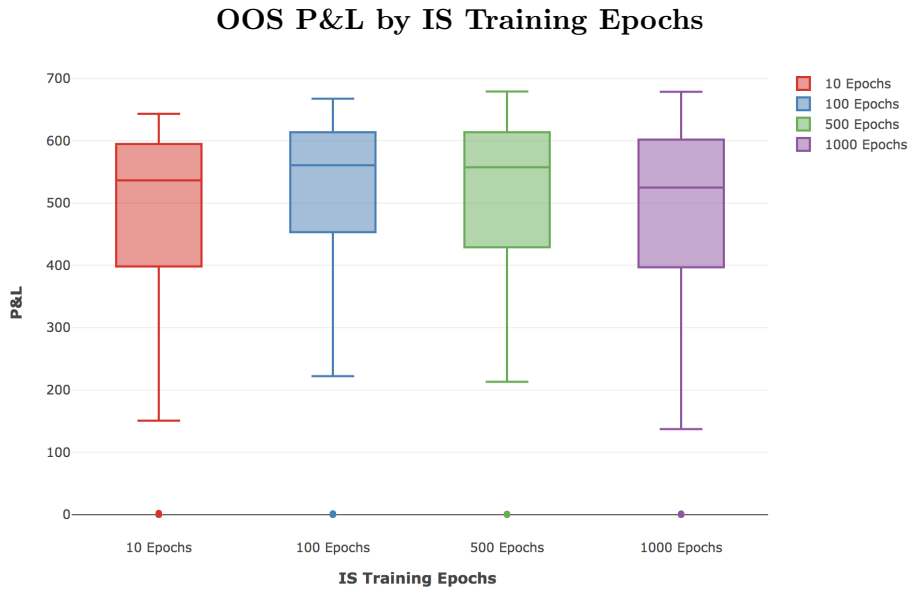


Figure 19: Dataset: Actual10 dataset (7.1.1), Configuration 13 (11.3.13)

The box plots above show OOS P&L grouped by the number of epochs in the SGD IS training phase (i.e. the number of times the IS data was trained on). In this set of configurations, 100 Epochs offers the best overall performance, and further training to 500 or 1000 epochs degrades performance due to the network overfitting on the IS data. The results here are noteworthy as they show that the benefit of historical data is limited - having a network become better at learning return relationships from 10 years ago is not leading to increased OOS P&L for more current data. The small difference in the upper half of observations between 10 and 100 Epochs further emphasises this point.

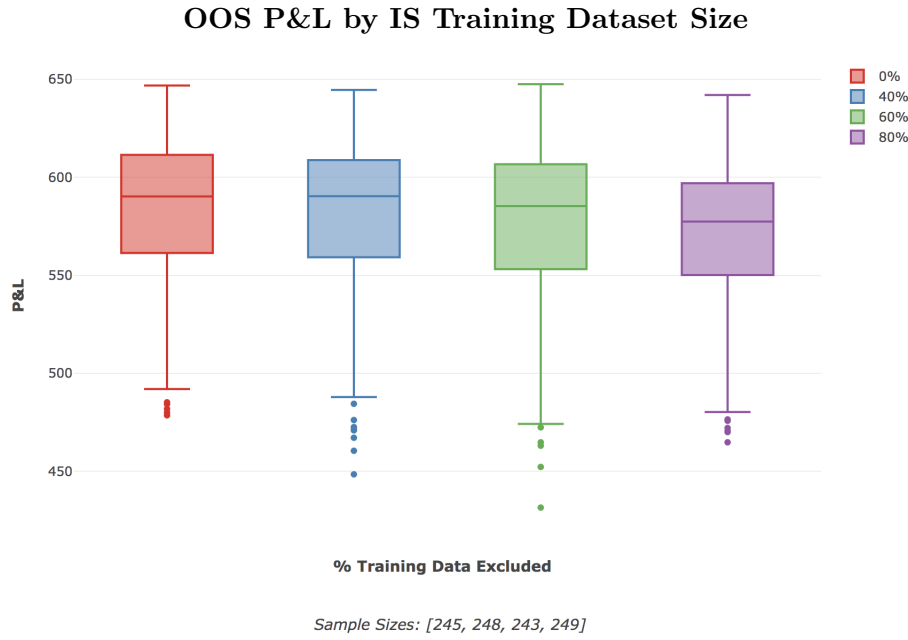


Figure 20: Dataset: Actual10 dataset ([7.1.1](#)), Configuration 16 ([11.3.16](#)) (some samples with 0 P&L were excluded for more effective visualization)

To further explore the effect of IS training on historical data, configurations were run with a percentage of the usual training data excluded, with the P&L results grouped above. The exclusion of up to 80% of the IS training data resulted in only a 2.2% drop in median OOS P&L for those networks. The training in these instances were not adjusted to increase the number of epochs according to the size of IS data, and so the configurations with more data excluded were also in essence trained less. These results, combined with those in Figure 19 show the limited use in training on historical data, and hence the far greater value in current cross sectional information.

8.4 Weight Initializaton Techniques

Neural network weight initialization has been one of the primary barriers to effective deep learning, with incorrect initializations leading to poor learning performance in deep networks. New techniques for initializing weights were one of the main reasons for the recent progress in the field [59]. Sections 8.2 and 8.3 clearly show that historical data and training are of limited value. The most profitable models learn quickly from recent data, and have had less training on historical data. The issue of weight initialization then is even more prominent when in the context of financial time series. The two most popular methods, RBM pre-training and Variance based initialization, have both been explored and are detailed below.

8.4.1 RBM Pretraining for Sigmoid Networks

While previously considered the best approach for training deep neural networks, the methodology of greedy layerwise RBM pre-training for Sigmoid SAE networks (as described in [59]) had detrimental effects on network performance, as seen in Figure 21.

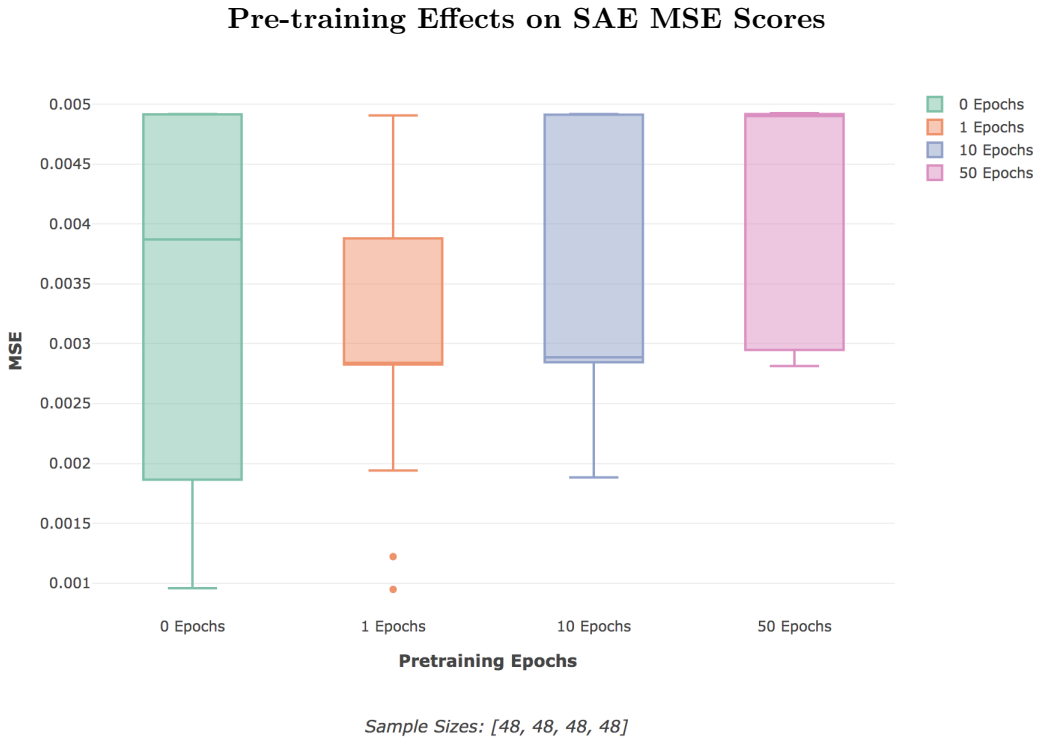


Figure 21: Dataset AGL&ACL (7.1.3); Configuration 6 (11.3.6)

The boxplots here show the summary of configuration performances, by minimum MSE achieved, grouped according to the number of pre-training epochs which the network had. There is an evident benefit to having no pre-training in this scenario as there is a clear decrease in performance as the number of epochs increase (the low value outliers that can be seen for the 1 epoch configuration were with learning rates which were low enough to approximate no epochs).

The RBM pre-training technique does assume that data is Independent and Identically Distributed (IID), and does ultimately traverse a different solution space and loss function. While it may be effective in some contexts, it was shown to result in a counterproductive exploration of the weight space for this non-IID dataset, and that ultimately the financial time series data is pathological for RBM pre-training. It may also again emphasise the value of more recent data over historical data ².

8.4.2 Variance Based Weight Initialization Techniques

More recent research has focused on the use of weight initialization using variance based methodologies, as discussed fully in Section 4.5. Our expectation, theoretically, is that the He initialization will generally outperform Xavier due to it being more appropriate for the ReLU activations being used. Additionally, in networks with varying layer sizes, we expect He-Adj and possibly Xavier

²The RBM greedy layerwise training implementation was effectively tested and validated on known datasets such as MNIST, example results for which can be seen in Section 11.1.2 of the Appendix

to outperform He which is subject to imbalanced initializations. Ultimately, He-Adj as presented in Section 4.5, should present the best of both for an initialization that is suited to Leaky ReLU activations and the varying layer sizes found in SAE networks.

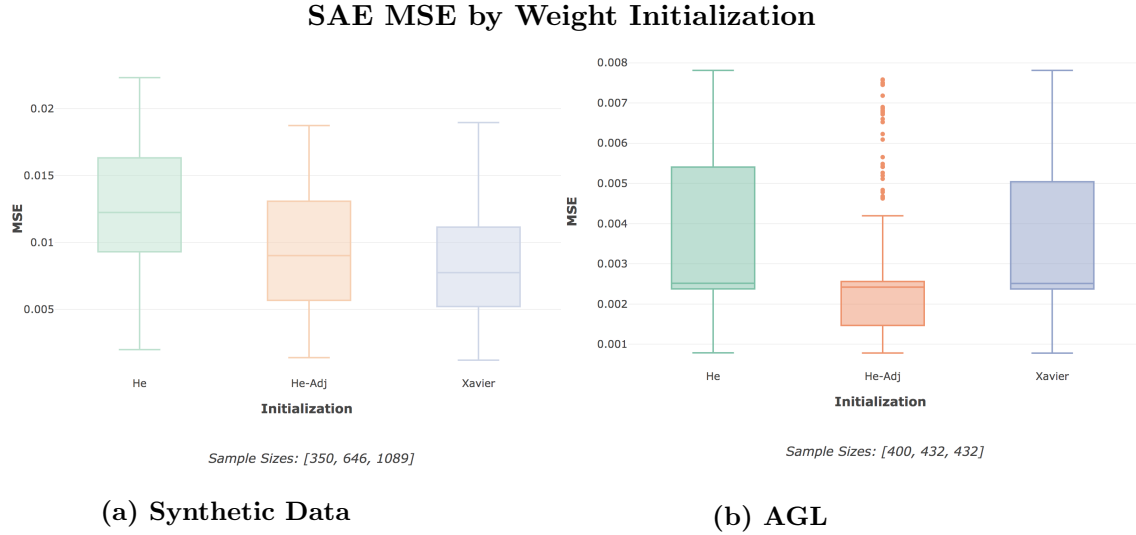


Figure 22: Dataset: Synthetic10 (7.2.2), AGL 7.1.3, Configuration 7 (11.3.7) & Configuration 8 (11.3.8) Training SAE networks across the Synthetic10 and AGL datasets, we mostly see the expected patterns emerge. He-Adj consistently outperforms He due to being better suited to the network structures, as seen in the plots above. We also see that He-Adj clearly outperforms Xavier for AGL data, but has performance that is mostly the same (or even marginally worse) than Xavier for the synthetic dataset. Similar trends as AGL are seen when SAEs were trained for the full 10 asset dataset, which can be seen in Appendix 11.1.2.

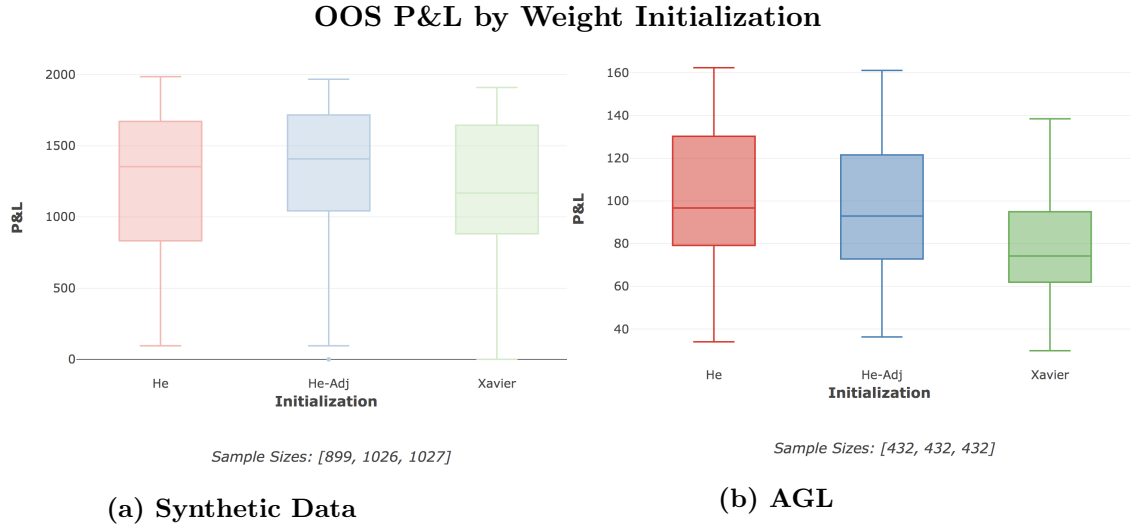


Figure 23: Dataset: Synthetic10 (7.2.2), AGL (7.1.3), Configuration 9 (11.3.9) & Configuration 10 (11.3.10)

Figure (a) shows OOS P&L performance for synthetic data. The networks with more consistent layer sizes result in the performance between He and He-Adj becoming comparable, while both outperform Xavier (as expected, with ReLU activations). In Figure (b), the P&L results for AGL data shows clear outperformance of Xavier by the He based initializations, but a less clear comparison between He and He-Adj.

The results here mostly conform to the theoretical expectations, though there are some inconsistencies. As discussed more fully in Section 8.5, the GBM data in synthetic datasets will have assets that are configured to certain mean and variances. As these movements are processed, scaled and aggregated over time through the data processing, the movements will generally be more similar and less complex than those of actual stock data which will show greater variance over time (this is shown more concretely in Figure 12a). The learning process then is not required to be able to pass through error signals that change dynamically over time, and so there is less pressure on the initial starting weights. This consideration may account for the unexpected performance of the Xavier initialization in the Synthetic SAE networks. Further, some of the assumptions of these techniques, such as data being IID, may not apply in the first place, making their results less predictable. Due to the generally better or comparable performance of He-Adj, it was the only initialization chosen for further trials.

8.5 Synthetic Data

8.5.1 GBM Generated Data

Geometric Brownian Motion (GBM), as discussed in Section 3.2, has been used to simulate synthetic datasets for the purposes of testing implementations and configurations without influencing the likelihood of backtest overfitting. GBM is a popular choice for synthetic financial data as it is a Markov process, thus following a random walk and is generally consistent with the efficient market hypothesis in that the next price movements is conditionally independent of past movements. In line with this though, the series will exhibit a constant drift with price shocks according to it's stationary configuration, and changes in price follow a particular distribution. It is worth noting that as GBM are non ergodic series, one should be wary of considering ensemble based predictions with much confidence [90]. GBM generated data provides a valuable tool in assessing ideas without taking on any risks, but these results need to be considered correctly. This section details how the behaviour of synthetic data differs from actual data in some of the more critical areas.

8.5.2 Synthetic Data Horizon Effects

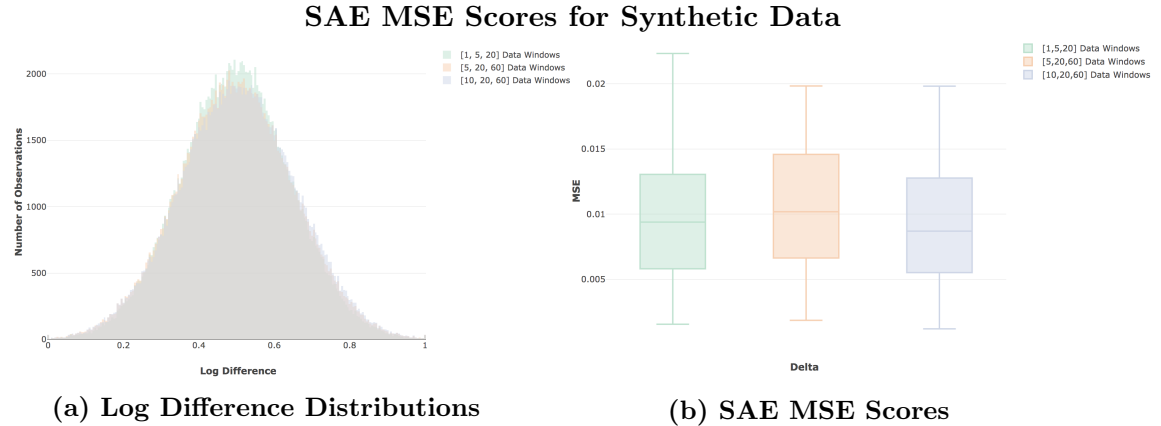


Figure 24: Dataset: Synthetic10 dataset (7.2.2), Configuration 7 (11.3.7)

Figure (a) shows the distribution of values to be replicated by the SAE for synthetic data. Geometric Brownian Motion generates discrete changes that follow a log-normal distribution, the log difference and scaling of which (as per the data processing described in Section 3.1) result in normally distributed price changes. We see small differences in the distributions according to the data horizons used, as one would expect, with slightly lower variances occurring for smaller data horizons ($\sigma_{[1,5,20]} = 0.145$, $\sigma_{[5,20,60]} = 0.152$, $\sigma_{[10,20,60]} = 0.154$). There were some differences in SAE performance as indicated in Figure (b), though not to large extents and considering the very similar distribution of values, there isn't any expectation of seeing fundamental differences in the networks ability to compress and replicate them.

Figure 12 shows the equivalent for actual data, where there is a significant difference in variances for longer data horizons which are more difficult to replicate.

OOS P&L by Data Horizon (Synthetic Data)

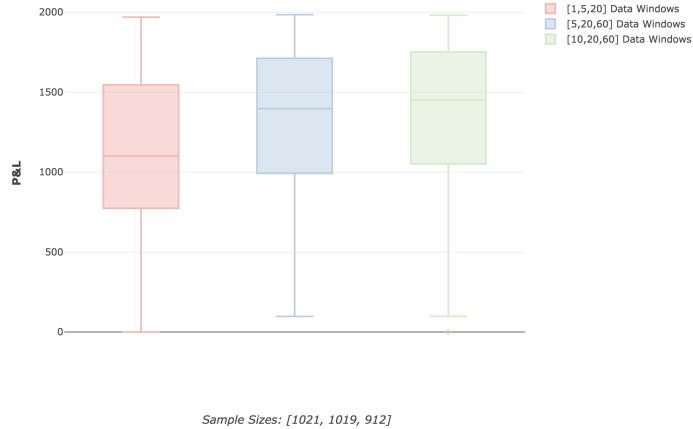


Figure 25: Dataset: Synthetic10 dataset (7.2.2), Configuration 9 (11.3.9)

The boxplots here show the P&L from the MMS grouped by the data horizon configurations. There's a clear trend of P&L increasing as the length of the windows increase. Shorter term GBM data would be more likely to represent fluctuations, whereas the longer term windows will be more representative of the constant mean in the asset price fluctuations, leading to easier predictive performance and higher P&L. This is in clear contrast to the effects seen in actual data, where both long term and short term strategies are present, with the highest strategies occurring for shorter horizon aggregations (these can be seen in Figure 13).

8.5.3 Synthetic Data Feature Selection

OOS P&L by Feature Selection Size and OGD Learning Rate

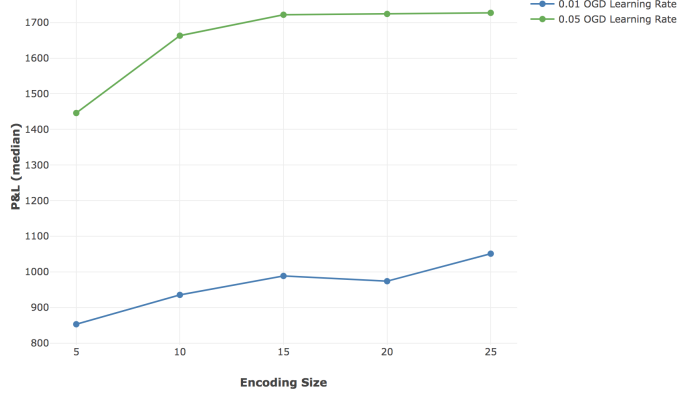


Figure 26: Dataset: Synthetic10 (7.2.2) ; Configurations 9 (11.3.9)

The trends in the synthetic data are relatively straightforward in comparison to actual data. Feature reduction is possible, with OOS P&L increasing as encoding size increases. There does however appear to be an optimal point around 15, after which performance plateaus. Given the stable nature of GBM data, this is to be expected. The results seen for synthetic data here offer a nice counterpoint to what is seen in the actual data. With the GBM data having constant characteristics throughout the whole dataset, there is no potential for the SAE to overfit to IS data and have a potentially detrimental effect as the learning rate increases (as was the case with actual data).

Results for SAE MSE were largely the same, which can be seen in Appendix 11.1.1.

8.6 Complexity of Financial Time Series

The complex nature of financial markets, with a high noise to signal ratio and constantly changing dynamics, presents challenges during the learning process. A model's success lies in its ability to reduce noise without losing signal, and being able to capture determinant features of importance. This section considers how these issues affect data preparation in terms of scaling, as well as SAE reproduction (Unsupervised Learning) and FFN prediction (Supervised Learning), and how SGD learning optimizations are able to help improve performance therein.

8.6.1 Data Scaling

The effects of different scaling techniques (Normalization and Standardization), as described in Section 3.1.2, had significant impacts on SAE performance as seen in Figure 27. The suggested implementation of the limited scaling approaches for the FFN networks was tested on Synthetic data (seen in Figure 28), showing a relatively small impact, though this is expected to be more significant when applied to actual data which would contain unstable variances over time.

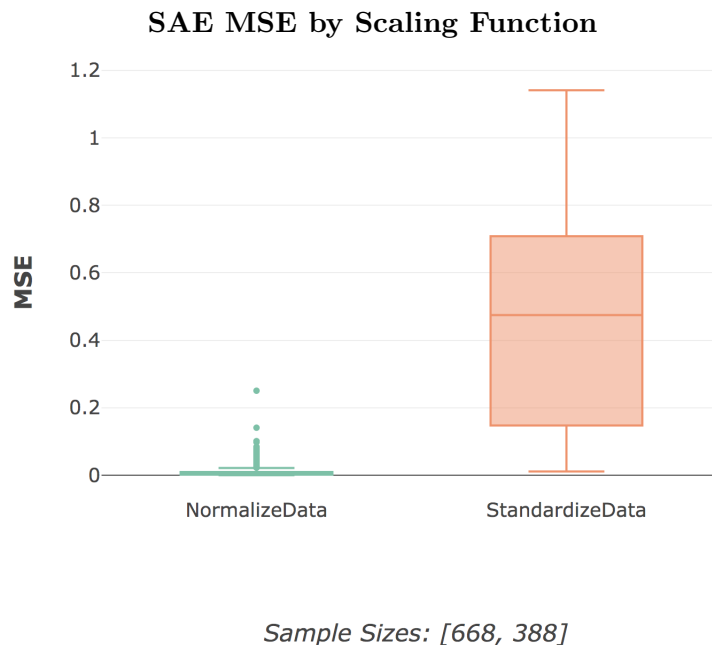
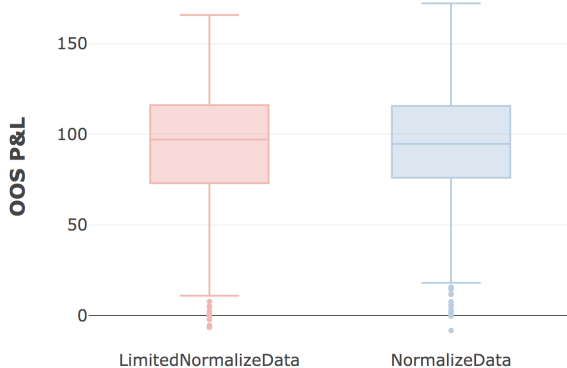


Figure 27: Dataset: Scaling10 dataset (7.1.2), Configuration 1 (11.3.1)

The figure here shows SAE MSE performance according to the scaling techniques as described in Section 3.1.2. As discussed more fully in Section 5.6, the use of standardization for scaling the data doesn't allow for effective outlier treatments, resulting in the significantly worse performance seen here. This again shows the difficulty of dealing with financial time series, which are likely to have many outliers.

OOS P&L by Scaling (Synthetic Data)

Sample Sizes: [480, 480]

Figure 28: Dataset Synthetic6 (7.2.1), Configuration 3 (11.3.3) & Configuration 4 (11.3.4)

The figure here shows the impact of the limited scaling technique (as described in Section 3.1.2) in comparison to the non-limited version. There is a minor detrimental effect as a result of OOS no longer falling within the defined bounds for the scaling used, though the use of a Linear output layer has been shown to assist in reducing the impact of this effect, as in Figure 36. The implementation of this is not a choice when interested in simulating a real world implementation, and with real assets which have changing variance over time it is expected the impact is actually more significant.

8.6.2 SAE Reproduction

The ability of an SAE to reproduce data to a smaller encoding is directly related to the variability and complexity of the underlying data, and the extent to which it can be reduced to fundamental underlying features. The impact of data complexity and variance, as well as the different natures of encodings learnt is discussed fully in Section 8.2 for actual data, and Section 8.5 for synthetic data. What is noted here is how learning optimizations can affect the traversal of a complex solution space.

Figure 29 shows the impact of L1 regularization (implemented as per Section 4.2.5) at both the aggregate and encoding size level, with results emphasising the different nature of features learnt at different encoding sizes, as discussed in Section 8.2. Figure 30 shows that denoising optimizations (implemented as per Section 4.4.3) have detrimental effects, highlighting the lack of benefits in adding noise to an already noisy feature space. Figure 31 shows the effects of learning rate schedules (implemented as per Section 4.2.6), with increased performances shown for different configurations.

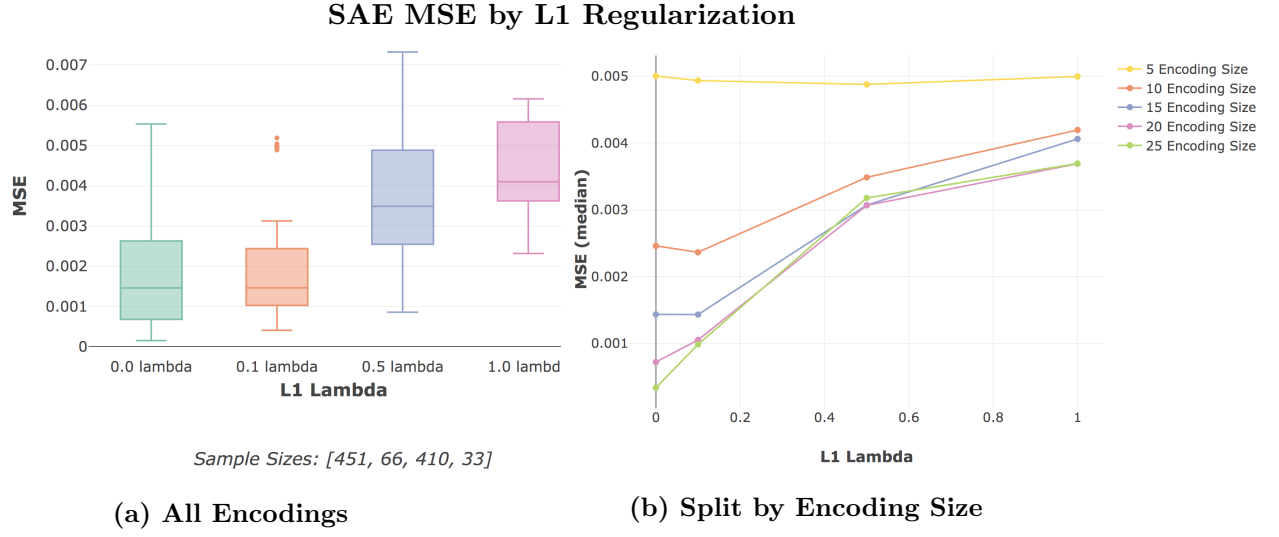


Figure 29: Dataset: Actual10 dataset (7.1.1), Configuration 12 (11.3.12)

Figure (a) shows the aggregate performance of SAE networks at different degrees of regularization, with a generally detrimental trend. Figure (b) however, grouping by encoding size, provides a better understanding. As per the results in Section 8.2, encodings of 5 are learning highly generalisable features, and so benefit from regularization with their best performance at $\lambda = 0.5$. Encodings of 10 have their best performance at $\lambda = 0.1$, learning less generalisable features. Higher encoding levels are operating in a different solution space, and do not benefit from the regularization.

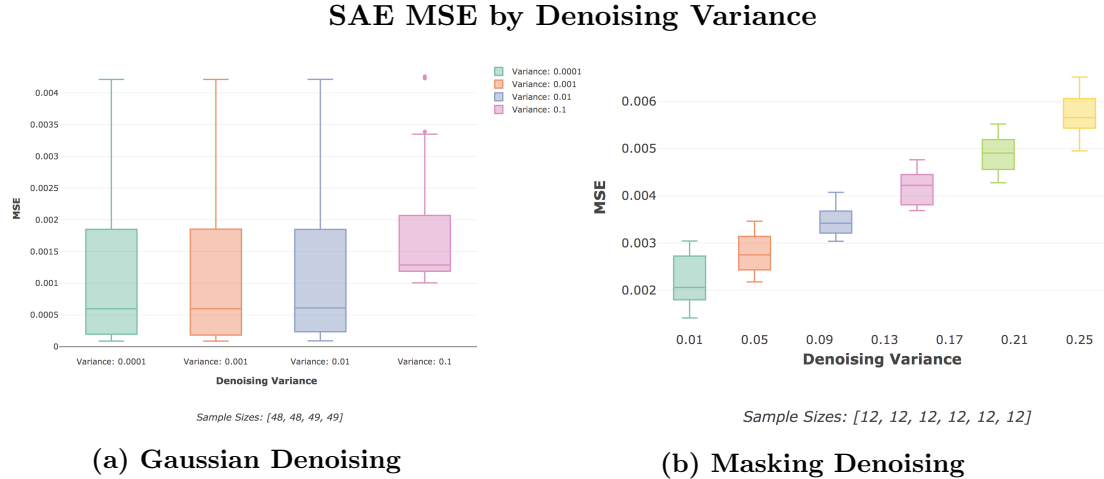


Figure 30: Dataset: Scaling 10 (7.1.2) , Configuration 14 (11.3.14) & Configuration 15 (11.3.15)

Figure (a) shows the effects of gaussian denoising on SAE MSE scores, with scores becoming worse as the denoising increases. This may once again reflect the differences between IID datasets with a model that is likely to overfit in comparison to financial time series data which already have a significant amount of noise present. Figure (b), with masking denoising, was not expected to have a beneficial effect on SAE performance from a conceptual perspective, which the results are certainly in line with.

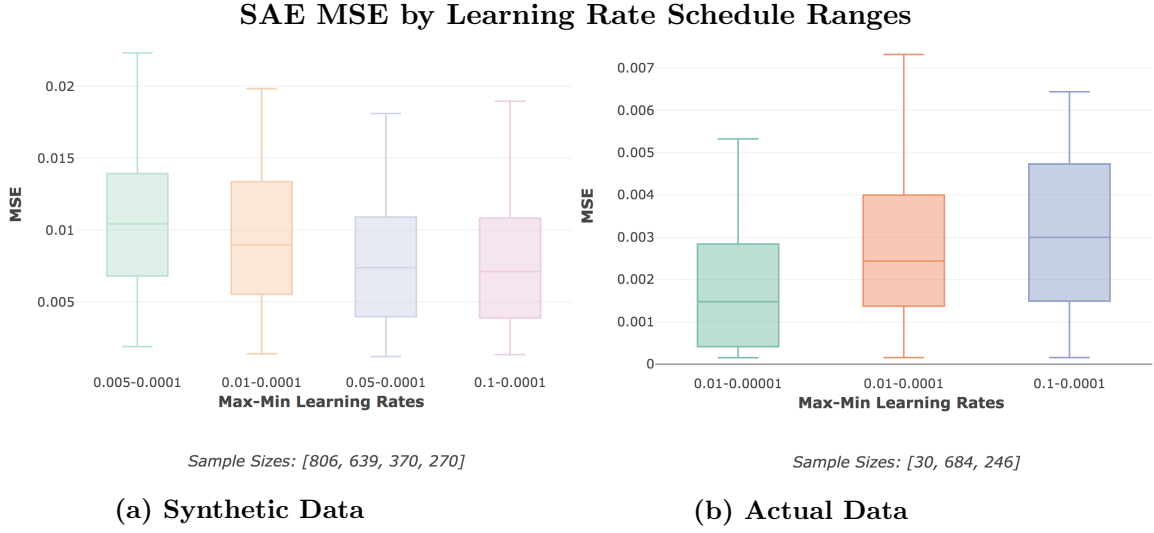


Figure 31: Dataset: Synthetic10 dataset (7.2.2), Actual10 dataset (7.1.1), Configuration 7 (11.3.7) & Configuration 12 (11.3.12)

It is interesting to note that the effects here are quite different for Synthetic and Actual data, with networks for Synthetic data favouring learning rate ranges with a higher upper bound, and Actual data networks trending in favour of lower upper bound ranges. The synthetic data is structurally less complex, as discussed further in Sections 8.5.1 and 8.3, and so the larger learning rates will allow for quicker optimisation. Conversely, SAE networks for actual data benefit from a more careful exploration of the solution space. The effects of the epoch length had a marginal effect, which can be viewed in Appendix 11.1.3.

8.6.3 FFN Prediction

As discussed in Section 8.3, the effects of supervised training on the IS dataset with SGD had limited benefits for OOS performance, and ultimately may be approximating the equivalent of pretraining weight initialization rather than an effective structural learning. The best performing networks were those which were able to quickly adapt to new solution spaces, rather than those which had trained effectively to old ones. Naturally then, the numerous SGD optimizations employed had very little effect on the OOS performance. That said, the effects they have on IS performance do give some insights into the nature of financial data being considered, and do suggest that implementing such optimizations in the OGD phase could be beneficial.

Figure 32 shows the effects of learning rate schedules (implemented as per Section 4.2.6), with notable impact across different epoch lengths. Figure 33 shows the impact of L1 regularization (implemented as per Section 4.2.5), with results showing only a minor potential improvement and ultimately highlighting the unstable dynamics of financial time series. Lastly, Figure 30 shows that input Dropout (implemented as per Section 4.2.7) was ineffective in prompting the network to learn interactive relations between assets.

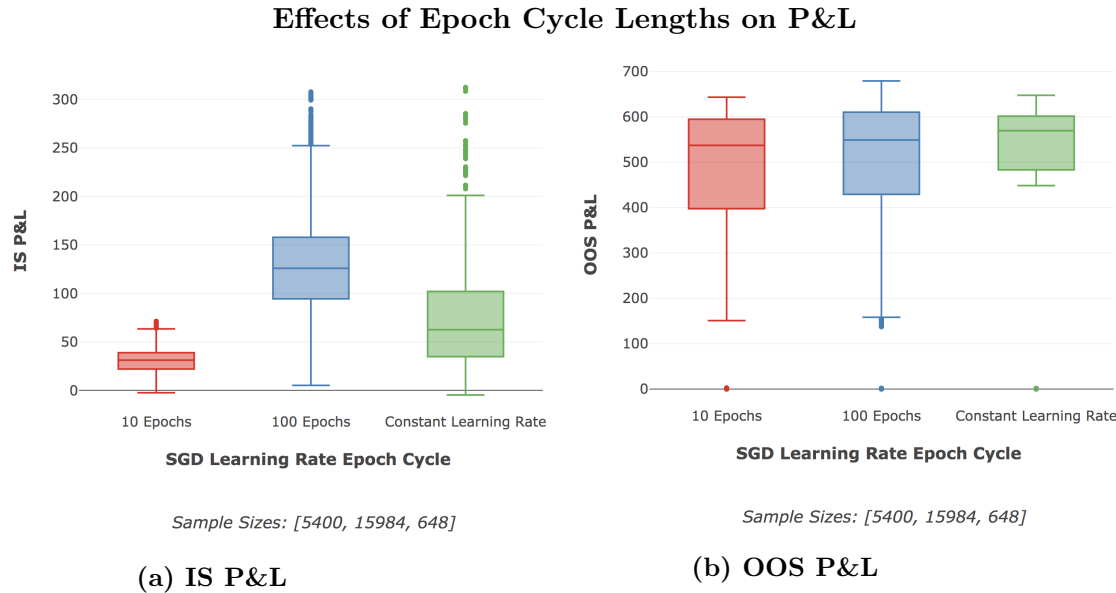


Figure 32: Dataset: Actual10 dataset (7.1.1), Configuration 13 (11.3.13)

Figure (a) shows significant differences in the P&L compared across different learning rate epochs, with 100 offering notable improvement over a constant learning rate. The 10 epoch cycles were used for configurations which only ran for 10 epochs, and so the performance may just be indicative of the amount of training. As expected, the performance increase IS doesn't have significant impacts on the OOS performance, but it does give an indication that a more careful exploration of the complex solution space would be beneficial where possible.

The learning rate ranges themselves were set to the best values seen for the data in the SAE training, and small variations did not result in notable changes. These can be seen in Appendix 11.1.3.

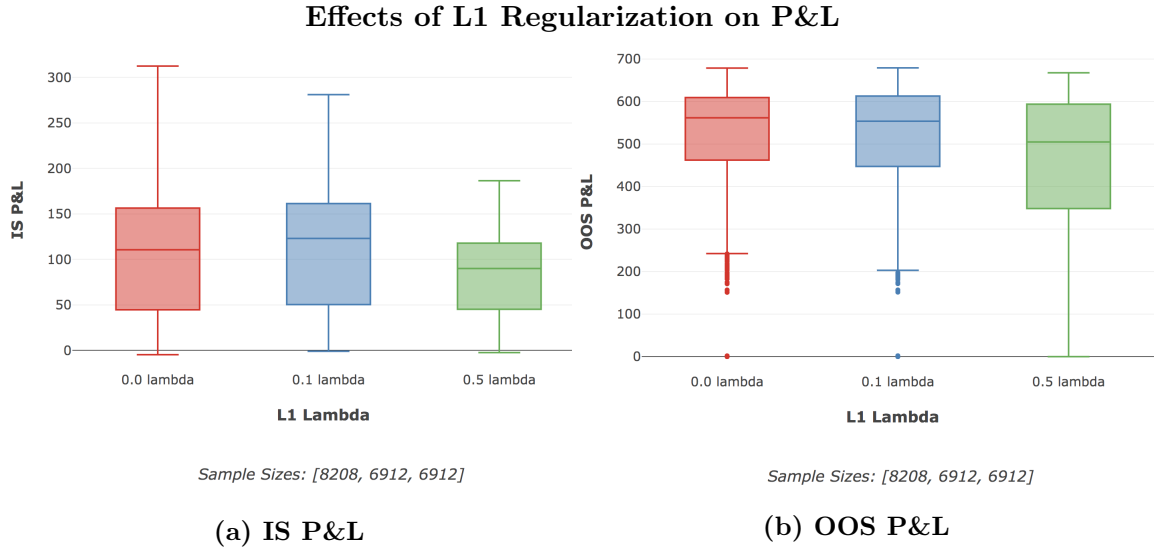


Figure 33: Dataset: Actual10 dataset (7.1.1), Configuration 13 (11.3.13)

L1 Regularization in Figure (a) shows a minor improvement in aggregate IS performance, though with lower maximum P&L and with only detrimental follow through to the OOS performance, as seen in Figure (b). This highlights that even when a model generalises to IS data, the changing dynamics of financial time series means that it may not be generalising well to OOS data. L1 regularization is expected to work well in instances of IID data, but for time series financial data, where the model isn't overfitting, it is just affecting model fidelity. This effect is amplified both IS and OOS when $\lambda = 0.5$.

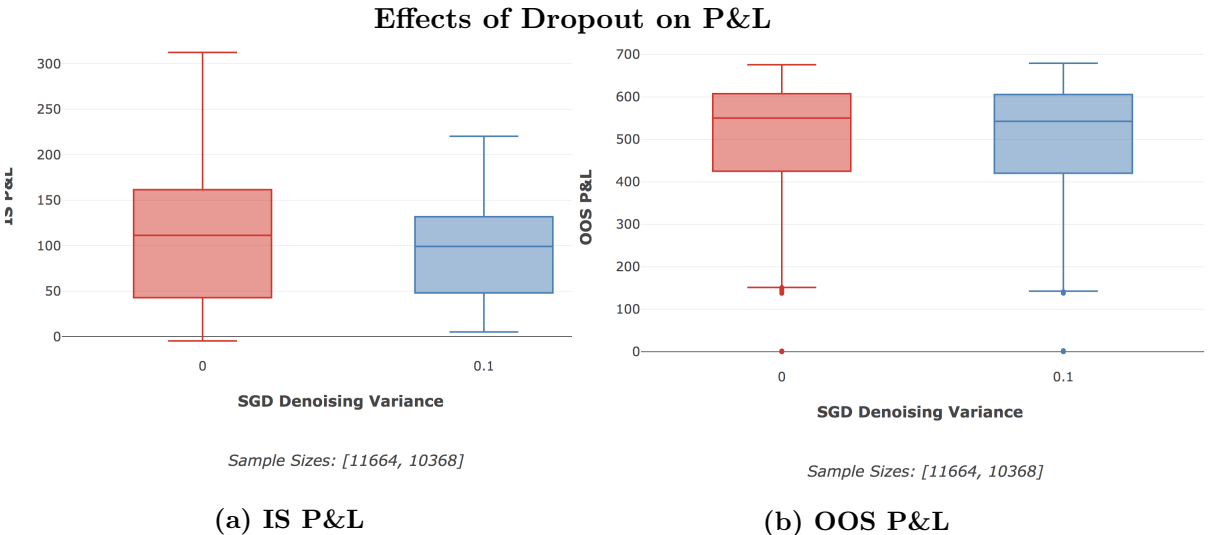


Figure 34: Dataset: Actual10 dataset (7.1.1), Configuration 13 (11.3.13)

Input Dropout was tested on the predictive FFN networks in the hope that it might encourage the network to increase learning about the relationships between assets. The results for 10% variation had a detrimental impact on IS performance, though with little impact on OOS P&L.

8.7 Network Structure

8.7.1 Effects of Network Size

The effects of networks size on SAE MSE performance and the predictive P&L performance are shown in Figure 35 below. The trends for both actual and synthetic data were largely the same, and so only actual data has been considered here.

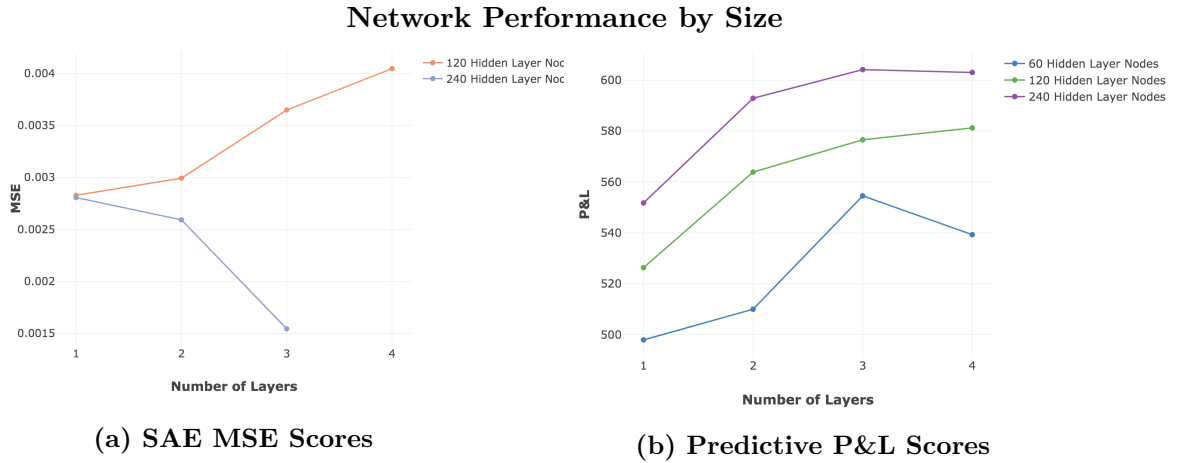


Figure 35: Dataset: Actual10 dataset (7.1.1), Configuration 12 (11.3.12) & Configuration 13 (11.3.13) Figure (a) shows the median MSE by SAE networks achieved with the indicated number of layers and layer nodes. It's worth noting that the number of layers here indicate the final SAE structure of N hidden layers, rather than the training structure of $2N + 1$ hidden layers. Interestingly, the networks with 120 node layers seem to struggled with training, and performance decreases as layers increased. This is to be expected if the learning parameters (e.g. SGD learning rate) are not ideal for the structure, the effects of which are amplified as network sizes increase. This is resolved in the larger 240 node networks which show significant improvement as more layers are added (as one would generally expect, subject to effective SGD).

Figure (b) shows the median OOS P&L achieved by predictive networks with the indicated number of layers and layer nodes. The behaviour is as expected here, where network performance generally increases with size. The exception is the four layer network of 60 nodes, where the training parameters were no longer effective in passing signal back (larger layer sizes are less likely to suffer from this, particularly with ReLU activations).

8.7.1.1 SAE Network Structures

It was interesting to note that the typically accepted SAE network structure, where layers decrease in size between the input layer and the encoding layer, resulted in worse performance when compared to the same number of layers with constant numbers of nodes. As detailed in Section 8.4, the RBM based greedy layerwise pre-training proved to be ineffective, and so weight initialization with SGD training on the entire network was used instead. It is possible that a greedy layerwise training using these methods (rather than RBM initialization) may have shown increased performance in the decreasing layer size structure, but for SGD training it was clear that larger layers at all stages

increased performance. The box plots showing these trends can be seen for actual and synthetic data in Appendix 11.1.4.

8.7.2 Effects of Activation Functions

A range of activation functions (Linear, ReLU and Sigmoid) (as described in Section 4.2.2) were tested on actual data for SAE networks in order to determine the best configuration choices going forward. It's shown that Linear activations are best for the encoding and output layers, and that ReLU activations largely outperform Sigmoid or Linear activations for the hidden layers (Figures 36 and 37). This makes sense with the non-linear benefit at hidden layers but with less loss of error signal and information at the output and encoding layers. These results were used for subsequent parameter choices.

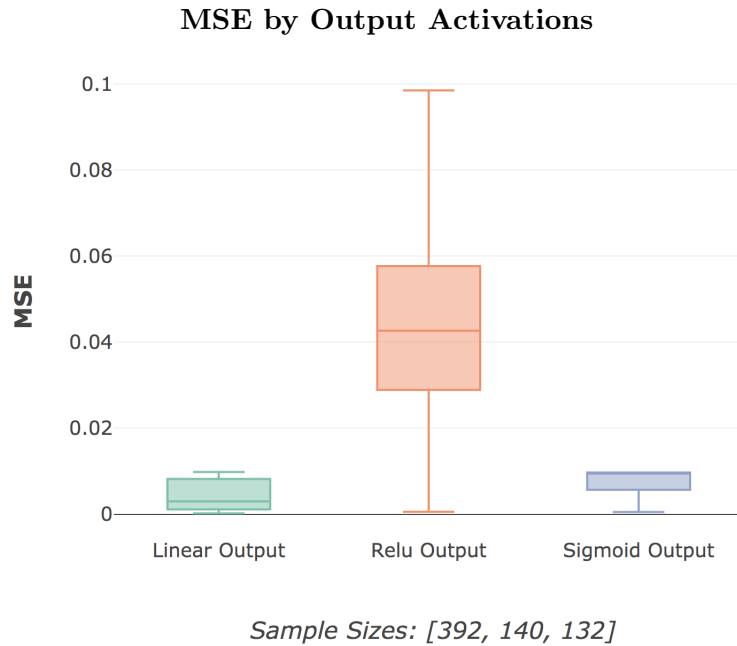


Figure 36: Dataset: Scaling10 dataset (7.1.2), Configuration 1 (11.3.1)

This figure shows the effects of the output activation for configurations using Normalized scaling. The ReLU activations also seemed to result in very poor performance, most likely due to the loss of error signal in the output layer where it is most critical.

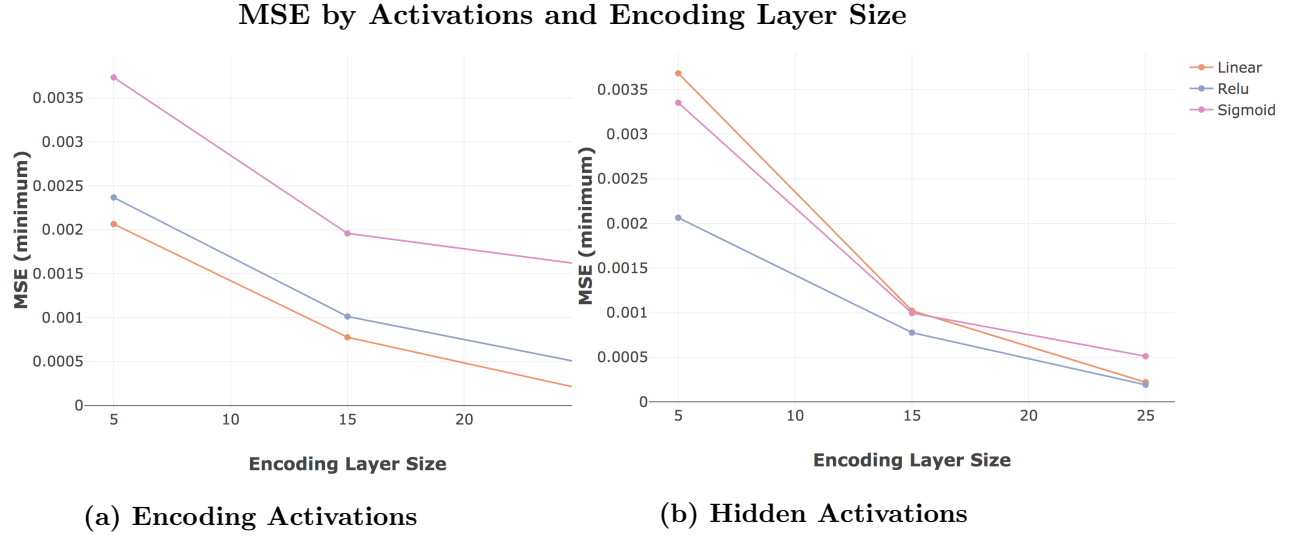


Figure 37: Dataset: Scaling10 dataset (7.1.2), Configuration 2 (11.3.2)

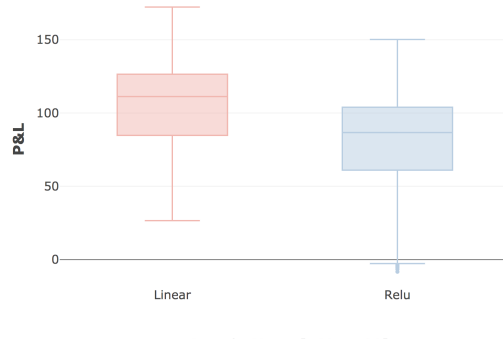
Figure (a) shows the best (minimum) MSE scores for different encoding activations at the different encoding layer sizes (with a network input of 30). There is a consistent out performance of Linear activations in the encoding layer, which is expected from literature [59], and in line with reducing loss of error signal at critical points.

Figure (b) shows the best (minimum) MSE scores for different hidden layer activations at the different encoding layer sizes (with a network input of 30). At larger encoding layers, there is a competitive performance from fully linear networks, where they are less pressured to take advantage of non-linear effects. As the size of the encoding layer is reduced, the advantages of non-linear activations become more apparent, with outperformance by ReLU and Sigmoid activations. Sigmoid activations are known to suffer from learning slow down as a result of saturation and so have increased sensitivity to vanishing gradients [51]. SAE networks are deep by nature, and so it is not surprising that the Sigmoid activations are resulting in worse performance over the same training period when compared to ReLU activations.

8.7.3 Predictive FFN Activations and Scaling

In the interest of reducing likelihood of backtest overfitting, as well as having seen results for SAE networks on actual data, predictive network activation functions were only tested with Synthetic data. The effect seen, and discussed more below, is that reconstruction of aggregated GBM data was able to be performed quite effectively through linear activations, so long as the network (and encoding layers) were large enough to allow for sufficient transformations. Linear activations weren't tested further on actual data, as there is no reason to believe the time series would continue to exhibit the constant drift with non-independent price jumps over time.

P&L by Scaling and Activations (Synthetic Data)



(a) Hidden Activations

Figure 38: Dataset Synthetic6 (7.2.1)), Configuration 3 (11.3.3) & Configuration 4 (11.3.4)

This figure offers a comparison of Linear and ReLU hidden layer activations on P&L, with the linear activations resulting in notably better P&L when compared to ReLU activations. Unlike the SAE networks, this persists even when the network size is decreased - this difference highlights the effects of GBM data and that it can be represented linearly, as per Section 8.5.1, whereas we would see actual asset data benefit from a non-linear representation. Linear configurations for actual data were not run, as real stock data is not expected to follow patterns that are linear through time, thus offering little value.

8.7.4 Sigmoid Activation Functions

Due to the poor performance seen in Sigmoid function based SAE's, as well as the poorer results when compared to ReLU activations, Sigmoid functions were largely excluded from further configuration testing.

8.7.5 Leaky ReLU vs ReLU

Leaky ReLU activations were implemented, and showed negligible effects for SAE, which can be seen in Appendix 11.1.4. For the predictive network, the LeakyReLU did offer some more significant improvements (3% - 10%) on OOS P&L for Synthetic data, as seen in Figure 60 in the appendix. Subsequently, Leaky ReLU was used as the hidden layer activation of choice for most trials.

8.8 Money Management Strategy

This section details the financial returns generated from the MMS implemented, as per Section 4.6, both in terms of OOS P&L as well as the strategy Sharp Ratios. The benchmark noted represents returns that would have been generated from the same MMS if the underlying network making predictions had 100% accuracy, and so in this way represents an upper bound on performance.

The benchmark return rate is 3.04%, so while the strategies' proximity to the benchmark do represent a framework success, they are not necessarily representative of a feasible market solution. Ultimately, this enforces the notion that the MMS implementation is of exceeding importance in a live trading process, and predictive accuracy is only able to achieve so much.

Figure 39 shows the distributions of OOS P&L with and without trading costs being accounted for, with a significant number of distributions which are within the 20%-30% range of the benchmark. While the costs do have a notable impact on the overall P&L distribution, it does not seem to indicate that the strategy would suffer from implementation limitations due to trading costs. The trials with 0 P&L are networks which suffered from either exploding or vanishing gradients, and were not able to make sufficient predictions. The distribution of Sharpe Ratios are shown in Figure 40a, and are expectedly following a similar pattern to the P&L distributions. The Sharpe Ratio's are not providing exceedingly good returns, though this is as representative of the basic trading strategy and selection of stocks used as any performance assessment of the underlying networks, as further emphasised by the distribution of correct trade percentages in Figure 40b.

As noted earlier, the P&L reported on here is a relative unit measurement, rather than a particular currency (as discussed in Section 3.3). Additionally, the MMS, as described in Section 4.6, only trades 1 stock unit at a time and so any P&L figures are relative indications rather than absolute limits.

MMS OOS P&L Distributions

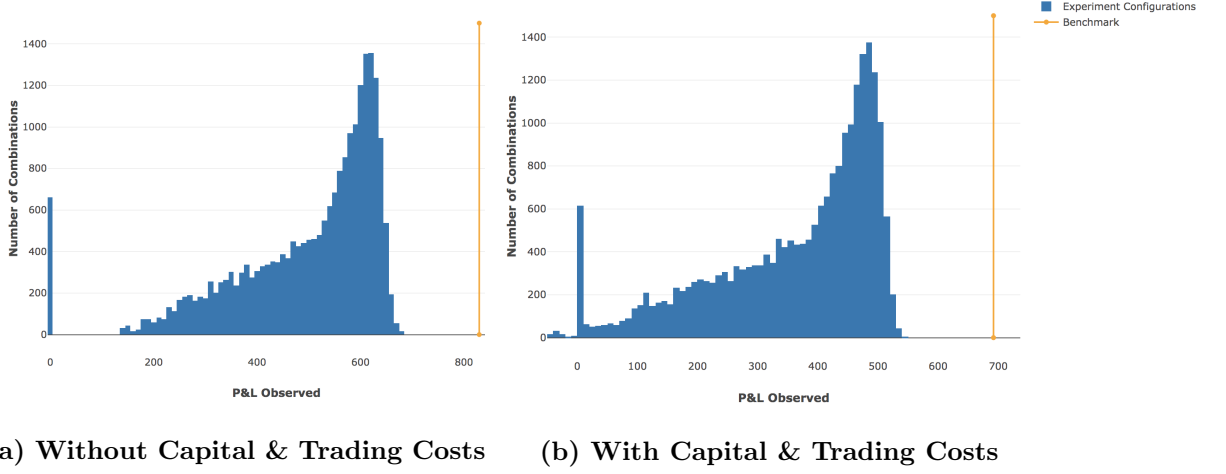


Figure 39: Dataset: Actual10 (7.1.1) ; Configuration 11 (11.3.11) & Configuration 16 (11.3.16)

The distributions of all OOS P&L values, with the benchmark P&L indicated in orange, give an encouraging view of the results. There is a significant negative skew, with a proportionally small number of strategies resulting in negative returns, even with capital and trading costs applied (as per equation (52)). There are a large proportion of strategies near the OOS upper bound, which in turn is within 22% and 28% of the benchmark for Figure (a) and (b), respectively (these percentages apply similarly to return rates as they do to OOS P&L).

MMS Sharpe Ratios and Correct Trades

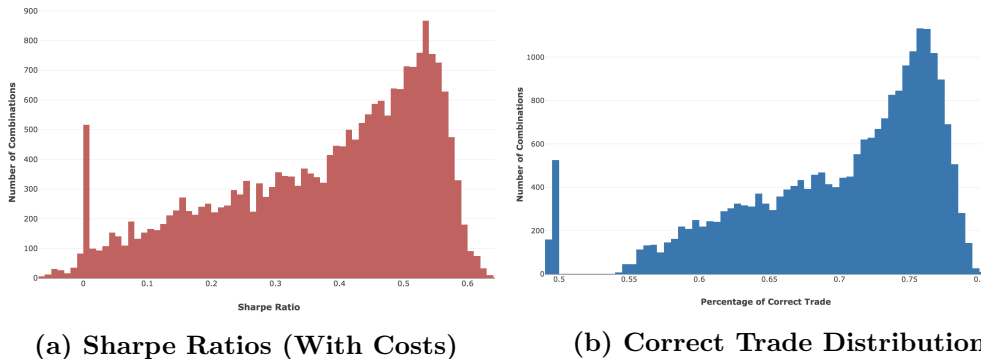


Figure 40: Dataset: Actual10 (7.1.1) ; Configuration 11 (11.3.11) & Configuration 16 (11.3.16)

Figure (a) shows the distribution of all strategies' Sharpe Ratios, with costs taken into account. Figure (b) shows the correct trade percentages made by the strategies (i.e. purchasing an asset when they should have). Naturally, these are all highly correlated measures, showing the same overall distribution patterns as those seen in the OOS P&L in Figure 39. This once again indicates the successful implementation of the underlying framework.

8.9 Probability of Backtest Overfitting

8.9.1 Concerns Regarding the PBO Calculation

The CSCV and PBO techniques, as detailed in Section 4.7, were developed by Bailey et al. [7] in order to offer a robust methodology of assessing whether a selected strategy is likely to have been justified through backtest overfitting, a common and problematic phenomenon (as discussed in Section 2.6). The crux of the methodology lies on the idea that for overfitting to occur, the strategies that deliver the best IS performance will systematically underperform in the OOS datasets (thus reflecting the model having overfit to the IS noise).

Their methodology offers several key benefits:

1. The CSCV methodology is generic, model-free and non-parametric, allowing it to arguably be used in any model case.
2. There is no requirement of a hold-out set, which removes potential credibility issues regarding whether the holdout set was treated appropriately or not.
3. While the Sharpe Ratio is the typically chosen performance metric, the technique is generic enough to allow any performance measure to be used.
4. The logit distribution developed through the assessment offers a useful view on the robustness of the strategies used and the nature of the PBO score.

While the methodology is in substance a model free approach to assessing overfitting, the application in a machine learning context has highlighted some shortfalls and dynamics that are worth considering in its usage. Conceptually, overfitting occurs from model parameters being applied to the IS set which perform poorly OOS. For an online learning neural network though, the model parameters which are applied IS for prior training are not necessarily the same parameters that are used for the OOS results (i.e. one may not use the same learning rates for IS SGD training as for OOS OGD training). Further, the parameters of a neural network model are for the most part the weights of the network, which change and adapt during the online learning (OOS) phase. This is the primary strength of the model - while it may very well be overfit to the IS data, an effective learning implementation will result in the model adapting relatively quickly and so move out of the overfit solution space (evidence of IS overfitting can be seen in Section 8.3). Notably, this behaviour would not occur in many static financial econometric models that might typically be more closely associated with backtest overfitting issues.

The use of the logit metric in the CSCV method also creates some potentially problematic issues due to its basis in an ordinal ranking, and whether the best strategy in the IS set is higher than the median in the OOS set. The effect is that strategies which perform poorly both in the IS and OOS datasets

are able to artificially bolster the ordinal position of the best strategy such that it is past the median point and does not result in an increased likelihood of overfitting. As the authors correctly noted, the addition of trials that are doomed to fail will bias results, and if configurations are obviously flawed then they shouldn't have been tried in the first place. In practice though, the issue is more pervasive than suggested. The combinatorial grid search approach as outlined in Section 5.3 results in certain parameter combinations that cause networks to perform very poorly. Individually, these parameters may work well in other combinations though, and so there would be no obvious reason to exclude them to begin with. In this sense, an honest search of the solution space where there is no prior knowledge about what will work OOS may result in a PBO score that is lower than it should be. This dynamic is concerning in that it is easy to create poor performance models and so allows the PBO method to be used fraudulently, and is even more so in the case where it might occur without the researcher realising.

Further to this, the parameter space search methodology (Section 5.3) also results in a lower likelihood of PBO due to the way of combining parameters across IS and OOS stages. By way of example, any configuration which performs well IS will have all possible OOS parameters tested in combination with it. While some of these combinations may result in poor performance, there will always be a combination of the best IS and best OOS parameter choices. This makes it unlikely that the best configurations will be past the median point for the logit calculation, resulting in a systematically low PBO.

Another potential implementation concern with CSCV and PBO is the choice of the S parameter, which is the number of splits for the data to be sampled into. As seen in Figure 41, the number of splits can have an overwhelming effect on the PBO score reported for the same data sets and results. This is not a problem if the implementation is done honestly and openly, but does allow for misuse and a potential inability to compare PBO scores. Further, while the authors do provide guidelines for choosing S such that the splits will be representative of trading periods, there is still no clearly defined method of choosing the time spans of these periods. The exponential growth in combinations to be tested as S increases also quickly results in reaching computational resource limits, which may further lead to the choice in S being made according to reasons that are not in line with prioritising the correct PBO score to report. These combination sizes can be seen below in Figure 42.

PBO Scores by Split Values

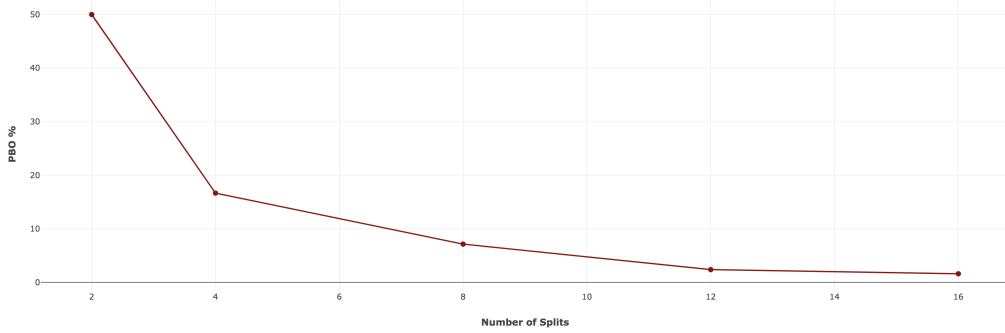


Figure 41: Dataset: Actual10 (7.1.1) ; Configuration 11 (11.3.11) & Configuration 16 (11.3.16)
The curve here shows the significant impact that the choice in the split parameter S has for the PBO score calculated, with a monotonically decreasing score as S increases (these scores were for the same set of results). This highlights the contextual nature of a PBO score and the problems raised with score-wise comparisons as well as upfront configuration choices.

Number of CSCV Combinations by Split Value

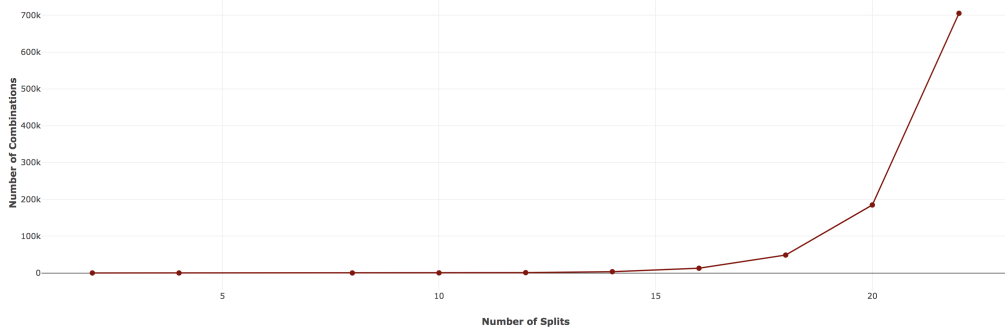


Figure 42:
The number of combinations that have to be processed by the CSCV method according to the value of the split parameter (S) chosen. The exponential increase in combinations to be processed as S crosses a value of 16 once again highlights configuration choice challenges. It is unlikely higher splits than 16 will be chosen, regardless of whether they are more appropriate or not.

8.9.2 PBO Results

The full set of tests run ($n = 22248$) on the Actual10 (7.1.1) dataset had a final PBO of 1.6%, having been run with a split of 16. There were 15 years of data, making it a reasonable choice as the split parameter (which needs to be even). Ideally, the splits would represent shorter periods, but the exponential increase in computational time (as seen in Figure 42) made this impractical, and 16 also happens to be the typical choice recommended by the authors. The full logit distribution can be seen below in Figure 43.

Logit Distribution for All Configurations

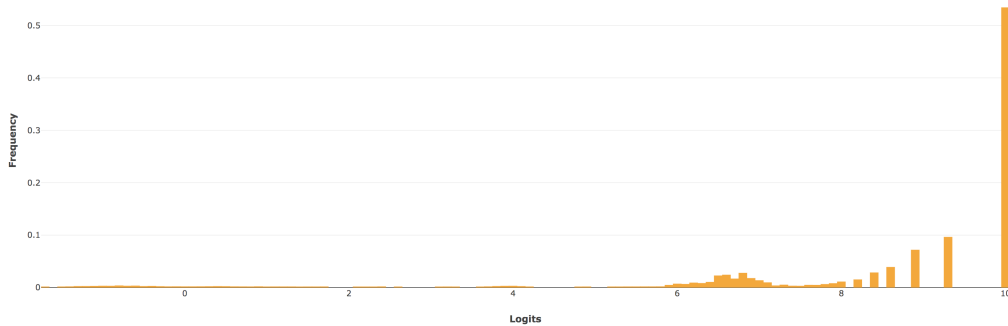


Figure 43: Dataset: Actual10 (7.1.1) ; Configuration 11 (11.3.11) & Configuration 16 (11.3.16)
The CSCV logit distribution for all 22248 configurations run, with a calculated PBO of 1.6%. The strong negative skew is indicative of IS and OOS strategy returns being closely matched in rank, thus resulting in the low PBO score. This is a favourable assessment for the efficacy of the full framework presented here, showing that training was able to occur without much risk of backtest overfitting.

It is of interest to note the dynamics and contribution towards the PBO results. The configuration process went through 2 primary phases: an extremely broad combinatorial grid search, consisting of 20736 configurations; and a second much narrower search of 1512 configurations. Assessing only the configurations from the second phase, results in a PBO score of 6.3%, which is significantly higher than the overall PBO score, the logit distribution for which can be seen in Figure 44 below. The effect here highlights two important aspects of the PBO calculation:

1. The scores are much higher for the configurations which were picked more specifically after having already seen a large number of results, which is correctly indicative of increased likelihood to overfit.
2. However, the PBO score is not monotonically increasing with N, as one would expect. This is counterintuitive and is in line with the concerns raised in Section 8.9.1 regarding the effects of increasing configuration sample size.

Logit Distribution for Subset of Configurations

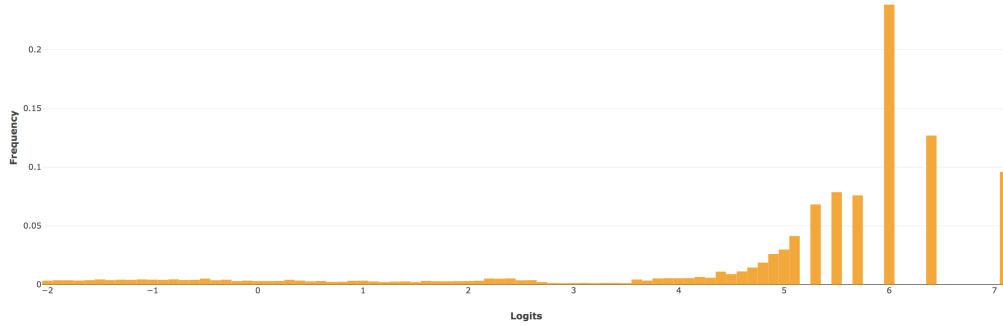


Figure 44: Dataset: Actual10 (7.1.1) ; Configuration 16 (11.3.16)

The CSCV logit distribution for a narrower subset of configurations run, with a calculated PBO of 6.3%. This subset consists of 1512 configurations, out of the total 22248 configurations run (presented in Figure 43). The higher PBO score (compared to the 1.6% for all configurations) is indicative of both a higher risk of PBO for the second phase of configurations tested, as well as a potential issues with PBO scoring, as raised above in Section 8.9.2.

8.9.3 Framework Success

While the CSCV and PBO implementations do raise some concerns, the results here do also highlight the efficacy of the framework which has been implemented. The low PBO scores presented here show that the combinatorial search approach combined with an online machine learning model allows researchers to take on a broad exploration of the possible solution space while maintaining a low risk of backtest overfitting, and such that P&L results which are comparable to the benchmark are achieved, as seen in Section 8.8.

8.10 Deflated Sharpe Ratio

8.10.1 Computational Complexity

One of the primary drawbacks of the DSR algorithm presented by Lopez de Prado and Lewis [81] is the computational complexity which arises with the iterative K-means implementation. A standard Lloyds implementation of the K-means algorithm has a computational complexity of $\mathcal{O}(knt)$, for k clusters, n components and t iterations³. The suggested implementation modification (as discussed in Section 4.8.1) would be for $t = 10$ and to run the algorithm iteratively for $k = 1, \dots, (n - 1)$, which can in turn be expressed as $n(n + 1)/2$. This leads to a computational complexity with an $\mathcal{O}(n^3)$ magnitude. Including the final modification suggested, which could run the algorithm recursively on subclusters, has the potential to increase this even further. This high degree of complexity presents a problem for cases where a large number of strategy permutations have been attempted, as is the case here (with $n > 20000$). With this in mind, the algorithm was implemented for a maximum of $k = 10$, though the results do not suggest this hindered the findings.

Trials with Sharpe Ratio's of 0 were excluded from the ONC clustering analysis due to divide by zero errors from the covariance matrix (this results in a sample size of 21815, rather than the larger 22248 available for the PBO process).

8.10.2 ONC Results

The ONC algorithm produced only 2 clusters for the components, which were partitioned exactly by the choice in input price fluctuation horizon aggregations (as per the calculations in Section 3). Cluster One contains all the trials with horizon aggregations of [1, 5, 10], and Cluster Two contains all trials with horizon aggregations of [5, 20, 60] and [10, 20, 60]. The nature of the experimentation process, with the combinatorial parameter space exploration (as detailed in Section 5.3), is such that other parameters are evenly split across the 2 clusters (e.g. OGD learning rate, network sizes, initializations and so on).

Under consideration of a single and consistent MMS trading strategy, the clusters here then indicate that the networks adapted to at least two different general strategies for predicting prices: one which was more influenced by the short term fluctuations in the 1 day aggregation, and the second which was more influenced by the long term fluctuations in the 60 day aggregation. The results presented in Section 8.2, such as the effect of the OGD learning rate on P&L, are then indicative of the networks ability to execute these overarching strategies effectively.

The best Sharpe Ratio value (with trading costs applied) was 0.64 and part

³<https://scikit-learn.org/stable/modules/generated/sklearn.cluster.KMeans.html>

of Cluster One, with the [1, 5, 10] price fluctuation horizon aggregations. The distributions seen in Figure 45 indicate that at a general level, Cluster Two has more consistent performance, with a higher mean ($\mu_{c1} = 0.367$, $\mu_{c2} = 0.387$) and more negative skewness ($\tilde{\mu}_{3,c1} = -0.529$, $\tilde{\mu}_{3,c2} = -0.746$). Cluster One on the other hand has higher variance ($\sigma_{c1} = 0.03$, $\sigma_{c2} = 0.022$), with more strategies at both the lower and higher range of SR. This shows that relying on the longer term trends for prediction can offer more reliable and consistent returns. Using shorter term fluctuations can offer higher rewards, though with more variance and risk involved, as per the efficacy of the implementation. These higher and lower variances in P&L returns were seen more concretely in Figure 13. The same patterns are presented in the OGD MSE scores, as seen in Figure 46. This is perhaps not entirely surprising when the price prediction horizon was 5 days.

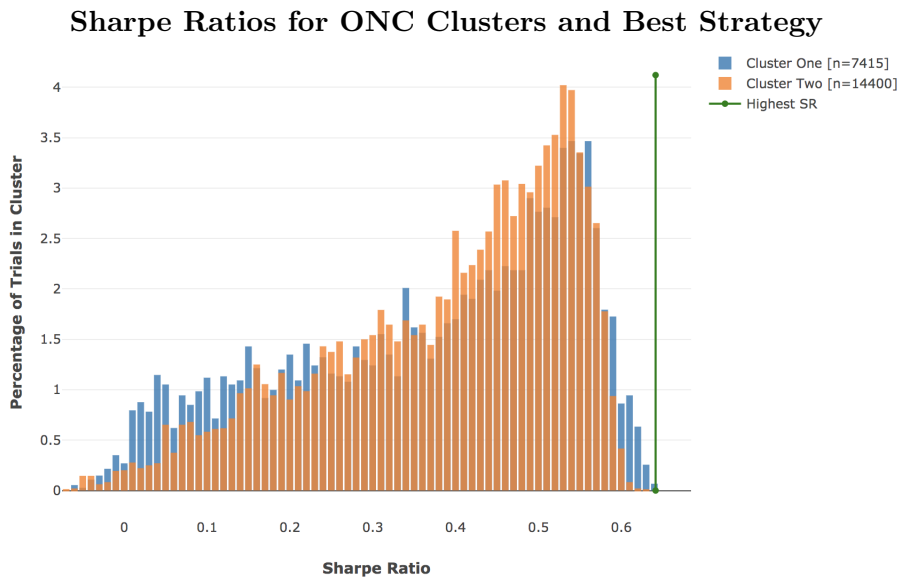


Figure 45: Dataset: Actual10 (7.1.1) ; Configuration 11 (11.3.11) & Configuration 16 (11.3.16)
The graph here shows the distributions of all Sharpe Ratios, grouped by the 2 clusters produced by the ONC algorithm, and an indication for the best Sharpe ratio, which is in Cluster One. As note above, Cluster Two has more consistent SR values, with a higher mean ($\mu_{c1} = 0.367$, $\mu_{c2} = 0.387$) and more negative skewness ($\tilde{\mu}_{3,c1} = -0.529$, $\tilde{\mu}_{3,c2} = -0.746$). Cluster One on the other hand has higher variance ($\sigma_{c1} = 0.03$, $\sigma_{c2} = 0.022$), with more strategies at both the lower and higher range of SR, including the highest SR from all trials.

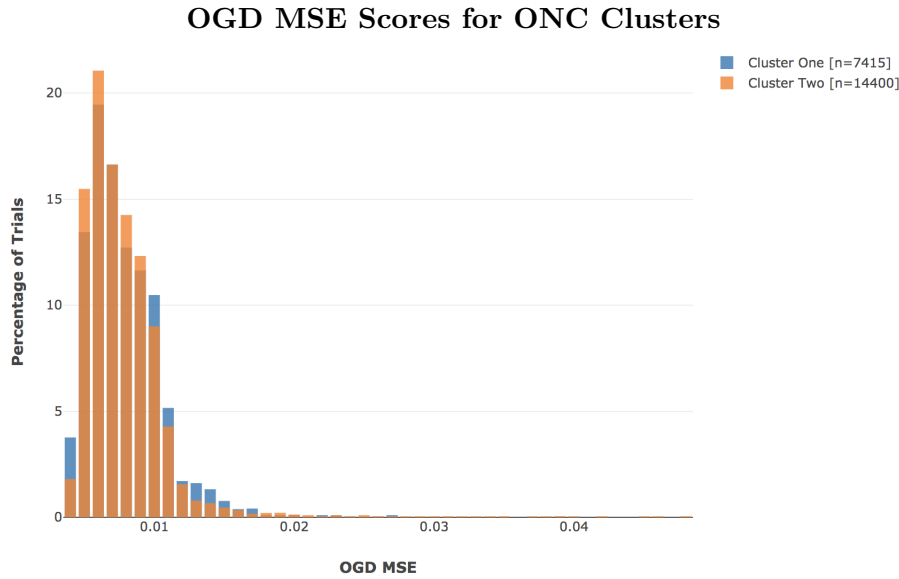


Figure 46: Dataset: Actual10 (7.1.1) ; Configuration 11 (11.3.11) & Configuration 16 (11.3.16)
The distributions of OGD MSE scores can be seen for both clusters here, indicating how precise the predictions were. The patterns tie in with those seen in Figure 45, with Cluster One having a higher variance which leads to more configurations at either end of the MSE range, and including the best performing one.

The lack of further clusterings was probed manually for Cluster One, running the algorithm for a range of values between 2 and 7000⁴. It was found that while there were sub-clusterings which resulted in a higher mean silhouette score (as per equation (78)), the variance of the silhouette scores also increased dramatically. This in turn, resulted in a lower score for the cost function \mathbf{q} (as per equation (79)), and so the ONC algorithm did not cluster further.

8.10.3 DSR and PSR Results

Using the clusters produced by the ONC Algorithm (Section 8.10.2), the DSR process as presented in Section 4.8 was followed. The aggregate cluster time series returns were calculated using equations 84 and 85 (Section 4.8.4.1). These are annualized, which allows their variance estimates to then be used to calculate SR^* , which represents the maximum expected observed Sharpe Ratio due to variance under the null hypothesis of $H_0 : \widehat{SR} = 0$ (as discussed in Sections 4.8.2 and 4.8.3). Using this SR^* as the benchmark, the PSR calculation ($\widehat{PSR}[SR^*]$) can then be used to determine if the observed \widehat{SR} is a false positive or not (as per Section 4.8.4). This figure is the DSR as a confidence for whether the observed best SR is actually positive.

In this case, the benchmark SR^* calculated was 0.023, and the best \widehat{SR} observed was 0.64, leading to a $\widehat{PSR}[SR^*]$ of 1.0, thus indicating that the trials certainly contain a strategy which has a positive SR rate. This does seem like

⁴[2,3,...,49,50,500,1000,1500,2000,2250,2400,2500,2600,2750,3000,4000,5000,6000]

a reasonable conclusion, considering the SR distributions in Figure 45. The calculations for all steps can be seen in Appendix 11.2.

8.10.4 Framework Success

Much like the results from the CSCV and PBO methodologies, the DSR assessment here provides assurance that a large configuration space can be explored effectively and still have confirmable effects which can be successfully incorporated into a profitable trading strategy. In this case, the DSR indicates that even with the expected variation amongst trial Sharpe Ratios, we were still able to find a strategy with a positive SR with full confidence.

8.11 Summary of Actual and Synthetic Data Effects

The usages of GBM generated synthetic data to perform conceptual testing without increasing the risk of backtest overfitting does has some benefits, though the stabler characteristics of the data lead to different results from actual data in many areas. The primary reason for the different behaviour links back to the complexity of financial time series with unstable dynamics. GBM data, conversely, has asset price fluctuations which follow a stable Log-normal distribution over time. This is seen clearly in the fluctuation distributions in Section 8.5.

As a result of this stable characteristic, longer data horizon aggregations lead to better performance for synthetic data as they were more likely to smooth over noise and capture the constant long term means. This is seen in both in SAE reproduction and P&L prediction in Section 8.5. Section 8.6 also showed on Synthetic data that the Limited Normalization (5) did impact P&L, but within reasonable margins.

The other prominent difference in Synthetic data was in the SAE features learnt. Results for SAE networks trained on actual data displayed different classes of features being learnt according to the input horizons, which had fluctuating performances across time periods. Synthetic data however has less inherent features to learn, and so responded with a monotonic performance according to feature size, as seen in Figure 26. In assessing data aggregations and encoding sizes, synthetic data was not an effective indicator for results on actual data.

The results for weight initialization techniques, as discussed in Section 8.4, were slightly different from actual data, but did still follow theoretical expectations and lead to similar conclusions. In this sense, synthetic data seemed to be a good indicator. Similarly, while synthetic results for Linear network activations would be misleading for actual data, the results for non-linear activations seemed to be effective in leading to similar decisions (as discussed in Section 8.7).

More typical implementation aspects, such as learning rates and network sizes, also followed similar patterns to actual data when training. These parameters tend to be discovered through exploration on any given data set though, and so the added benefit of synthetic data results is marginal.

Ultimately, the inherent differences between synthetic and actual data result in more differences than similarities. GBM generated data can be used to test process and framework implementations, but the behaviours seen in results should be considered very carefully before being applied to actual data (if at all).

9 Conclusion

The work presented here builds on mechanistic machine learning approaches to financial market data, and in doing so provides a novel framework which is shown to be effective in both training and validation. The framework embodies a configurable approach, based on decoupled modules throughout the process, and incorporating several key techniques: deep learning neural networks for stock price fluctuation prediction, Stacked AutoEncoders for the purpose of feature selection, both CSCV & PBO in order to assess the returns from the MMS and the likelihood that backtest overfitting has taken place, and DSR in order to assess the likelihood of a positive Sharpe Ratio having been observed. The results from trials based on the presented framework highlight the efficacy of such an approach, whilst also developing a refined perspective on how these techniques behave within the phenomenology of financial markets.

The nature of neural networks as non-linear universal approximators combined with the brute force approach to learning market dynamics allow us to establish market characteristics, and how they relate to models which, conceptually, could not be made more complex. The most pervasive observation in this sense, was the highly dynamic and complex nature of financial time series, with the unstable behaviour of assets over time being highlighted as one of the more challenging barriers to learning. While machine learning models are expected to excel in big data environments, in financial markets there is in fact a lack of data with relevant information and signal (especially if one considers the need of validation datasets).

To this point, it was shown in Section 8.3 that the IS training on historical data had a limited benefit, which could become detrimental if trained on extensively. This was confirmed by showing the negligible impact of increasing training time as well as the surprisingly small impact of large reductions in the training data. It was made clear that increased performance for IS data was not necessarily linked to OOS performance, emphasising the changing dynamics of financial markets over time. This gives weight to the importance of online learning methods for financial applications, which in turn makes network initialization a significant configuration choice. Methodologies for effective initialization are explored in Section 8.4, with positive results shown for the He-adj initialization presented in Section 4.5, as well as a poor performance in RBM based pre-training.

Naturally then, the primary determinants of OOS P&L were shown to be those which affected the online learning data and the model’s ability to adapt to it. The horizon length of input data aggregations was shown to be the primary distinguishing property of trade correlations in Section 8.10. In Section 8.2, the differences between these groups were explored. It’s seen that networks provided with 1 day fluctuations adapt to short term price prediction

strategies, and so excel in configurations which allow them to adapt quickly to new information. Conversely, networks provided with longer horizons, such as 60 day fluctuations, adapted to following long term trends and performed best under configurations which had more careful adaptations. Notably, the short term strategies had the highest OOS P&L returns, but also the highest variance in these returns. This highlights both the increased value in recent information in financial markets, as well as the difficulty in using it due to the amount of noise present.

Reducing the noise through the usage of SAE based feature reduction provided interesting results, as also noted in Section 8.2. It was shown that SAE networks would learn fundamentally different features according to the encoding sizes made available which then had a non-linear effect in its impact on OOS P&L. Larger encodings (15, 20, 25) lead to a denoising effect on the input data, with performance being generally better at higher encoding when used in strategies focusing on short term fluctuations. Smaller encodings (5, 10) were shown to learn more inherent features, resulting in higher performance in many circumstances when compared to the larger encoding feature sets. These features are not necessarily stable through time though, which was shown through the inconsistent performance of features learnt for an encoding size of 10. This issue was not present in the networks which were limited to 5 features, which learnt more robust and generalisable features. These smaller networks had competitive performance when compared to networks learning larger feature sets, showing that feature reduction in financial time series is both possible and beneficial, despite the complexity present.

This general complexity of financial time series was also explored through the results of data processing and learning optimizations in Section 8.6. The effects of outliers was seen to be significant when comparing scaling techniques, with substantial differences between standardization and normalization. A strong relation was shown between regularization benefits and the smaller SAE encodings, in line with the extent of generalisable features being learnt. Learning optimizations for IS batch training, such as regularization and learning rate schedules, were shown to have benefits for IS results, but little carry through to OOS performance. This once again indicates the complex but unstable nature of financial solution spaces.

Comparisons of results against synthetic data generated through Geometric Brownian Motion (GBM) are made throughout the findings, though particularly so in Sections 8.5 and 8.11. GBM generated data exhibits constant characteristics by design, which contrasts heavily against the non-stationary nature of financial time series. It was shown that, for the most part, these differences lead to results for synthetic data being non-transferable to actual data. The use of synthetic data is still valuable in that it allows very effective framework and process testing without increasing the likelihood of backtest overfitting, but beyond that it's usage is somewhat limited.

The full set of returns are explored in Section 8.8, with the distributions of OOS P&L and Sharpe Ratios being considered relative to the benchmark (a model with 100% prediction accuracy). It was seen that the framework presented is able to generate effective models, with returns distributions showing significant negative skewness, and achieving returns in the region of 20%-30% from the upper bound benchmark. That said, the benchmark itself only had a return rate of 3.04%, so while the strategies seem to be objectively profitable, they are being considered in a region that would not be competitive in the market. This speaks to a more foundational issue in financial markets, in that the MMS put into places is a critical component of profitability. The predictability of trading signal in and of itself is not enough to generate competitive gains.

The most challenging aspect of such a mechanistic approach to learning is ensuring that the model has not resulted in backtest overfitting, as discussed extensively in Section 2.6. Probing and validation of the generalisation error in the case was done through the use of Bailey’s Probability of Backtest Overfitting (PBO) methodology [7], as well as the use of Prado’s Deflated Sharpe Ratio (DSR) [81]. The results, as discussed in Sections 8.9 and 8.9, show a low likelihood of the models having overfit, and a certain likelihood of the true best Sharpe Ratio being positive. This lends weight to validity and efficacy of the full framework presented, showing that the solution space for financial asset price fluctuation prediction can be explored in a brute force fashion without necessarily overfitting.

The system presented then, was successful in achieving the aims set out for it and presents a cohesive view of how components interact and might be changed in a future implementation. Feedforward neural network training parameters are explored and presented, including network sizes, activation functions and learning optimizations. Stacked AutoEncoders, initialized using both RBM pre-training as well as variance based techniques, are presented and shown to be able to perform effective feature selection. An extensive comparison of synthetic and actual data, including data pre-processing, is covered such that it might guide further usage of the system. The CSCV and PBO methodologies are implemented, considered, and shown that they are able to work for a novel implementation on machine learning models and provide rigorous assessment of results. Their results are further validated through the usage of the ONC and DSR algorithms to detect positive Sharpe Ratios.

Further to this, a view on the phenomenology of financial markets has been developed and presented, based on the experiments results. The results presented for limited in-sample training of the networks (both by length of training and dataset size), the effects of feature selection developed in-sample, as well as out of sample training parameters all provide a clear notion that there is a positive but very limited benefit to training on long term historical financial time series. The results show that the value of a cross sectional view of the

data has far more weight in delivering out of sample returns, which is particularly noteworthy in the context of a neural network with few structural model limitations. Similarly, online learning approaches are shown to have greater efficacy in this context.

Ultimately, the system has been presented and shown to not only deliver promising P&L figures for out of sample data, but has also done so while being able to incur a low probability of backtest overfitting or spurious results otherwise.

10 Future Work

Several areas of the system have been highlighted as worthy of further work based on the results seen so far:

1. The incorporation of Open, High, Low and Volume data into the feature set would likely offer significantly beneficial signal gains for the predictive networks.
2. In light of the historical data redundancy seen, an improved and optimized online learning phase would be worth considering.
3. The updating of SAE models is the another likely area of beneficial development, possibly based on rolling time windows in order to fully take advantage of recent data benefits, or using a bootstrapped dataset in order to add time based weights to observations.
4. While RBM pre-training was shown to be ineffective, it is possible that a greedy layerwise approach using variance based weight initialization could still be used in order to train more efficient SAE networks.
5. Data processing methods such as the Error Function could be implemented in order to better deal with outliers, which are shown to be prominent in financial data.
6. Further exploration of using input Dropout for price fluctuation prediction is warranted, in order to try and enforce correlation and relationship recognition within the FNN.
7. A more extensive exploration of how to best benefit from historical data would be particularly beneficial, especially with its potential application outside of just the presented system.

11 Appendix

11.1 Additional Results

11.1.1 Additional Results for Section 8.2 - Feature Selection

MSE By Feature Selection Size (Synthetic Data)

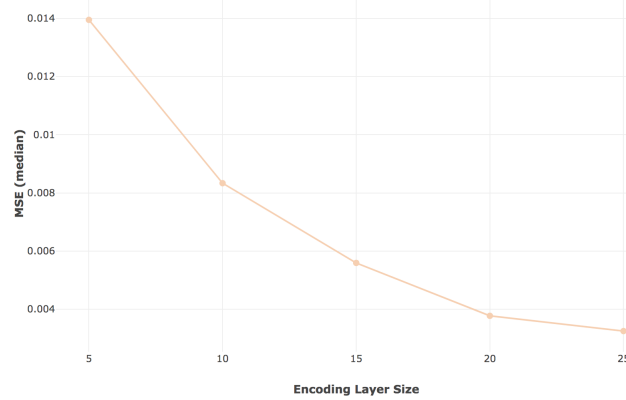


Figure 47: Dataset: Synthetic10 (7.2.2) ; Configuration 7 (11.3.7)

The MSE scores here show that while feature selection and reduction is possible through the SAE networks, the ability to reproduce input does decrease monotonically with the encoding layer size. This is not of real concern though unless exact reproduction (with noise included) is of interest.

11.1.2 Additional Results for Section 8.4 - Weight Initialization Techniques

Prediction Accuracy by Training Epochs (MNIST Data)

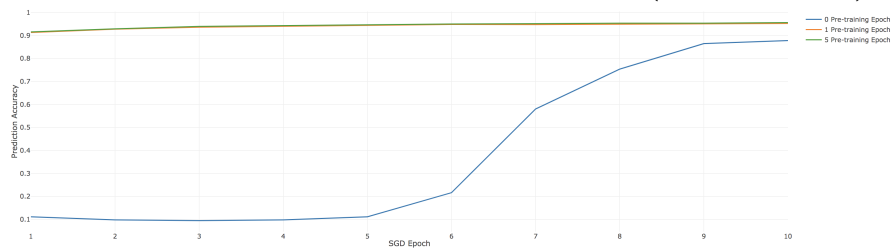


Figure 48: The plot above shows the prediction accuracy achieved on the MNIST dataset according to the number of pre-training epochs using the RBM greedy layerwise methodology as per Section 4.3. There's a clear indication that pre-training allows the network to achieve much higher accuracy much quicker.

SAE MSE by Initialization (Actual Data)

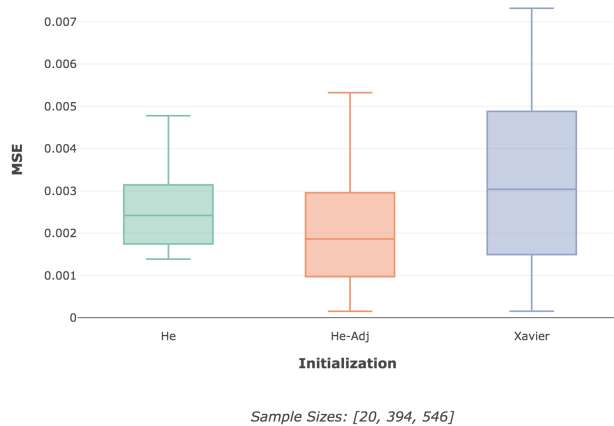


Figure 49: Dataset: Actual10 (7.1.1) ; Configuration 12 (11.3.12)

The SAE MSE results here continue the trend seen for AGL, where He-Adj offers the best performance. Both He and He-Adj suffered with larger learning rates, resulting in dying ReLU's and networks with null outputs, hence the smaller sample sizes. It's possible a more suitable set of learning rates would lead to better results, though the results presented in Section 8.4 lead to a favouring of He-Adj in any case.

11.1.3 Additional Results for Section 8.6 - Complexity of Financial Time Series

11.1.3.1 Effects of Learning Rate Epoch Cycles

SAE MSE by Learning Rate Epoch Cycles (Actual Data)

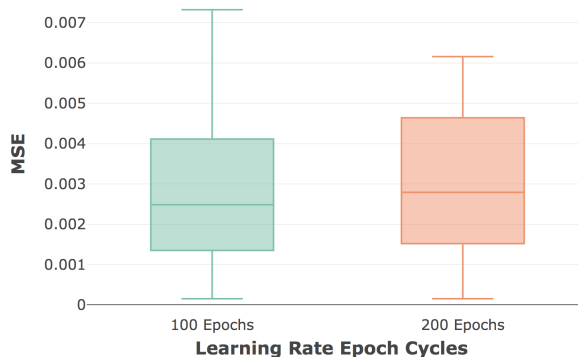


Figure 50: MSE for SAE Networks

This figure shows the MSE scores for SAE networks, with the shorter epoch cycle offering the best (and the worst) results. Synthetic data for the SAE MSE scores behaved similarly, as seen in Figure 51.

SAE MSE by Learning Rate Epoch Cycles (Synthetic Data)

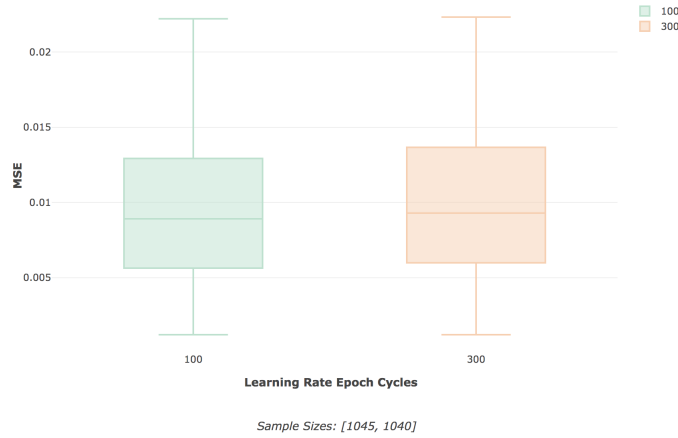


Figure 51: Dataset: Synthetic10 (7.2.2) ; Configuration 7 (11.3.7)

The SAE networks didn't show significant differences according to the epoch cycles. As discussed in Sections 8.5.1 and 8.3, the structure of synthetic data for SAE replication is structurally less complex, and so learning optimizations are less likely to produce large differences.

11.1.3.2 Effects of Learning Rate Epoch Cycles

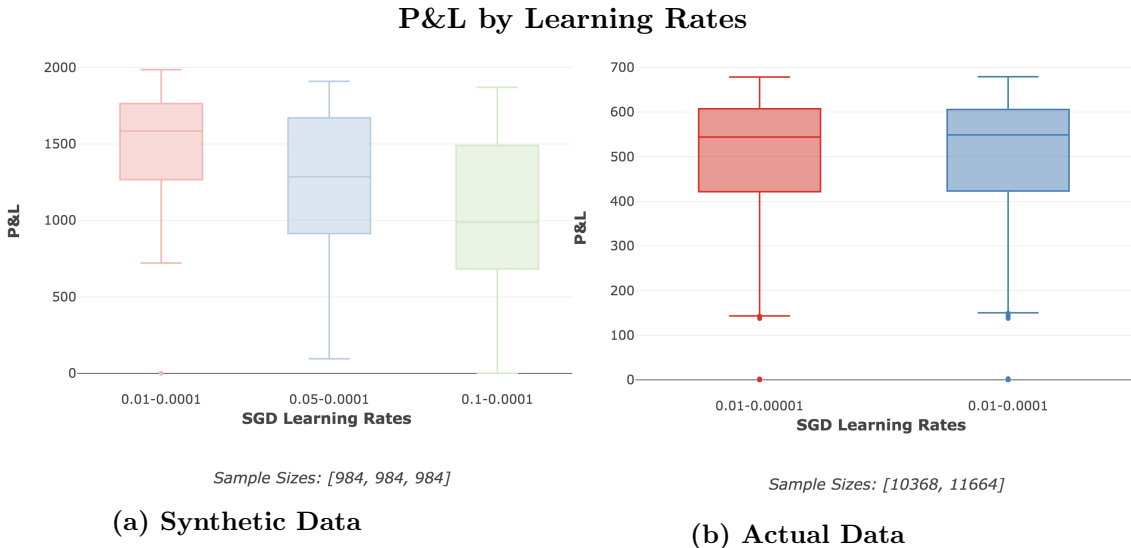


Figure 52: Dataset: Synthetic10 dataset (7.2.2), Actual10 dataset (7.1.1), Configuration 9 (11.3.9) & Configuration 13 (11.3.13)

The learning rates for Actual data shown in Figure (b) here were chosen according to the best rates seen in the SAE training. There's no substantial difference shown by changing the lower bound by a factor. The results for Synthetic data were interesting in that the networks had higher P&L when trained with smaller learning rates, suggesting that the predictive task still warrants a more careful solution space exploration despite the less complex nature of the data.

11.1.4 Additional Results for Section 8.7 - Network Structure and Training

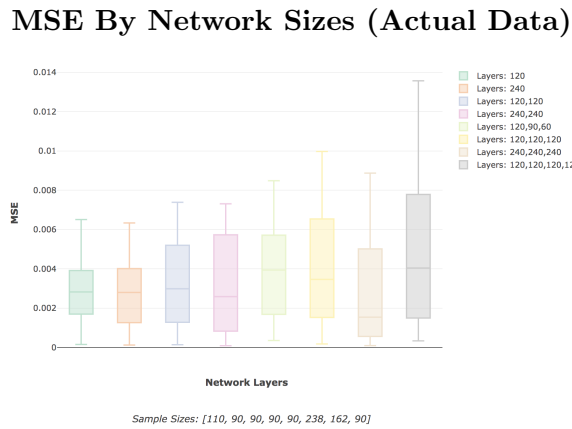


Figure 53: Dataset: Actual10 (7.1.1) ; Configuration 12 (11.3.12)

This figure shows the MSE achieved by SAE networks with the indicated sizes, showing a general increase in performance as both layers and layer sizes increase. The network sizes here indicate the final N layers for the SAE, rather than the $2N + 1$ that are present in training. Training parameters such as number of SGD epochs were not adjusted for network size, and so some smaller networks achieved higher performance as they had more accommodating training. The general trends should be focused on as the indicator for more tailored training. As noted in Section 8.7, the more typical structure of SAEs with descending layer sizes did not show better performance.

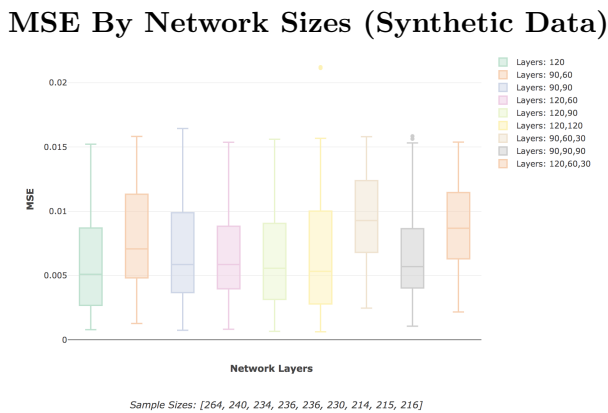


Figure 54: Dataset: Synthetic10 (7.2.2) ; Configuration 7 (11.3.7)

This figure shows the MSE achieved by networks with the indicated sizes, showing a general increase in performance as both layers and layer sizes increase. The network sizes here indicate the final N layers for the SAE, rather than the $2N + 1$ that are present in training. Training parameters such as number of SGD epochs were not adjusted for network size, and so some smaller networks achieved higher performance as they had more accommodating training. The general trends should be focused on as the indicator for more tailored training. As noted in Section 8.7, the more typical structure of SAEs with descending layer sizes did not show better performance.

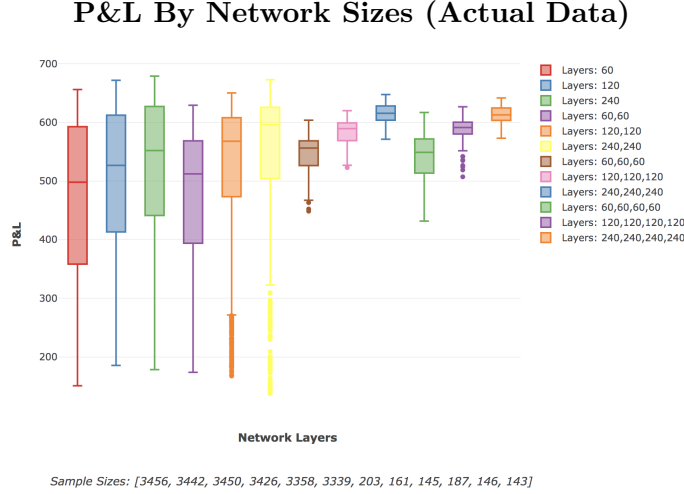


Figure 55: Dataset: Actual10 (7.1.1) ; Configuration 13 (11.3.13)

This figure shows the P&L achieved by networks with the indicated sizes, showing a general increase in performance as both layers and layer sizes increase. Networks that suffered from exploding ReLU's (and hence have approximately 0 P&L) have been excluded for the more effective visualization. Training parameters such as number of SGD epochs were not adjusted for network size, and so some smaller networks achieved higher performance as they had more accommodating training. The general trends should be focused on as the indicator for more tailored training.

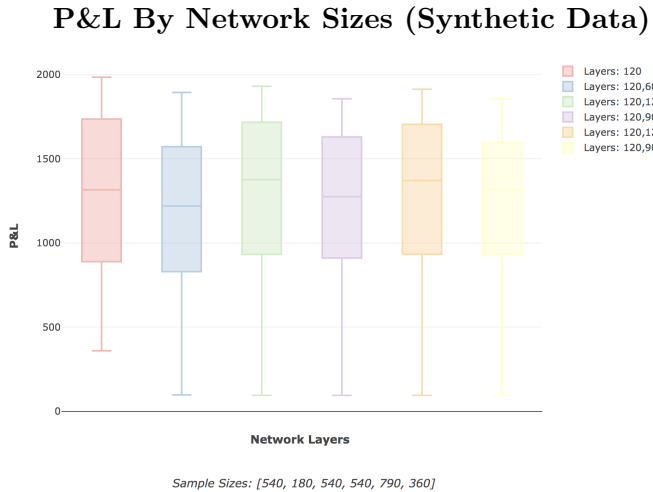


Figure 56: Dataset: Synthetic10 (7.2.2) ; Configuration 9 (11.3.9)

This figure shows the P&L achieved by networks with the indicated sizes, showing a general increase in performance as both layers and layer sizes increase. Networks that suffered from exploding ReLU's (and hence have approximately 0 P&L) have been excluded for the more effective visualization. Training parameters such as number of SGD epochs were not adjusted for network size, and so some smaller networks achieved higher performance as they had more accommodating training. The general trends should be focused on as the indicator for more tailored training.

Predictive P&L by OGD Learning Rate (Synthetic Data)

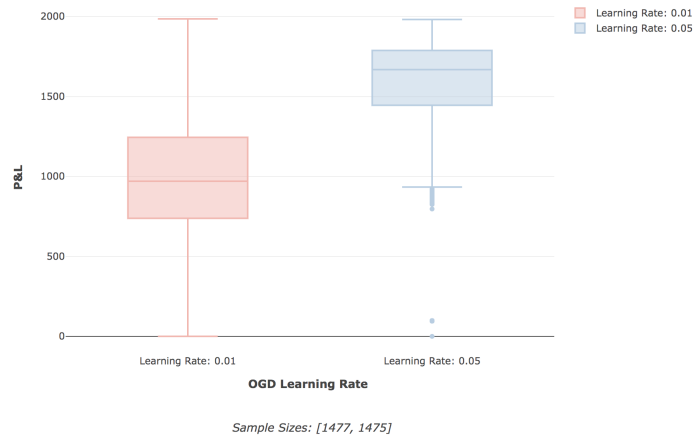


Figure 57: Dataset: Synthetic10 (7.2.2) ; Configuration 9 (11.3.9)

The networks trained on Synthetic data showed a sharp P&L increase as the OGD learning rate increased. It wasn't tested if they would experience the same turning point and begin to degrade as seen in networks for Actual data in Section 8.2

Predictive P&L by L1 Regularization (Synthetic Data)

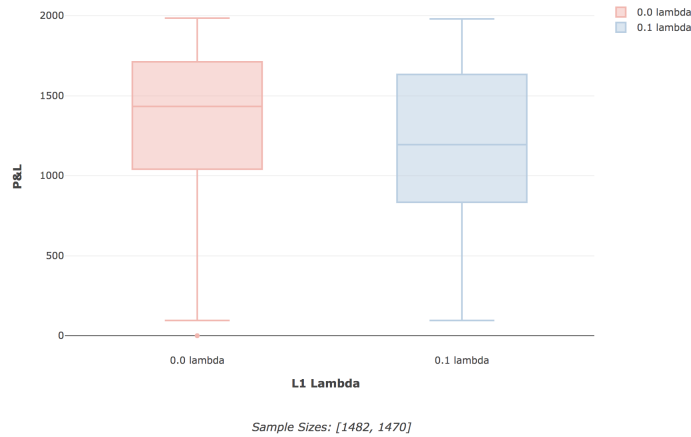


Figure 58: Dataset: Synthetic10 (7.2.2) ; Configuration 9 (11.3.9)

SAE: Leaky ReLU vs ReLU (Synthetic Data)

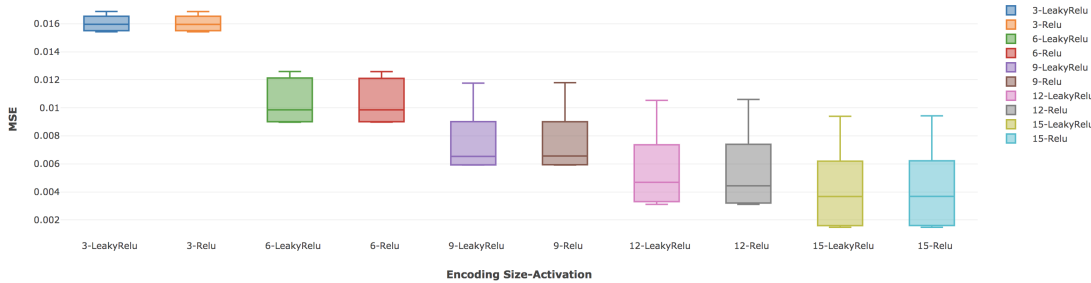


Figure 59: Dataset Synthetic6 (7.2.1) ; Configuration 17 (11.3.17)

The plot above shows the SAE MSE, grouped by encoding size and activations, showing a marginal increase in performance for Leaky ReLU activations.

P&L by ReLU Activations (Synthetic Data)

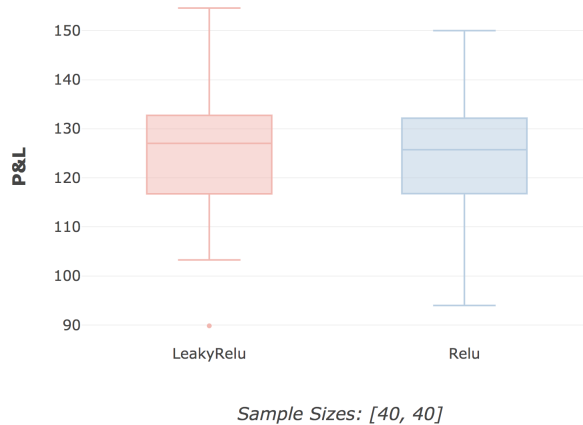


Figure 60: Dataset Synthetic6 (7.2.1) ; Configuration 5 (11.3.5)

The plot shows the FFN P&L, grouped by activation, showing some improvements from the Leaky ReLU activation. The effect is most noticeable in reducing the lower bounds of performance (10.8%), though has a clear benefit in the upper bounds as well (3.4%).

11.2 Additional Calculations for Section 8.10 - DSR and ONC

11.2.1 DSR and PSR calculations

1 Calculated the Aggregate Cluster Strategy Time Series Return:

Using the ONC results from Section 8.10.2, as well as equations 84 and 85 from Section 4.8.4.1, the 2 cluster SR metrics were calculated to be $\widehat{SR}_1 = 0.395059$ and $\widehat{SR}_2 = 0.483543$.

2 Annualize the Cluster Strategy Sharpe Ratios:

$$\widehat{aSR}_k = \widehat{SR}_k \sqrt{Frequency_k} \quad (88)$$

$$\widehat{aSR}_1 = 0.395059\sqrt{365.25} = 7.550167 \quad (89)$$

$$\widehat{aSR}_2 = 0.483543\sqrt{365.25} = 9.241242 \quad (90)$$

3 Estimate the Variance of Strategy Sharpe Ratios:

Using equation (87), the cluster strategy Sharpe ratios can be used to estimate the SR variance.

$$E[V[\{\widehat{SR}_k\}]] = \frac{V[\{\widehat{aSR}_k\}]}{\text{Frequency}_{k^*}} \quad (91)$$

$$= \frac{V[7.550167, 9.241242]}{365.25} \quad (92)$$

$$= 0.001957 \quad (93)$$

4 Calculate the Benchmark SR*:

Using the estimated variance and equation (83), the benchmark SR^* can then be calculated (where $Z[.]$ is the CDF of the standard Normal Distribution and γ is the Euler-Mascheroni constant).

$$SR^* = \sqrt{V[\{\widehat{SR}_k\}]} \left((1 - \gamma)Z^{-1} \left[1 - \frac{1}{K} \right] + \gamma Z^{-1} \left[1 - \frac{1}{Ke} \right] \right) \quad (94)$$

$$= \sqrt{0.001957} \left((1 - \gamma)Z^{-1} \left[1 - \frac{1}{2} \right] + \gamma Z^{-1} \left[1 - \frac{1}{2e} \right] \right) \quad (95)$$

$$= 0.022995 \quad (96)$$

5 Calculate DSR:

Using the benchmark, the final DSR calculation can be done with equation (81) (where T is the number of observed returns, $\hat{\gamma}_3$ is the skewness of r_t and $\hat{\gamma}_4$ is the kurtosis of r_t ())

$$\widehat{SR} = 0.641676 \quad (97)$$

$$\widehat{PSR}[SR^*] = Z \left[\frac{(\widehat{SR} - SR^*)\sqrt{T-1}}{\sqrt{1 - \hat{\gamma}_3 \widehat{SR} + \frac{\hat{\gamma}_4 - 1}{4} \widehat{SR}^2}} \right] \quad (98)$$

$$= Z \left[\frac{(0.641676 - 0.022995) \sqrt{1555 - 1}}{\sqrt{1 - 1.860821 * 0.641676 + \frac{9.083369 - 1}{4} 0.641676^2}} \right] \quad (99)$$

$$= Z \left[\frac{24.388922}{0.798770} \right] \quad (100)$$

$$= 1.0 \quad (101)$$

11.3 Configuration Sets Used

11.3.1 Configuration 1

- category: SAE
 - sae_config_id: 0
 - steps: 5000
 - deltas: 1,5,20
 - process_splits: 0.6
 - training_splits: 0.8,1.0
 - prediction_steps: 2
 - scaling_function: NormalizeData;StandardizeData
 - layer_sizes: (30,60,5); (30,60,60,5); (30,60,60,60,5); (30,120,5); (30,120,120,5); (30,120,120,120,5); (30,60,15); (30,60,60,15); (30,60,60,60,15); (30,120,15); (30,120,120,15); (30,120,120,120,15); (30,60,25); (30,60,60,25); (30,60,60,60,25); (30,120,25); (30,120,120,25); (30,120,120,120,25)
 - layer_activations: SigmoidActivation,ReluActivation,LinearActivation
 - initialization: XavierGlorotUniformInit
 - encoding_activation: LinearActivation;SigmoidActivation;ReluActivation
 - output_activation: LinearActivation;SigmoidActivation;ReluActivation
 - learning_rate: 0.001;0.1;1.0;0.01;0.05;0.25;2.0
 - minibatch_size: 20
 - max_epochs: 500
 - l1_lambda: 0.0
 - min_learning_rate: 0.0
 - epoch_cycle_max: 0
 - ogd_learning_rate: 0.0
- Samples: 1129

11.3.2 Configuration 2

- category: SAE
- sae_config_id: 0
- steps: 5000
- deltas: 1,5,20
- process_splits: 0.6
- training_splits: 0.8,1.0
- prediction_steps: 2
- scaling_function: NormalizeData

- layer_sizes: (30,60,5); (30,60,60,5); (30,60,60,60,5); (30,120,5); (30,120,120,5); (30,120,120,120,5); (30,60,15); (30,60,60,15); (30,60,60,60,15); (30,120,15); (30,120,120,15); (30,120,120,120,15); (30,60,25); (30,60,60,25); (30,60,60,60,25); (30,120,25); (30,120,120,25); (30,120,120,120,25)
 - layer_activations: SigmoidActivation,ReluActivation,LinearActivation
 - initialization: XavierGlorotUniformInit
 - encoding_activation: LinearActivation;SigmoidActivation;ReluActivation
 - output_activation: LinearActivation;SigmoidActivation;ReluActivation
 - learning_rate: 0.001;0.1;1.0;0.01;0.05;0.25
 - minibatch_size: 20
 - max_epochs: 500
 - l1_lambda: 0.0
 - min_learning_rate: 0.0
 - epoch_cycle_max: 0
 - ogd_learning_rate: 0.0
- Samples: 648

11.3.3 Configuration 3

- category: FFN
- sae_config_id: 3560;3574;3580;3590;3613;3620;3626;3638;3650;3671
- steps: 5000
- deltas: 1,5,20
- process_splits: 0.6
- training_splits: 0.8,1.0
- prediction_steps: 2
- scaling_function: NormalizeData;LimitedNormalizeData
- layer_sizes: (15,40,6); (12,40,6); (9,40,6); (6,40,6); (3,40,6); (15,40,40,40,6); (12,40,40,40,6); (9,40,40,40,6); (6,40,40,40,6); (3,40,40,40,6); (15,80,6); (12,80,6); (9,80,6); (6,80,6); (3,80,6); (15,80,80,80,6); (12,80,80,80,6); (9,80,80,80,6); (6,80,80,80,6); (3,80,80,80,6)
- layer_activations: SigmoidActivation,ReluActivation,LinearActivation
- initialization: XavierGlorotNormalInit
- encoding_activation: ;LinearActivation
- output_activation: LinearActivation;ReluActivation
- learning_rate: 1.0e-5;0.0001;0.001;0.01
- minibatch_size: 20
- max_epochs: 500

- l1_lambda: 0.0
- min_learning_rate: 0.0
- epoch_cycle_max: 0
- is_denoising: 0
- denoising_variance: 0.0
- ogd_learning_rate: 0.0001;0.001

Samples: 960

11.3.4 Configuration 4

- category: FFN
- sae_config_id: 3560;3574;3580;3590;3613;3620;3626;3638;3650;3671
- steps: 5000
- deltas: 1,5,20
- process_splits: 0.6
- training_splits: 0.8,1.0
- prediction_steps: 2
- scaling_function: NormalizeData;LimitedNormalizeData
- layer_sizes: (15,40,6); (12,40,6); (9,40,6); (6,40,6); (3,40,6); (15,40,40,40,6); (12,40,40,40,6); (9,40,40,40,6); (6,40,40,40,6); (3,40,40,40,6); (15,80,6);(12,80,6); (9,80,6); (6,80,6); (3,80,6); (15,80,80,80,6); (12,80,80,80,6); (9,80,80,80,6); (6,80,80,80,6); (3,80,80,80,6); (15,20,6); (12,20,6); (9,20,6); (6,20,6); (3,20,6); (15,20,20,6); (12,20,20,6); (9,20,20,6); (6,20,20,6); (3,20,20,6); (15,20,20,20,6); (12,20,20,20,6); (9,20,20,20,6); (6,20,20,20,6); (3,20,20,20,6)
- layer_activations: SigmoidActivation,ReluActivation,LinearActivation
- initialization: XavierGlorotNormalInit
- encoding_activation: ;LinearActivation
- output_activation: LinearActivation;ReluActivation
- learning_rate: 1.0e-5;0.0001;0.001;0.01
- minibatch_size: 20
- max_epochs: 500
- l1_lambda: 0.0
- min_learning_rate: 0.0
- epoch_cycle_max: 0
- is_denoising: 0
- denoising_variance: 0.0
- ogd_learning_rate: 0.0001;0.001

Samples: 1680

11.3.5 Configuration 5

- category: FFN
 - sae_config_id: 8860;8872;8876;8888;8910;8800;8812;8816;8828;8850
 - steps: 5000
 - deltas: 1,5,20
 - process_splits: 0.6
 - training_splits: 0.8,1.0
 - prediction_steps: 2
 - scaling_function: LimitedNormalizeData
 - layer_sizes: (15,40,6); (12,40,6); (9,40,6); (6,40,6); (3,40,6); (15,40,40,40,6); (12,40,40,40,6); (9,40,40,40,6); (6,40,40,40,6); (3,40,40,40,6); (15,80,6);(12,80,6); (9,80,6); (6,80,6); (3,80,6); (15,80,80,80,6); (12,80,80,80,6); (9,80,80,80,6); (6,80,80,80,6); (3,80,80,80,6)
 - layer_activations: SigmoidActivation,ReluActivation,LinearActivation
 - initialization: XavierGlorotNormalInit
 - encoding_activation: LinearActivation
 - output_activation: LinearActivation
 - learning_rate: 0.001;0.01
 - minibatch_size: 20
 - max_epochs: 500
 - l1_lambda: 0.0
 - min_learning_rate: 0.0
 - epoch_cycle_max: 0
 - is_denoising: 0
 - denoising_variance: 0.0
 - ogd_learning_rate: 0.001
- Samples: 80

11.3.6 Configuration 6

- category: SAE
- sae_config_id: 0
- steps: 5000
- deltas: 1,5,20
- process_splits: 0.6
- training_splits: 0.8,1.0
- prediction_steps: 2

- scaling_function: NormalizeData
 - layer_sizes: (6,15,5); (6,15,15,5)
 - layer_activations: SigmoidActivation,ReluActivation,LinearActivation
 - initialization: XavierGlorotNormalInit
 - encoding_activation: LinearActivation;SigmoidActivation
 - output_activation: SigmoidActivation
 - learning_rate: 1.0;2.0;4.0
 - minibatch_size: 20
 - max_epochs: 100
 - l1_lambda: 0.0
 - min_learning_rate: 1.0
 - epoch_cycle_max: 1
 - ogd_learning_rate: 0.0
- Samples: 192

11.3.7 Configuration 7

- category: SAE
- sae_config_id: 0
- steps: 5000
- deltas: 1,5,20;5,20,60;10,20,60
- process_splits: 0.6
- training_splits: 0.8,1.0
- prediction_steps: 5
- scaling_function: LimitedNormalizeData
- layer_sizes: (30,120,60,25); (30,120,60,20); (30,120,60,15); (30,120,60,10);
 (30,120,60,5); (30,120,25); (30,120,20); (30,120,15); (30,120,10); (30,120,5);
 (30,120,120,25); (30,120,120,20); (30,120,120,15); (30,120,120,10); (30,120,120,5);
 (30,120,90,25); (30,120,90,20); (30,120,90,15); (30,120,90,10); (30,120,90,5);
 (30,90,60,25); (30,90,60,20); (30,90,60,15); (30,90,60,10); (30,90,60,5); (30,90,60,30,25);
 (30,90,60,30,20); (30,90,60,30,15); (30,90,60,30,10); (30,90,60,30,5); (30,120,60,30,25);
 (30,120,60,30,20); (30,120,60,30,15); (30,120,60,30,10); (30,120,60,30,5);
 (30,90,90,90,25); (30,90,90,90,20); (30,90,90,90,15); (30,90,90,90,10); (30,90,90,90,5); (30,90,90,25);
 (30,90,90,20); (30,90,90,15); (30,90,90,10); (30,90,90,5)
- layer_activations: SigmoidActivation,ReluActivation,LinearActivation
- initialization: XavierGlorotUniformInit;HeUniformInit;DCUniformInit
- encoding_activation: LinearActivation
- output_activation: LinearActivation
- learning_rate: 0.005;0.01;0.05;0.1

- minibatch_size: 20
- max_epochs: 400
- l1_lambda: 0.0
- min_learning_rate: 0.0001
- epoch_cycle_max: 100;300
- is_denoising: 0
- denoising_variance: 0.0
- ogd_learning_rate: 0.0

Samples: 3266

11.3.8 Configuration 8

- category: SAE
- sae_config_id: 0
- steps: 5000
- deltas: 1,5,20;5,20,60;10,20,60
- process_splits: 0.6
- training_splits: 0.8,1.0
- prediction_steps: 5
- scaling_function: LimitedNormalizeData
- layer_sizes: (3,12,6,2); (3,12,2); (3,12,12,2); (3,12,9,2); (3,9,6,2); (3,9,6,3,2); (3,12,6,3,2); (3,9,9,9,2); (3,9,9,2); (3,12,6,1); (3,12,1); (3,12,12,1); (3,12,9,1); (3,9,6,1); (3,9,6,3,1); (3,12,6,3,1); (3,9,9,9,1); (3,9,9,1)
- layer_activations: SigmoidActivation,ReluActivation,LinearActivation
- initialization: XavierGlorotUniformInit;HeUniformInit;DCUniformInit
- encoding_activation: LinearActivation
- output_activation: LinearActivation
- learning_rate: 0.005;0.01;0.05;0.1
- minibatch_size: 20
- max_epochs: 400
- l1_lambda: 0.0
- min_learning_rate: 0.0001
- epoch_cycle_max: 100;300
- is_denoising: 0
- denoising_variance: 0.0
- ogd_learning_rate: 0.0

Samples: 1296

11.3.9 Configuration 9

- category: FFN
 - sae_config_id: 18140;18914;18259;18311;19481;20662;18917;18260;18314;18766;18119;18191;19343
 - steps: 5000
 - deltas: 1,5,20;5,20,60;10,20,60
 - process_splits: 0.6
 - training_splits: 0.8,1.0
 - prediction_steps: 5
 - scaling_function: LimitedNormalizeData
 - layer_sizes: (25,120,120,10); (20,120,120,10); (15,120,120,10); (10,120,120,10); (5,120,120,10); (25,120,120,120,10); (20,120,120,120,10); (15,120,120,120,10); (10,120,120,120,10); (5,120,120,120,10); (25,120,90,90,60,10); (20,120,90,90,60,10); (15,120,90,90,60,10); (10,120,90,90,60,10); (5,120,90,90,60,10); (25,120,90,60,10); (20,120,90,60,10); (15,120,90,60,10); (10,120,90,60,10); (5,120,90,60,10); (25,120,10); (20,120,10); (15,120,10); (10,120,10); (5,120,10); (25,120,60,10); (20,120,60,10); (15,120,60,10); (10,120,60,10); (5,120,60,10)
 - layer_activations: SigmoidActivation,ReluActivation,LinearActivation
 - initialization: XavierGlorotUniformInit;DCUniformInit;HeUniformInit
 - encoding_activation: None
 - output_activation: LinearActivation
 - learning_rate: 0.01;0.05;0.1
 - minibatch_size: 20
 - max_epochs: 400
 - l1_lambda: 0.0;0.1
 - min_learning_rate: 0.0001
 - epoch_cycle_max: 100
 - is_denoising: 0
 - denoising_variance: 0.0
 - ogd_learning_rate: 0.01;0.05
- Samples: 3313

11.3.10 Configuration 10

- category: FFN
- sae_config_id: 25339;25778;25684;25846;25640;25767
- steps: 5000
- deltas: 1,5,20;5,20,60;10,20,60
- process_splits: 0.6

- training_splits: 0.8,1.0
- prediction_steps: 5
- scaling_function: LimitedNormalizeData
- layer_sizes: (2,12,6,1); (1,12,6,1); (2,12,12,1); (1,12,12,1); (2,12,12,12,1); (1,12,12,12,1); (2,12,9,9,6,1); (1,12,9,9,6,1); (2,12,9,6,1); (1,12,9,6,1); (2,12,1); (1,12,1)
- layer_activations: SigmoidActivation,ReluActivation,LinearActivation
- initialization: HeUniformInit; XavierGlorotUniformInit; DCUniformInit
- encoding_activation: None
- output_activation: LinearActivation
- learning_rate: 0.01;0.05;0.1
- minibatch_size: 20
- max_epochs: 400
- l1_lambda: 0.0;0.1
- min_learning_rate: 0.0001
- epoch_cycle_max: 100
- is_denoising: 0
- denoising_variance: 0.0
- ogd_learning_rate: 0.01;0.05

Samples: 1296

11.3.11 Configuration 11

- category: FFN
- sae_config_id: 1533;1497;1554;1639;147;1534;1468;1501;318;1284;1535;1553;1059;1508;333
- steps: 1
- deltas: 1,5,20;5,20,60;10,20,60
- process_splits: 0.6
- training_splits: 0.8,1.0
- prediction_steps: 5
- scaling_function: LimitedNormalizeData
- layer_sizes: (25,60,10); (20,60,10); (15,60,10); (10,60,10); (5,60,10); (25,120,10); (20,120,10); (15,120,10); (10,120,10); (5,120,10); (25,240,10); (20,240,10); (15,240,10); (10,240,10); (5,240,10); (25,120,120,10); (20,120,120,10); (15,120,120,10); (10,120,120,10); (5,120,120,10); (25,240,240,10); (20,240,240,10); (15,240,240,10); (10,240,240,10); (5,240,240,10); (25,60,60,10); (20,60,60,10); (15,60,60,10); (10,60,60,10); (5,60,60,10); (30,60,10); (30,120,10); (30,240,10); (30,60,60,10); (30,120,120,10); (30,240,240,10)
- layer_activations: SigmoidActivation,ReluActivation,LinearActivation

- initialization: DCUniformInit
 - encoding_activation: None
 - output_activation: LinearActivation
 - learning_rate: 0.01
 - minibatch_size: 32
 - max_epochs: 100;500;1000;10
 - l1_lambda: 0.0;0.1;0.5
 - ifnull(tp.l2_lambda,0): 0
 - min_learning_rate: 0.0001;1.0e-5
 - epoch_cycle_max: 100;10
 - is_denoising: 1
 - denoising_variance: 0.0;0.1
 - ogd_learning_rate: 0.005;0.01;0.05;0.1
- Samples: 20737

11.3.12 Configuration 12

- category: SAE
- sae_config_id: 0
- steps: 1
- deltas: 1,5,20;5,20,60;10,20,60
- process_splits: 0.6
- training_splits: 0.8,1.0
- prediction_steps: 5
- scaling_function: LimitedNormalizeData
- layer_sizes: (30,120,25); (30,120,20); (30,120,15); (30,120,10); (30,120,5);
 (30,120,120,25); (30,120,120,20); (30,120,120,15); (30,120,120,10); (30,120,120,5);
 (30,120,120,120,25); (30,120,120,120,20); (30,120,120,120,15); (30,120,120,120,10);
 (30,120,120,120,5); (30,120,120,120,120,25); (30,120,120,120,120,20); (30,120,120,120,120,15);
 (30,120,120,120,120,10); (30,120,120,120,120,5); (30,240,240,25); (30,240,240,20);
 (30,240,240,15); (30,240,240,10); (30,240,240,5); (30,240,240,25); (30,120,90,60,25);
 (30,120,90,60,20); (30,120,90,60,15); (30,120,90,60,10); (30,120,90,60,5);
 (30,240,25); (30,240,20); (30,240,15); (30,240,10); (30,240,5); (30,240,240,240,20);
 (30,240,240,240,15); (30,240,240,240,10); (30,240,240,240,5)
- layer_activations: SigmoidActivation,ReluActivation,LinearActivation
- initialization: XavierGlorotUniformInit;HeUniformInit;DCUniformInit
- encoding_activation: LinearActivation
- output_activation: LinearActivation
- learning_rate: 0.01;0.1

- minibatch_size: 32
- max_epochs: 2000;10000;20000
- l1_lambda: 0.5;0.0;0.1;1.0
- ifnull(tp.l2_lambda,0): 0
- min_learning_rate: 0.0001;1.0e-5
- epoch_cycle_max: 100;200
- is_denoising: 0
- denoising_variance: 0.0
- ogd_learning_rate: 0.0

Samples: 1665

11.3.13 Configuration 13

- category: FFN
- sae_config_id: 1533;1497;1554;1639;147;1534;1468;1501;318;1284;1535;1553;1059;1508;333
- steps: 1
- deltas: 1,5,20;5,20,60;10,20,60
- process_splits: 0.6
- training_splits: 0.8,1.0
- prediction_steps: 5
- scaling_function: LimitedNormalizeData
- layer_sizes: (25,60,10); (20,60,10); (15,60,10); (10,60,10); (5,60,10); (25,120,10); (20,120,10); (15,120,10); (10,120,10); (5,120,10); (25,240,10); (20,240,10); (15,240,10); (10,240,10); (5,240,10); (25,120,120,10); (20,120,120,10); (15,120,120,10); (10,120,120,10); (5,120,120,10); (25,240,240,10); (20,240,240,10); (15,240,240,10); (10,240,240,10); (5,240,240,10); (25,60,60,10); (20,60,60,10); (15,60,60,10); (10,60,60,10); (5,60,60,10); (30,60,10); (30,120,10); (30,240,10); (30,60,60,10); (30,120,120,10); (30,240,240,10); (10,60,60,60,10); (10,120,120,120,10); (10,240,240,240,10); (10,60,60,60,10); (10,120,120,120,10); (10,240,240,240,10)
- layer_activations: SigmoidActivation,ReluActivation,LinearActivation
- initialization: DCUniformInit
- encoding_activation: None
- output_activation: LinearActivation
- learning_rate: 0.01
- minibatch_size: 32
- max_epochs: 100;500;1000;10
- l1_lambda: 0.0;0.1;0.5
- ifnull(tp.l2_lambda,0): 0
- min_learning_rate: 0.0001;1.0e-5

- epoch_cycle_max: 100;10;-1
- is_denoising: 1;0
- denoising_variance: 0.0;0.1
- ogd_learning_rate: 0.005;0.01;0.05;0.1

Samples: 22033

11.3.14 Configuration 14

- category: SAE
- sae_config_id: 0
- steps: 5000
- deltas: 1,5,20
- process_splits: 0.6
- training_splits: 0.8,1.0
- prediction_steps: 2
- scaling_function: NormalizeData
- layer_sizes: (6,30,5); (6,30,30,5); (6,30,3); (6,30,30,3); (30,60,5); (30,60,60,5); (30,60,60,60,5); (30,120,5); (30,120,120,5); (30,120,120,120,5); (30,60,15); (30,60,60,15); (30,60,60,60,15); (30,120,15); (30,120,120,15); (30,120,120,120,15); (30,60,25); (30,60,60,25); (30,60,60,60,25); (30,120,25); (30,120,120,25); (30,120,120,120,25)
- layer_activations: SigmoidActivation,ReluActivation,LinearActivation
- initialization: XavierGlorotUniformInit
- encoding_activation: LinearActivation
- output_activation: LinearActivation
- learning_rate: 0.05;0.1
- minibatch_size: 20
- max_epochs: 1;1000
- l1_lambda: 0.0
- min_learning_rate: 0.0
- epoch_cycle_max: 0
- is_denoising: 1
- denoising_variance: 0.1;0.01;0.001;0.0001;1.0e-11
- ogd_learning_rate: 0.0

Samples: 243

11.3.15 Configuration 15

- category: SAE
- sae_config_id: 0
- steps: 5000
- deltas: 1,5,20
- process_splits: 0.6
- training_splits: 0.8,1.0
- prediction_steps: 2
- scaling_function: LimitedNormalizeData
- layer_sizes: (30,60,25); (30,60,60,25); (30,120,25); (30,120,120,25); (30,60,15); (30,60,60,15); (30,120,15); (30,120,120,15); (30,60,5); (30,60,60,5); (30,120,5); (30,120,120,5)
- layer_activations: SigmoidActivation,ReluActivation,LinearActivation
- initialization: XavierGlorotUniformInit
- encoding_activation: LinearActivation
- output_activation: LinearActivation
- learning_rate: 0.001
- minibatch_size: 20
- max_epochs: 500
- l1_lambda: 0.0
- min_learning_rate: 0.0
- epoch_cycle_max: 0
- is_denoising: 1
- denoising_variance: 0.01;0.05;0.1;0.15;0.2;0.25
- ogd_learning_rate: 0.0

Samples: 73

11.3.16 Configuration 16

- category: FFN
- sae_config_id: 318;1508;1639
- steps: 1
- deltas: 5,20,60;10,20,60;1,5,20
- process_splits: 0.6
- training_splits: 0.8,1.0
- prediction_steps: 5
- scaling_function: LimitedNormalizeData

- layer_sizes: (10,60,60,60,10); (10,120,120,120,10); (10,240,240,240,10); (10,60,60,60,10); (10,120,120,120,120,10); (10,240,240,240,240,10); (10,60,10); (10,120,10); (10,240,10); (10,60,60,10); (10,120,120,10); (10,240,240,10)
 - layer_activations: SigmoidActivation,ReluActivation,LinearActivation
 - initialization: DCUniformInit
 - encoding_activation: None
 - output_activation: LinearActivation
 - learning_rate: 0.01
 - minibatch_size: 32
 - max_epochs: 100;500;10;2000
 - l1_lambda: 0.0
 - ifnull(tp.l2_lambda,0): 0
 - min_learning_rate: 0.0001;0.001;1.0e-5
 - epoch_cycle_max: -1;100;10
 - is_denoising: 0
 - denoising_variance: 0.0
 - ogd_learning_rate: 0.01;0.05;0.1;0.001
- Samples: 1512

11.3.17 Configuration 17

- category: SAE
- sae_config_id: 0
- steps: 5000
- deltas: 1,5,20
- process_splits: 0.6
- training_splits: 0.8,1.0
- prediction_steps: 2
- scaling_function: LimitedNormalizeData
- layer_sizes: (18,40,15); (18,40,40,15); (18,40,40,40,15); (18,80,15); (18,80,80,15); (18,80,80,80,15); (18,40,12); (18,40,40,12); (18,40,40,40,12); (18,80,12); (18,80,80,12); (18,80,80,80,12); (18,40,9); (18,40,40,9); (18,40,40,40,9); (18,80,9); (18,80,80,9); (18,80,80,80,9); (18,40,6); (18,40,40,6); (18,40,40,40,6); (18,80,6); (18,80,80,6); (18,80,80,80,6); (18,40,3); (18,40,40,3); (18,40,40,40,3); (18,80,3); (18,80,80,3); (18,80,80,80,3)
- layer_activations: SigmoidActivation,ReluActivation,LinearActivation
- initialization: XavierGlorotUniformInit
- encoding_activation: LinearActivation
- output_activation: LinearActivation

- learning_rate: 0.001;0.01
- minibatch_size: 20
- max_epochs: 500
- l1_lambda: 0.0
- min_learning_rate: 0.0
- epoch_cycle_max: 0
- is_denoising: 0
- denoising_variance: 0.0
- ogd_learning_rate: 0.0

Samples: 120

11.4 Diagnostic Charts

| Function Name | Configuration Dimensions | Type |
|-------------------------------------|---|------------|
| PL_ScalingOutputActivation | Scaling Methodology, Network Output Activation Function | Box Chart |
| PL_ScalingHiddenOutputActivation | Scaling Methodology, Network Hidden Activation Function | Box Chart |
| PL_LearningRates_MaxMin | Min and Max SGD Learning Rates | Box Chart |
| PL_L1Reg | SGD L1 Regularization Lambda | Box Chart |
| PL_ValidationSplit | Percentage of SGD dataset used for training / testing | Box Chart |
| PL_OGD_LearningRate | OGD Learning Rate | Box Chart |
| PL_Denoising | SGD Denoising Variance | Box Chart |
| PL_MaxEpochs | SGD Training Epochs | Box Charts |
| PL_EpochCycle | SGD Learning Rate Epochg Cycle Length | Box Chart |
| PL_LayerActivation_OutputActivation | Network Hidden Activations and Output Activation | Box Chart |
| PL_Activations | Network Hidden Activations | Box Chart |
| PL_Activations_NetworkSize | Network Hidden Activations and Layer Sizes | Box Chart |
| PL_NetworkSize | Network Layers | Box Chart |
| PL_NetworkSizeLines | Network Layers | Line Graph |
| PL_SAE_Encoding_SizeLines | Feature Selection Size | Line Graph |

| | | |
|--|---|-----------|
| PL_SAE_Encoding_Size | Feature Selection Size | Box Chart |
| PL_DataDeltas | Price Fluctuation Aggregation Horizons | Box Chart |
| PL_Init | Network Initialization Method | Box Chart |
| PL_Heatmap_LearningRate_MaxEpochs | OGD Learning Rate and SGD Training Epochs | Heatmap |
| PL_Heatmap_NetworkSize_DataAggregation | Network Number of Layers and Price Fluctuation Aggregation Horizons | Heatmap |
| PL_Heatmap_LayerSize_DataAggregation | Network Layer Sizes and Price Fluctuation Aggregation Horizons | Heatmap |

Table 5: P&L Diagnostic EDA Functions

| Function Name | Configuration Dimensions | Type |
|------------------------------|--|------------|
| MSE_ActivationsEncodingSizes | Network Activation Functions and Encoding Layer Size | Box Chart |
| MSE_LayerSizesLines | Network Layer Sizes | Line Graph |
| MSE_LayerSizes | Network Layer Sizes | Box Chart |
| MSE_LearningRate_MaxMin | SGD Min and Max Learning Rates | Box Chart |
| MSE_Lambda1 | SGD L1 Regularization Lambda | Box Chart |
| MSE_EpochCycle | SGD Learning Rate Epoch Cycle Length | Box Chart |
| MSE_Init | Network Initialization Method | Box Chart |

| | | |
|--------------------------------------|---|-----------|
| MSE_Deltas | Price Fluctuation Aggregation Horizons | Box Chart |
| MSE_Min_EncodingSize_Activation | Encoding Layer Activation Function and Size | Box Chart |
| MSE_Activation_Scaling_Filters | All Activation Functions and Data Scaling Methodology | Box Chart |
| MSE_OutputActivation_Scaling_Filters | Output Activation Function and Data Scaling Methodology | Box Chart |
| MSE_Output_Activation | Output Activation Function | Box Chart |
| MSE_Encoding_Activation | Encoding Layer Activation | Box Chart |
| MSE_Hidden_Activation | Hidden Layer Activation Functions | Box Chart |
| MSE_Scaling_Filters | Data Scaling Methodology | Box Chart |
| MSE_Pretraining | Pretraining Epochs | Box Chart |
| MSE_Denoising | SGD Denoising Variance | Box Chart |

Table 6: P&L Diagnostic EDA Functions

12 References

- [1] Susanne Albers. Online algorithms: a survey. *Mathematical Programming*, 97:3–26, 05 2003. doi: 10.1007/s10107-003-0436-0. URL <https://link.springer.com/content/pdf/10.1007%2Fs10107-003-0436-0.pdf>.
- [2] Diego Aparicio and Marcos Lopez de Prado. How hard is it to pick the right model? mcs and backtest overfitting. *Algorithmic Finance*, 7:53–61, 01 2018. doi: 10.3233/AF-180231. URL <https://ssrn.com/abstract=3044740>.
- [3] B. Arthur. Complexity in economics and financial markets. *Complexity*, 1:20–25, 10 1995. doi: 10.1002/cplx.6130010106. URL <https://onlinelibrary.wiley.com/doi/epdf/10.1002/cplx.6130010106>.
- [4] David Bailey and Marcos Lopez de Prado. The sharpe ratio efficient frontier. *The Journal of Risk*, 15:3–44, 12 2012. doi: 10.21314/JOR.2012.255.
- [5] David Bailey and Marcos Lopez de Prado. The deflated sharpe ratio: Correcting for selection bias, backtest overfitting, and non-normality. *The Journal of Portfolio Management*, 40:94–107, 09 2014. doi: 10.3905/jpm.2014.40.5.094.
- [6] David H. Bailey, Jonathan Borwein, Marcos Lopez de Prado, and Qiji Jim Zhu. Pseudo-mathematics and financial charlatanism: The effects of backtest overfitting on out-of-sample performance. *Notices of the American Mathematical Society*, 61:458–471, 4 2014. doi: 10.1090/noti1105. URL <https://ssrn.com/abstract=2308659>.
- [7] David H. Bailey, Jonathan Borwein, Marcos Lpez de Prado, and Qiji Jim Zhu. The probability of backtest overfitting. *Journal of Computational Finance*, 20:39–69, 4 2017. doi: 10.21314/JCF.2016.322. URL <https://www.davidhbailey.com/dhbpapers/backtest-prob.pdf>.
- [8] Wei Bao, Jun Yue, and Yulei Rao. A deep learning framework for financial time series using stacked autoencoders and long-short term memory. *PLoS ONE*, 12, 07 2017. doi: 10.1371/journal.pone.0180944.
- [9] Peter Bartlett, Elad Hazan, and Alexander Rakhlin. Adaptive online gradient descent. *Advances in Neural Information Processing Systems 20 - Proceedings of the 2007 Conference*, 01 2007.
- [10] Y. Bengio and Samy Bengio. Modeling high-dimensional discrete data with multi-layer neural networks. 02 2001. URL <http://papers.nips.cc/paper/1679-modeling-high-dimensional-discrete-data-with-multi-layer-neural-networks.pdf>.

- [11] Y. Bengio, Pascal Lamblin, D. Popovici, and Hugo Larochelle. Greedy layer-wise training of deep networks. *Adv. Neural Inf. Process. Syst.*, 19: 153–160, 01 2007.
- [12] Y. Bengio, Aaron Courville, and Pascal Vincent. Representation learning: A review and new perspectives. *IEEE transactions on pattern analysis and machine intelligence*, 35:1798–1828, 08 2013. doi: 10.1109/TPAMI.2013.50.
- [13] L Bottou and Yann Lecun. Large scale online learning. *Advances in Neural Information Processing Systems 16*, 03 2004.
- [14] L. Bottou and N. Murata. *Stochastic Approximations and Efficient Learning, The Handbook of Brain Theory and Neural Networks*. The MIT Press, 2 edition, 2019.
- [15] Chris Brooks and Harry Kat. The statistical properties of hedge fund index returns. *Henley Business School, Reading University, ICMA Centre Discussion Papers in Finance*, 01 2001.
- [16] Steve Christie. Is the sharpe ratio useful in asset allocation? *SSRN Electronic Journal*, 05 2005. doi: 10.2139/ssrn.720801.
- [17] Dan Cirean, Ueli Meier, Luca Gambardella, and Jrgen Schmidhuber. Deep, big, simple neural nets for handwritten digit recognition. *Neural computation*, 22:3207–20, 12 2010. doi: 10.1162/NECO_a_00052.
- [18] JuliaLang.org contributors. The julia programming language, 2019. URL <https://julialang.org/>.
- [19] James Crutchfield. Between order and chaos. *Nature Physics*, 9:382–382, 06 2013. doi: 10.1038/nphys2639.
- [20] Joel da Costa. Dissertation github - activationfunctions, 2019. URL <https://github.com/joel11/Masters/blob/master/Code%20Libraries/ActivationFunctions.jl>.
- [21] Joel da Costa. Dissertation github - csv, 2019. URL <https://github.com/joel11/Masters/blob/master/Code%20Libraries/CSV.jl>.
- [22] Joel da Costa. Dissertation github - configtestsffn, 2019. URL <https://github.com/joel11/Masters/blob/master/Code%20Libraries/ConfigTestsFFN.jl>.
- [23] Joel da Costa. Dissertation github - configtestssae, 2019. URL <https://github.com/joel11/Masters/blob/master/Code%20Libraries/ConfigTestsSAE.jl>.
- [24] Joel da Costa. Dissertation github - costfunctions, 2019. URL <https://github.com/joel11/Masters/blob/master/Code%20Libraries/CostFunctions.jl>.

- [25] Joel da Costa. Dissertation github - dsrdataproc, 2019. URL https://github.com/joel11/Masters/blob/master/Code%20Libraries/DSR/DSR_dataproc.py.
- [26] Joel da Costa. Dissertation github - dsrproc, 2019. URL https://github.com/joel11/Masters/blob/master/Code%20Libraries/DSR/DSR_proc.py.
- [27] Joel da Costa. Dissertation github - datagenerator, 2019. URL <https://github.com/joel11/Masters/blob/master/Code%20Libraries/DataGenerator.jl>.
- [28] Joel da Costa. Dissertation github - dataprocessor, 2019. URL <https://github.com/joel11/Masters/blob/master/Code%20Libraries/DataProcessor.jl>.
- [29] Joel da Costa. Dissertation github - databasecreator, 2019. URL <https://github.com/joel11/Masters/blob/master/Code%20Libraries/DatabaseCreator.jl>.
- [30] Joel da Costa. Dissertation github - databaseops, 2019. URL <https://github.com/joel11/Masters/blob/master/Code%20Libraries/DatabaseOps.jl>.
- [31] Joel da Costa. Dissertation github - experimentprocess, 2019. URL <https://github.com/joel11/Masters/blob/master/Code%20Libraries/ExperimentProcess.jl>.
- [32] Joel da Costa. Dissertation github - generator, 2019. URL <https://github.com/joel11/Masters/blob/master/Code%20Libraries/Generator.jl>.
- [33] Joel da Costa. Dissertation github - gradientfunctions, 2019. URL <https://github.com/joel11/Masters/blob/master/Code%20Libraries/GradientFunctions.jl>.
- [34] Joel da Costa. Dissertation github - initializationfunctions, 2019. URL <https://github.com/joel11/Masters/blob/master/Code%20Libraries/InitializationFunctions.jl>.
- [35] Joel da Costa. Dissertation github - networktrainer, 2019. URL <https://github.com/joel11/Masters/blob/master/Code%20Libraries/NetworkTrainer.jl>.
- [36] Joel da Costa. Dissertation github - rbm, 2019. URL <https://github.com/joel11/Masters/blob/master/Code%20Libraries/RBM.jl>.
- [37] Joel da Costa. Dissertation github root, 2019. URL <https://github.com/joel11/Masters/blob/master/Code%20Libraries>.

- [38] Joel da Costa. Dissertation github - sgd, 2019. URL <https://github.com/joel11/Masters/blob/master/Code%20Libraries/SGD.jl>.
- [39] Joel da Costa. Dissertation github - trainingstructures, 2019. URL <https://github.com/joel11/Masters/blob/master/Code%20Libraries/TrainingStructures.jl>.
- [40] Yann Dauphin, Razvan Pascanu, Caglar Gulcehre, Kyunghyun Cho, Surya Ganguli, and Y. Bengio. Identifying and attacking the saddle point problem in high-dimensional non-convex optimization. *NIPS*, 27, 06 2014.
- [41] David Donoho. High-dimensional data analysis: The curses and blessings of dimensionality. *AMS Math Challenges Lecture*, pages 1–32, 01 2000.
- [42] John Duchi, Elad Hazan, and Yoram Singer. Adaptive subgradient methods for online learning and stochastic optimization. *Journal of Machine Learning Research*, 12:2121–2159, 07 2011.
- [43] Dumitru Erhan, Y. Bengio, Aaron Courville, Pierre-Antoine Manzagol, Pascal Vincent, and Samy Bengio. Why does unsupervised pre-training help deep learning? *Journal of Machine Learning Research*, 11:625–660, 02 2010. doi: 10.1145/1756006.1756025.
- [44] Eugene Fama. The behavior of stock market price. *Journal of Business - J BUS*, 38, 01 1965. doi: 10.1086/294743.
- [45] Jianqing Fan and Yingying Fan. High dimensional classification using features annealed independence rules. *Annals of statistics*, 36:2605–2637, 02 2008. doi: 10.1214/07-AOS504.
- [46] Jianqing Fan and Runze Li. Statistical challenges with high dimensionality: Feature selection in knowledge discovery. *Proc. Madrid Int. Congress of Mathematicians*, 3, 03 2006.
- [47] Python Software Foundation. Python, 2019. URL <https://www.python.org/>.
- [48] Rong Ge, Furong Huang, Chi Jin, and Yang Yuan. Escaping from saddle points — online stochastic gradient for tensor decomposition. 03 2015. URL <http://proceedings.mlr.press/v40/Ge15.pdf>.
- [49] Tim Gebbie and Fayyaaz Loonat. Learning zero-cost portfolio selection with pattern matching. *PLOS ONE*, 13, 05 2016. doi: 10.1371/journal.pone.0202788.
- [50] Xavier Glorot and Y. Bengio. Understanding the difficulty of training deep feedforward neural networks. *Journal of Machine Learning Research - Proceedings Track*, 9:249–256, 01 2010.

- [51] Xavier Glorot, Antoine Bordes, and Y. Bengio. Deep sparse rectifier neural networks. *Proceedings of the 14th International Conference on Artificial Intelligence and Statistics (AISTATS) 2011*, 15:315–323, 01 2011.
- [52] Ian Goodfellow, David Warde-Farley, Mehdi Mirza, Aaron Courville, and Y. Bengio. Maxout networks. *30th International Conference on Machine Learning, ICML 2013*, 1302, 02 2013.
- [53] Gerwin Griffioen. Technical analysis in financial markets. *SSRN Electronic Journal*, 03 2003. doi: 10.2139/ssrn.566882.
- [54] Peter Hansen, James Nason, and Asger Lunde. The model confidence set. *Econometrica*, 79:453–497, 03 2010. doi: 10.2139/ssrn.522382.
- [55] Campbell R. Harvey and Yan Liu. Backtesting. *The Journal of Portfolio Management*, 42:13–28, 07 2015. doi: <https://doi.org/10.3905/jpm.2015.42.1.013>.
- [56] Douglas Hawkins. The problem of overfitting. *Journal of chemical information and computer sciences*, 44:1–12, 05 2004. doi: 10.1021/ci0342472.
- [57] Kaiming He, Xiangyu Zhang, Shaoqing Ren, and Jian Sun. Delving deep into rectifiers: Surpassing human-level performance on imagenet classification. *IEEE International Conference on Computer Vision (ICCV 2015)*, 1502, 02 2015. doi: 10.1109/ICCV.2015.123.
- [58] G. Hinton. A practical guide to training restricted boltzmann machines[j]. *Momentum*, 9:926–947, 01 2010.
- [59] G.E. Hinton and R.R. Salakhutdinov. Reducing the dimensionality of data with neural networks. *Science (New York, N.Y.)*, 313:504–7, 08 2006. doi: 10.1126/science.1127647.
- [60] Geoffrey Hinton. Article training products of experts by minimizing contrastive divergence. *Neural computation*, 14:1771–800, 09 2002. doi: 10.1162/089976602760128018.
- [61] Geoffrey Hinton, Simon Osindero, and Yee-Whye Teh. A fast learning algorithm for deep belief nets. *Neural computation*, 18:1527–54, 08 2006. doi: 10.1162/neco.2006.18.7.1527.
- [62] Geoffrey Hinton, Nitish Srivastava, Alex Krizhevsky, Ilya Sutskever, and Ruslan Salakhutdinov. Improving neural networks by preventing co-adaptation of feature detectors. *arXiv preprint*, arXiv, 07 2012.
- [63] Sepp Hochreiter and Jrgen Schmidhuber. Long short-term memory. *Neural computation*, 9:1735–80, 12 1997. doi: 10.1162/neco.1997.9.8.1735.

- [64] K. Hornik. Multilayer feed-forward networks are universal approximators. *Neural Networks*, 2:359–366, 1989. doi: [https://doi.org/10.1016/0893-6080\(89\)90020-8](https://doi.org/10.1016/0893-6080(89)90020-8).
- [65] Daniel Hsu. Time series compression based on adaptive piecewise recurrent autoencoder. 07 2017.
- [66] John Ioannidis. Why most published research findings are false. *CHANCE*, 32:4–13, 01 2019. doi: 10.1080/09332480.2019.1579573.
- [67] A. Ivakhnenko. Polynomial theory of complex systems. ieee trans syst man cybern. *Systems, Man and Cybernetics, IEEE Transactions on*, 1: 364 – 378, 11 1971. doi: 10.1109/TSMC.1971.4308320.
- [68] Neil Johnson, Guannan Zhao, Eric Hunsader, Hong Qi, Nicholas Johnson, Jing Meng, and Brian Tivnan. Abrupt rise of new machine ecology beyond human response time. *Scientific reports*, 3:2627, 09 2013. doi: 10.1038/srep02627.
- [69] Michael N. Kahn. *Technical Analysis Plain and Simple: Charting the Markets in Your Language*. Financial Times Press, 2006.
- [70] Alex Krizhevsky, Ilya Sutskever, and Geoffrey Hinton. Imagenet classification with deep convolutional neural networks. *Neural Information Processing Systems*, 25, 01 2012. doi: 10.1145/3065386.
- [71] John Langford, Lihong Li, and Tong Zhang. Sparse online learning via truncated gradient. *Journal of Machine Learning Research*, 10, 07 2008. doi: 10.1145/1577069.1577097.
- [72] Martin Langkvist, Lars Karlsson, and Amy Loutfi. A review of unsupervised feature learning and deep learning for time-series modeling. *Pattern Recognition Letters*, 42, 06 2014. doi: 10.1016/j.patrec.2014.01.008.
- [73] Yann LeCun. A theoretical framework for back-propagation. 01 1992.
- [74] Yann LeCun, Y. Boser, B. Denker, D. Henderson, R. Howard, W. Hubbard, and L. Jackel. Back-propagation applied to handwritten zip-code recognition. *Neural Computation - NECO*, 01 1992.
- [75] Yann LeCun, Leon Bottou, Genevieve Orr, and Klaus-Robert Müller. *Efficient BackProp*, volume 1524, pages 546–546. 01 1998. doi: 10.1007/3-540-49430-8_2.
- [76] Yann LeCun, Y. Bengio, and G. Hinton. Deep learning. *Nature*, 521:436–44, 05 2015. doi: 10.1038/nature14539.
- [77] Andrew Lo. The statistics of sharpe ratios. *Financial Analysts Journal*, 58, 02 2003. doi: 10.2469/faj.v58.n4.2453.

- [78] Marcos Lopez de Prado. The future of empirical finance. *The Journal of Portfolio Management*, 41:140–144, 07 2015. doi: 10.3905/jpm.2015.41.4.140.
- [79] Marcos Lopez de Prado. Building diversified portfolios that outperform out of sample:. *The Journal of Portfolio Management*, 42:59–69, 07 2016. doi: 10.3905/jpm.2016.42.4.059.
- [80] Marcos Lopez de Prado and Michael Lewis. Dissertation github - dsr-pradolewis, 2019. URL https://github.com/joel11/Masters/blob/master/Code%20Libraries/DSR/DSR_PradoLewis.py.
- [81] Marcos Lopez de Prado and Michael Lewis. Detection of false investment strategies using unsupervised learning methods. *Quantitative Finance*, 19:1–11, 07 2019. doi: 10.1080/14697688.2019.1622311.
- [82] Ilya Loshchilov and Frank Hutter. Sgdr: Stochastic gradient descent with warm restarts. 08 2016.
- [83] Spencer Lyon. Plotlyjs, 2019. URL <http://spencerlyon.com/PlotlyJS.jl/>.
- [84] A. Maas, A. Hannun, and A. Ng. Rectifier nonlinearities improve neural network acoustic models. *Proceedings of the 30 th International Conference on Machine Learning*,, 28, 2013. URL https://ai.stanford.edu/~amaas/papers/relu_icml2013_final.pdf.
- [85] R. Mclean and Jeffrey Pontiff. Does academic research destroy stock return predictability? *The Journal of Finance*, 71, 05 2013. doi: 10.2139/ssrn.2156623.
- [86] Elmar Mertens. Comments on variance of the iid estimator in lo (2002). *Technical report, Working Paper University of Basel*, 11 2002.
- [87] Marvin Minsky and Seymour Papert. *Perceptrons: An Introduction to Computational Geometry*. 01 2017. ISBN 9780262343930. doi: 10.7551/mitpress/11301.001.0001.
- [88] John Murphy. Technical analysis of financial markets. 01 1999.
- [89] Nicholas Murphy and Tim Gebbie. Learning the population dynamics of technical trading strategies, 03 2019.
- [90] Alexander Adamou Ole Peters. *Ergodicity Economics*. London Mathematical Laboratory, 2018.
- [91] Aaron oord, Sander Dieleman, Heiga Zen, Karen Simonyan, Oriol Vinyals, Alex Graves, Nal Kalchbrenner, Andrew Senior, and Koray Kavukcuoglu. Wavenet: A generative model for raw audio. 09 2016.

- [92] J.D. Opdyke. Comparing sharpe ratios: So where are the p-values? *Journal of Asset Management*, 8, 12 2007. doi: 10.1057/palgrave.jam.2250084.
- [93] Norman Packard, J.P. Crutchfield, and R. Shaw. Geometry from a time series. *Phys. Rev. Lett.*, 45:712, 09 1980. doi: 10.1103/PhysRevLett.45.712.
- [94] Razvan Pascanu, Tomas Mikolov, and Y. Bengio. On the difficulty of training recurrent neural networks. *30th International Conference on Machine Learning, ICML 2013*, 11 2012.
- [95] Jeffrey M. Perkel. Julia: come for the syntax, stay for the speed. *Nature*, 572:141–142, 2019. doi: doi:10.1038/d41586-019-02310-3.
- [96] R.J. Peter. Silhouettes: a graphical aid to the interpretation and validation of cluster analysis. *J. Comput. Appl. Math.*, 20, 01 1987.
- [97] Marc'Aurelio Ranzato, Christopher Poultney, Sumit Chopra, and Yann Lecun. Efficient learning of sparse representations with an energy-based model. 01 2006.
- [98] Nicolas Roux and Y. Bengio. 1 representational power of restricted boltzmann machines and deep belief networks. *Neural computation*, 20:1631–49, 07 2008. doi: 10.1162/neco.2008.04-07-510.
- [99] D. Rumelhart, G. Hinton, and Williams RJ. Learning internal representations by error propagation. *Parallel Distributed Processing: Explorations in the Microstructure of Cognition*, 1, 07 1986. doi: 10.1016/B978-1-4832-1446-7.50035-2.
- [100] Robert Schaefer. Subset selection in regression. *Technometrics*, 34, 03 2012. doi: 10.1080/00401706.1992.10484917.
- [101] J Schmidhuber. Deep learning in neural networks: An overview. *Neural Networks*, 61:85–117, 01 2015. doi: <https://doi.org/10.1016/j.neunet.2014.09.003>.
- [102] Frank Schorfheide and Kenneth Wolpin. On the use of holdout samples for model selection. *American Economic Review*, 102, 05 2012. doi: 10.1257/aer.102.3.477.
- [103] Jack D. Schwager. *Getting Started in Technical Analysis*. Wiley, 1999. ISBN 0471295426.
- [104] Pierre Sermanet, Koray Kavukcuoglu, Soumith Chintala, and Yann Le-cun. Pedestrian detection with unsupervised multi-stage feature learning. *Proceedings / CVPR, IEEE Computer Society Conference on Computer Vision and Pattern Recognition. IEEE Computer Society Conference on Computer Vision and Pattern Recognition*, 12 2012. doi: 10.1109/CVPR.2013.465.

- [105] William Sharpe. Mutual fund performance. *Journal of Business*, 39: 119–138, 01 1966. doi: 10.1086/294846.
- [106] Hava Siegelmann. Theoretical foundations of recurrent neural networks. 11 2019.
- [107] Andrew Skabar and Ian Cloete. Neural networks, financial trading and the efficient markets hypothesis. *ACSC '02: Proceedings of the Twenty-fifth Australasian Conference on Computer Science*, 4, 02 2002. doi: 10.1145/563857.563829.
- [108] Leslie Smith. Cyclical learning rates for training neural networks. pages 464–472, 03 2017. doi: 10.1109/WACV.2017.58.
- [109] F. Takens. Detecting strange attractors in turbulence. *Dynamical Systems and Turbulence serial Lecture notes in Mathematics*, 898, 01 1981.
- [110] Lawrence Takeuchi. Applying deep learning to enhance momentum trading strategies in stocks. 2013.
- [111] Luigi Troiano, Elena Villa, and Pravesh Kriplani. On feature reduction using deep learning for trend prediction in finance. 04 2017.
- [112] Paul Tseng. An incremental gradient(-projection) method with momentum term and adaptive stepsize rule. *SIAM Journal on Optimization*, 8, 04 1999. doi: 10.1137/S1052623495294797.
- [113] Pascal Vincent, Hugo Larochelle, Isabelle Lajoie, Y. Bengio, and Pierre-Antoine Manzagol. Stacked denoising autoencoders: Learning useful representations in a deep network with a local denoising criterion. *Journal of Machine Learning Research*, 11:3371–3408, 12 2010.
- [114] Sida Wang and Christopher Manning. Fast dropout training. In Sanjoy Dasgupta and David McAllester, editors, *Proceedings of the 30th International Conference on Machine Learning*, volume 28 of *Proceedings of Machine Learning Research*, pages 118–126, Atlanta, Georgia, USA, 17–19 Jun 2013. PMLR. URL <http://proceedings.mlr.press/v28/wang13a.html>.
- [115] Sholom M. Weiss and Casimir A. Kulikowski. *Computer Systems That Learn: Classification and Prediction Methods from Statistics, Neural Nets, Machine Learning, and Expert Systems*. Morgan Kaufmann Publishers Inc., San Francisco, CA, USA, 1991. ISBN 1-55860-065-5.
- [116] Paul Werbos. *Applications of advances in nonlinear sensitivity analysis*, volume 38, pages 762–770. 01 1970. doi: 10.1007/BFb0006203.
- [117] Paul Werbos and Paul John. Beyond regression : new tools for prediction and analysis in the behavioral sciences /. 01 1974.

- [118] Diane Wilcox and Tim Gebbie. Hierarchical causality in financial economics. *SSRN Electronic Journal*, 08 2014. doi: 10.2139/ssrn.2544327.
- [119] Huaiqin Wu. Global stability analysis of a general class of discontinuous neural networks with linear growth activation functions. *Inf. Sci.*, 179: 3432–3441, 09 2009. doi: 10.1016/j.ins.2009.06.006.
- [120] Lv Yisheng, Yanjie Duan, Wenwen Kang, Zhengxi Li, and Fei-Yue Wang. Traffic flow prediction with big data: A deep learning approach. *IEEE Transactions on Intelligent Transportation Systems*, 16:865–873, 01 2014. doi: 10.1109/TITS.2014.2345663.
- [121] Matthew Zeiler. Adadelta: An adaptive learning rate method. 1212, 12 2012.
- [122] Yang Zhao, Jianping Li, and Lean Yu. A deep learning ensemble approach for crude oil price forecasting. *Energy Economics*, 66, 06 2017. doi: 10.1016/j.eneco.2017.05.023.